Alma Mater Studiorum · University of Bologna

School of Science
Department of Physics and Astronomy
Master Degree in Physics

A single-sided NMR approach to study structural differences of bovine articular tissue

Supervisor:
Prof. Claudia Testa

Co-supervisor:
Dr. Leonardo Brizi

Submitted by:
Carlo Golini

Academic Year 2020/2021

Abstract

This thesis work has been developed in collaboration between the Department of Physics and Astronomy of the University of Bologna and the *IRCCS* Rizzoli Orthopedic Institute during an internship period.

The study aims to investigate the sensitivity of single-sided *NMR* in detecting structural differences of the articular cartilage tissue and their correlation with mechanical behavior. Suitable cartilage indicators for osteoarthritis (*OA*) severity (e.g., water and proteoglycans content, collagen structure) were explored through four *NMR* parameters: T_2, T_1, D, and Slp. Structural variations of the cartilage among its three layers (i.e., superficial, middle, and deep) were investigated performing several *NMR* pulses sequences on bovine knee joint samples using the *NMR-MOUSE* device. Previously, cartilage degradation studies were carried out, performing tests in three different experimental setups. The monitoring of the parameters and the best experimental setup were determined. An *NMR* automatized procedure based on the acquisition of these quantitative parameters was implemented, tested, and used for the investigation of the layers of twenty bovine cartilage samples. Statistical and pattern recognition analyses on these parameters have been performed.

The results obtained from the analyses are very promising: the discrimination of the three cartilage layers shows very good results in terms of significance, paving the way for extensive use of *NMR* single-sided devices for biomedical applications. These results will be also integrated with analyses of tissue mechanical properties for a complete evaluation of cartilage changes throughout *OA* disease.

The use of low-priced and mobile devices towards clinical applications could concern the screening of diseases related to cartilage tissue. This could have a positive impact both economically (including for underdeveloped countries) and socially, providing screening possibilities to a large part of the population.

Contents

Introduction

Osteoarthritis (OA) is the most common joint disease in adults around the world. This is a painful and degenerative musculoskeletal condition characterized by the destruction of articular cartilage (loss of cellular integrity and cartilage volume) and pathophysiological changes in the underlying subchondral bone [1].

In 2010, the burden of this pathology was about the 6.8% of *DALY*s (Disability-Adjusted Life Years), which has been the key measure in Global Burden of Disease (*GBD*) studies to present a comprehensive assessment of the worldwide health impact of disease, injury and risk factors [2]. The burden is likely to grow steadily because of rising rates with age and with an aging world population. Because of the epidemiological pattern and associated costs, healthcare systems will need to develop effective and affordable strategies for dealing with this musculoskeletal disorder. For example, an early osteoarthritis diagnosis is crucial because once a certain degree of tissue damage is reached, it is almost impossible to recapture the articular cartilage functionality without surgery [3].

The technique of Nuclear Magnetic Resonance (*NMR*) and especially its extension towards imaging, denoted as Magnetic Resonance Imaging (*MRI*), is established as one of the most favored clinical tools for non-invasive diagnostic, evaluation, and monitoring of articular cartilage. *MRI* is widely accepted because of its ability to capture the integrity of soft tissue and subchondral bone. It is preferable to conventional radiography and computed tomography (*CT*) because of its superior soft-tissue contrast, multi-planar capabilities, and lack of ionizing radiation [4]. In general, the goal of many studies of cartilage is to determine the relationships between the composition, structure, and material properties of healthy cartilage, and to determine changes associated with pathologies (e.g. osteoarthritis) and aging [5]. *MRI* investigations which have been carried out so far have addressed predominantly the properties of articular cartilage in high magnetic fields (i.e. 1.5 to $3\,T$), such as the structural variations represented by the longitudinal and transverse relaxation times (i.e. T_1, T_2, T_2^* and $T_{1\rho}$) [6] [7]. Multiparametric *MRI* studies have also shown the possibility to evaluate cartilage degradation by assessing several quantitative parameters [8]. However, high-field clinical imaging usually provides limited resolution within the cartilage structure of a few *mm* in thickness; the rather short transverse relaxation times compared to most other tissues in the body constitute a significant problem for in vivo *MRI*. These facts limit the feasibility of high-field *MRI* studies of cartilage and especially the early diagnosis of osteoarthritis. Many fundamental studies of cartilage properties have therefore been performed ex vivo at various mag-

netic field strengths, in particular with micro-imaging equipment available at higher fields, allowing much better spatial resolution. Moreover, *NMR* cartilage studies focusing on orientation-dependent contrast and pressure influence were carried out, while spectroscopic and diffusion measurements elucidated the effect on molecular and transport properties [9] [10].

In recent years, a new generation of low-field solutions, either whole-body or extremity scanners, have entered the market; they combine reduction in cost with higher flexibility, for instance by allowing tilting of the patient together with the detection system to compare the state in joints with and without load, using the effect of the actual body weight. While low magnetic field strengths inevitably lead to a loss of Signal-to-Noise Ratio (*SNR*), and consequentially of spatial resolution, measurements at lower fields often experience higher contrast and potentially hold extra information about relaxation and diffusion properties not available at typical clinical field strengths [10]. A particular advantage of transferring typical *NMR* studies on cartilage to low magnetic field strength is found in the fact that relaxation contrast of T_1 is generally enhanced towards lower fields.

Moreover, low-field single-sided *NMR* may provide an appealing approach for the assessment of biological tissue properties. Single-sided *NMR* scanners allow direct contact of the resonator with a flat surface, such as a wall, a patient's skin, or any object in the vicinity of the receiver coil. Single-sided devices have demonstrated their potential in human and animal models like human skin, silicone breast implants, breast tissue, intestine, tendon, articular cartilage, bone, fluid components of trabecular bone, and human mummies. These devices allow the detection of the signal from a sensitive volume (a slab), suitably selected inside an object, regardless of its extension, and placed on the magnet surface. They have the additional advantages of low acquisition, running and maintenance costs, as they consist of small permanent magnets, and are portable [11]. Although the idea of using this type of equipment has been formulated over two decades before, systematic investigations of unilateral *NMR* did not appear in the scientific literature until the mid-1990s with the publication of the *NMR-MOUSE* [12], a single-sided mobile *NMR* surface scanner developed by Blumich et al. [13] in 1996. Because of its compactness and mobility, this device was named *NMR-MOUSE* for *mo*bile *u*niversal *s*urface *e*xplorer. This device has led to the development and understanding of *NMR* in highly inhomogeneous fields. It has been used and explored in such diverse fields as the non-destructive testing of rubber and polymer products, food and livestock analysis, as well as the state

assessment of objects of cultural heritage. In medicine, the reported studies focus on surface-near tissue like the Achilles tendon, skin and bones [12].

For 10 years now the *NMR-MOUSE* has also been used for studies on articular cartilage by a researchers group in Germany led by Erik Rossler and Carlos Mattea. Interesting results have been recently published in some papers (see [14] [9] [3] [15] [16]). The majority of these relaxometry studies are related to variations in Magnetization (M), diffusion coefficient (D), relaxation times (T_2 and T_1), which in turn can be related to water content or the presence of metabolites as well as cartilage tissue structure. It has been seen that water relaxation depends not only on water content but also on the kind of interaction with existing interfaces. It has also been observed that T_2 and T_1 measured in such low field and high spatial resolution can distinguish the four layers of the cartilage (superficial, middle, deep, calcified), which are usually all affected by *OA* disease. The layer structure of mammalian cartilage was found to meet the conditions required for obtaining a depth scan with the *NMR-MOUSE*. Curvature and other imperfections of the cartilage necessarily lead to partial averaging of the layer structure but were found to be acceptable for the main joints of larger mammalians such as bovine or human hip and knee joints. The variation of T_2, T_1, and D as a function of distance from the surface has been studied.

However, literature results on these topics are still poor, especially concerning the study on cartilage sample degradation. This phenomenon is due to the exposition at room temperature of the tissue in which it is subjected to dehydration with a consequent structural change. Moreover, *NMR* procedures, from which quantitative *NMR* parameters for each cartilage layer can be obtained, have not yet been submitted.

In this work, the *NMR-MOUSE* device was used to perform several *NMR* pulses sequences on bovine knee cartilage samples. Samples have been prepared at the Laboratory of Medical Technology of Rizzoli Orthopedic Institute under the supervision of Eng. Massimiliano Baleani and his collaborators. First of all, a study on cartilage degradation was carried out, performing several tests in three different experimental setups. Degradation test means the study of a certain *NMR* parameter trend during the time which starts immediately after the sample thawing (usually tens of hours were tested). These initial tests aimed to determine the changes during the time of four *NMR* parameters that would later be used in a final automatized procedure. This *NMR* procedure is capable to obtain quantitative *NMR* parameters (i.e. T_2, T_1, D and Slp) exactly from each cartilage layer of each sample. The approach behind this analysis is to determine whether and which *NMR* parameters can significantly

discriminate the differences in the cartilage structure among the three layers and among different coring zones of the knee. The aim is to correlate the anatomical characteristics with the *NMR* measures results. Finally, the ultimate goal of this work will be to correlate these two aspects with biomechanical measures performed in the Laboratory of Medical Technology (not reported here). This unified interpretation of Nuclear Magnetic Resonance and biomechanical measures will become more and more relevant in pre-clinical research for establishing a correlation between measured parameters and severity of the disease, such as osteoarthritis.

Materials and Methods

Chapter 1

The articular cartilage

In this Chapter, the composition and structure of the articular cartilage tissue are illustrated. The variations in composition, function, organization, morphology, and mechanical properties of cartilage components according to the depth from the articular surface, will lead to describe the cartilage through superficial, middle, deep, and calcified layers. Moreover, the bovine knee joint structure explanation will be carried out considering four main different zones that will be of interest to the studies of this work.

1.1 Composition and structure of articular cartilage tissue

Articular cartilage is a highly specialized connective tissue that covers the ends of long bones within the synovial joint cavity. The tissue facilitates the load-bearing of joints by cushioning the underlying subchondral bone from excess stresses and distributing the load during joint movements. The mechanical features of articular cartilage provide minimal friction and excellent lubrication within the joint [17]. These physical and mechanical properties are based on the specific chemical composition and metabolic activity of the tissue, which consists of a relatively small number (about 5% of adult tissue volume) of highly specialized cells (i.e. chondrocytes) distributed throughout an abundant extracellular substance. A particular feature of these chondrocytes is that they lack cell-cell contact; thus, communication between cells has to occur via the extracellular matrix (ECM). Articular cartilage is unique within the class of connective tissues because it contains no blood vessels, no nerve

fibers, no lymphatics, and also no separating basement membranes on either side of the tissue. So, the delivery of nutrients and removal of waste products is made by diffusion through the *ECM*.

The extracellular matrix is mainly composed of water (70-80% of adult tissue weight), collagen (10-20% of adult tissue weight), and proteoglycans, with lesser amounts of other non-collagenous proteins and glycoproteins [4]. In particular, it is characterized by a three-dimensional cross-linked network of insoluble collagen fibrils in which other more soluble components (i.e. highly hydrated negatively charged proteoglycan aggregates or glycoproteins) are trapped, immobilized, or even chemically attached, creating a fiber-reinforced composite solid matrix [18]. The majority of water is contained within the interstitial intrafibrillar space created by this collagen–proteoglycan matrix. Although there are 14 different types of collagen, approximately 90% of the adult articular cartilage collagen is of type II [17]. This molecule is composed of three identical polypeptide chains wound into a triple helix structure. The network formed by type II collagen fibrils provides tensile strength and is essential for maintaining the volume and shape of the cartilage. This tensile strength is increased by covalent, intermolecular cross-links which form between type II collagen molecules thanks to the mediation of collagen type IX [19]. The presence of collagen cross-links is crucial because the collagen network is under constant tension even in the unloaded state due to the swelling pressure of the proteoglycan/water gel. Collagen cross-links can be conceptually classed as either enzymatic or non-enzymatic, with enzymatic cross-linking representing an essential step in the development and repair of collagen connective tissues [20]. For this reason, cross-link concentration can be a suitable indicator of cartilage degradation due to age or diseases (e.g. osteoarthritis). As regards proteoglycans (*PG*s), they are highly hydrophilic macromolecules embedded in an underhydrated (i.e. compressed) form within the fibrillar network. They give articular cartilage its ability to undergo reversible deformation. The predominant *PG* of articular cartilage, termed aggrecan, contains a protein core to which glycosaminoglycan side chains (about 90% of the total mass of aggrecan) and oligosaccharides are covalently attached.

To form articular cartilage, chondrocytes organize the collagens, proteoglycans, and non-collagenous proteins into the just illustrated highly ordered structure. The composition, organization, and mechanical properties of the *ECM*, cell morphology, and cell function vary according to the depth from the articular surface. The morphological changes in chondrocytes and matrix from the articular surface to the

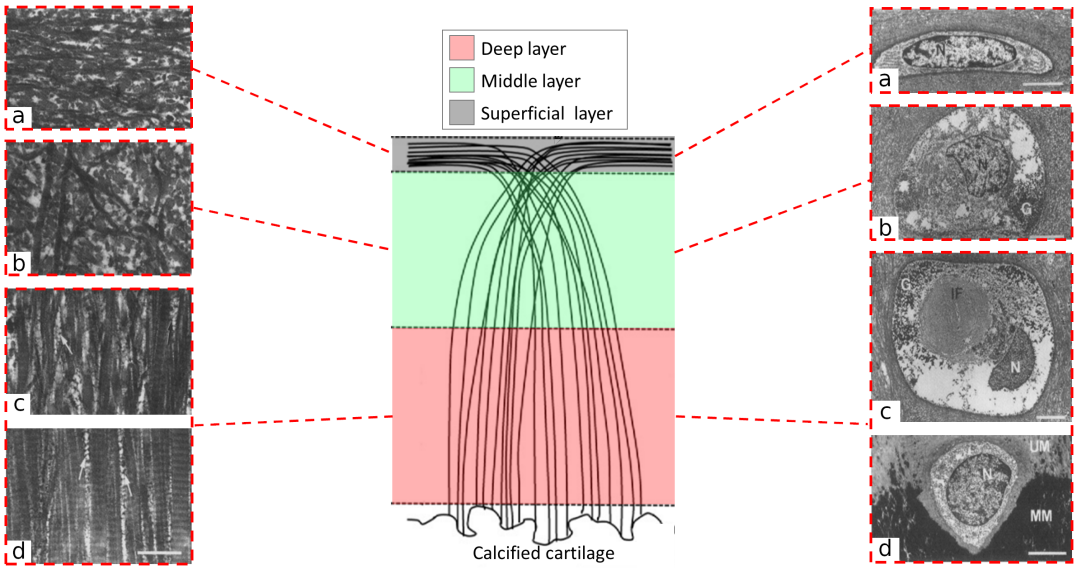

Figure 1.1: *The morphological changes of both (right) chondrocytes and (left) collagen fibrils from the articular cartilage surface to the subchondral bone (up to down). The four cartilage layers are identified as (a) superficial, (b) middle, (c, d) deep and calcified layers. Black lines in the central sketch represent collagen fibrils. Right and left figures are electron micrographs taken from [21]. N = nucleus, G = glycogen, IF = intermediate filaments, UM = unmineralized matrix, MM = mineralized matrix, bar = 3 μm.*

subchondral bone make it possible to identify four layers, which are superficial, middle, deep, and calcified layers. They are schematically represented in Figure 1.1, in which the change of both chondrocytes shape and collagen fibrils organization between cartilage layers is shown.

The relative size and appearance of these layers vary among species and among joints within the same species: although each zone has different morphological features, the boundaries between the layers cannot be sharply defined. Nonetheless, recent studies have shown that the zonal organization has functional importance: layers differ concerning concentrations of water, proteoglycan, and collagen and concerning the size of the aggregates. Cells in different layers differ not only in shape, size, and orientation relative to the articular surface but also in metabolic activity [21].

The superficial cartilage layer, also known as tangential layer (Fig. 1.1a, black), makes up approximately 10% to 20% of articular cartilage thickness [4]. It is characterized by two zones: an acellular sheet of fine fibrils in the joint surface and a

deeper zone in which flattened ellipsoid-shaped chondrocytes arrange themselves so that their major axes are parallel to the articular surface. The chondrocytes synthesize a matrix that has a high concentration of collagen and a low concentration of proteoglycans relative to the other cartilage layers. The concentration of water is also the highest in this layer. As shown in Figure 1.1, the collagen fibrils organization is parallel to the joint surface. These fibrils give this layer greater tensile stiffness and strength than the deeper layers to resist shear forces generated during the use of the joint. For this reason, mechanical tests, which will be correlated with *NMR* tests results of this work (Chapter 7), will be performed directly on the superficial cartilage layer. The total measured elastic modulus is indeed influenced mainly by the contribution of this layer, that deforms approximately 25 times more than the middle layer [4]. Moreover, alterations in the superficial layer may contribute to the development of osteoarthritis by changing the mechanical behavior of the tissue.

The middle cartilage layer (Fig. 1.1b, green) is characterized by intermediate morphology and matrix composition between the superficial layer and the deep layer. The middle layer usually has several times the volume of the superficial layer (40% to 60% of the cartilage volume [4]). The cells assume a spheroidal shape and synthesize a matrix that has larger-diameter collagen fibrils, higher concentration of proteoglycans, and lower concentrations of water and collagen than does the matrix of the superficial layer. As shown in Figure 1.1, the collagen fibrils organization is oblique to the joint surface: they start to bend along cartilage depth forming a mostly random orientation.

The deep cartilage layer (Fig. 1.1c and d, red) is characterized by spheroidal-shaped chondrocytes which tend to align themselves in columns perpendicular to the joint surface. This layer makes up 30% to 40% of the cartilage [4] and it contains the largest-diameter collagen fibrils, the highest concentration of proteoglycans, and the lowest concentration of water. As shown in Figure 1.1, the collagen fibrils are oriented perpendicular to the articular surface and they pass into the tidemark, a thin line of decalcified articular cartilage that roughly corresponds to the boundary between calcified and uncalcified cartilage.

The calcified cartilage layer (Fig. 1.1, white) is a thin layer that separates the deep layer (i.e. uncalcified cartilage) from the subchondral bone. The cells have a smaller volume than the cells of the deep layer. In some regions, these cells appear to be surrounded by calcified cartilage (see Fig 1.1d on the right part), suggesting that the cells have an extremely low level of metabolic activity. However, recent

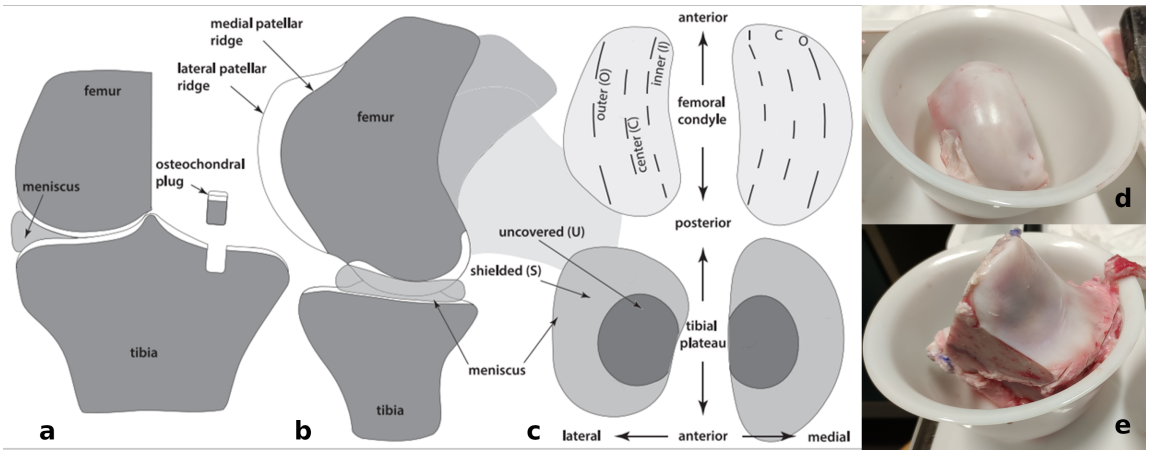

Figure 1.2: *The bovine knee (or stifle) joint: (a) a frontal plane view and (b) a sagittal plane view for three flexion angles. (c) The four different zones which have been considered for the studies of this work: from top left clockwise lateral femoral condyle, medial femoral condyle, medial tibial plateau and lateral tibial plateau. Figures are taken from [22]. (d, e) Photos of one lateral femoral condyle and one lateral tibial plateau used for this work.*

work suggests that they may have a role in the development and progression of osteoarthritis [21]. Of course, *ECM* macromolecules and their concentrations change during the different phases of development and aging to meet altered functional needs. The concentration and metabolic balance among them and their structural relationships and interactions reflect the character and function of articular cartilage within its layers and within different joints. This work will aim to catch these peculiarities through *NMR* measurements, trying to compare both different cartilage layers and different knee joint zones of a bovine. In the next Section, these zones will be described.

1.2 The bovine knee joint structure

The knee joint, more precisely called the stifle is the most complex joint located in the hind (i.e. pelvic) limbs of the bovine. The bovine knee joint is similar in several aspects to the human knee joint. This suggests that the obtained results on studying bovine knee are generally applicable and can be cautiously extrapolated to the human knee. In general, it is known that many properties of the human knee joint are almost certainly driven by the same fundamental biological processes that govern tissue development in other animal joints like the bovine one [22].

The knee joint includes two long bones, the femur, and the tibia, and it is stabilized by paired collateral and cruciate ligaments which act to prevent abduction/adduction [23]. 'Cushioning' of the joint is provided by two C-shaped pieces of cartilage (i.e. menisci) which sit between femoral condyles (i.e. the two reliefs in the bottom extremity of the femur) and tibial plateaus (i.e. the two concave plains in the top extremity of the tibia). The two femoral condyles can rotate on the two tibial plateaus. The articular cartilage is a thin layer of a few millimeters that covers and protects these two femora and tibia extremities and it is preserved and hydrated by the joint synovial liquid. Figure 1.2 shows a schematic representation of the bovine knee joint view in frontal and sagittal planes (a and b). The cartilage layer is represented in white and it is thicker in the center than in the periphery of the tibial plateaus [22].

The four different zones which have been considered for the studies of this work are shown in Figure 1.2c: from top left clockwise lateral femoral condyle, medial femoral condyle, medial tibial plateau, and lateral tibial plateau. Photos of one femoral condyle and one tibial plateau used for this work are also reported.

Chapter 2

Sample preparation

This Chapter contains all information about the samples used for *NMR* measurements in this work. The coring procedure of bovine knee joint pieces using the *ProLIGHT Machining Center* is illustrated. The treatment of the bovine samples from coring to *NMR* tests is also described. Finally, the preliminary part of *NMR* measures that were devoted to the choice of the best experimental setup is reported here. This represented a key step for understanding the role of degradation of the cartilage of the samples during the time.

2.1 The coring procedure

All the bovine knee joints were donated to the Rizzoli Orthopedic Institute by a butcher shop in Cesena. Each knee joint was taken the night before the coring day and it was put in the fridge until the following morning. The first step in the Laboratory of Medical Technology was the knee boning and sawing to obtain four different bovine pieces: two tibial plateaus and two femoral condyles. In Section 1.2, two of these four pieces have been shown, in particular a condyle and a plateau. The following step was the coring of the bovine knee joint pieces which was performed using the *ProLIGHT Machining Center* (Fig. 2.1), with a hollow cylinder drill of $10\,mm$ diameter. From each piece, about five cylindrical samples were obtained. During processing, the cartilage surface of the pieces was kept moist with a liquid solution which contained about 90% of distilled water and 10% of Phosphate Buffered Saline, *PBS* (concentration=10X, pH=7.4). Each coring step was of $0.5\,mm$ in the downward direction of the vertical axis, starting from the cartilage surface. After each step, the machine stopped the coring for a few seconds to give the possibility to keep

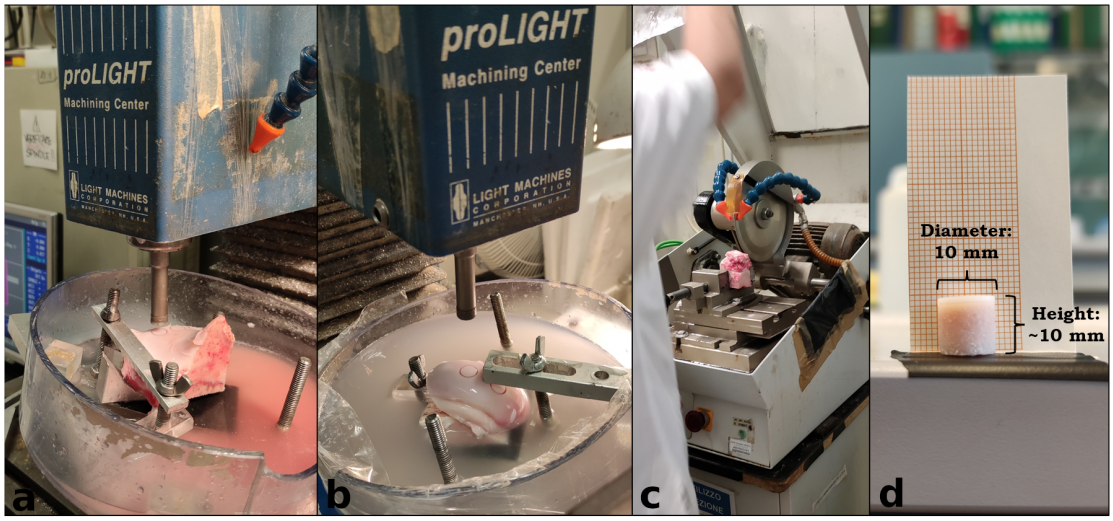

Figure 2.1: *The coring procedure of (**a**) bovine tibial plateau and (**b**) femoral condyle performed by the ProLIGHT Machining Center, taking the cartilage surface approximately perpendicular to the core axis. (**c**) The samples cutting procedure to get a uniform final sample height of about* 10 *mm (**d**).*

moist the sample. Usually, 36 steps were performed to reach a total sample depth of 18 *mm*. The time of the steps (so the coring velocity) was different in cartilage and bone: the first steps were done more slowly to better preserve the cartilage zone. The total coring time for one sample was about 10 minutes. For anatomical reasons in all the pieces the cartilage surface is not flat, there is curvature. For this research, it was essential to obtain samples with cartilage layers parallel to each other and all perpendicular to the core axis. In other words, the cartilage plate of each sample had to be as flat as possible. So, the bovine piece was placed so that to have the cartilage surface approximately perpendicular to the core axis, as it is shown in Fig. 2.1a and b.

After having cored the five samples (related to the same bovine piece), the samples were cut horizontally with a saw (Fig. 2.1c) in the bone part to obtain a uniform sample height of about 10 *mm*, starting from the initial coring depth of 18 *mm*. So, at the end of this procedure, the majority of the cylindrical samples had a diameter and height of 10 *mm* (see Fig. 2.1d). However, some samples were obtained with a smaller or bigger height depending on the coring position concerning the bovine piece's morphology. Immediately after being cut, the samples were immersed in the *PBS* solution for the entire coring procedure. In the end, all the samples were put in a freezer and defrosted one at a time in the following days for *NMR* measures.

2.2 The choice of the best experimental setup

The preliminary part of *NMR* measures was devoted to the choice of the experimental setup. This was a key step for understanding the role of degradation of the cartilage of the samples during the time. Considering this degradation was crucial because it was needed to analyze the samples cartilage as close as possible to the *in vivo* situation, in which the cartilage is preserved and hydrated by the synovial liquid (see Section 1.2). In this case, the degradation of the samples was mainly due to the evaporation of water molecules of the cartilage tissue with a consequent structural change, especially in the superficial layer because it was the most exposed to the air. Another degradation factor could be a high number of samples freezing and thawing cycles, but in this work, this was not relevant because the majority of the analyzed samples had only one cycle of freezing and thawing. So dehydration (i.e. the evaporation of water molecules) was considered as the main factor of the cartilage degradation during the time. In the preliminary part of this work it has been tried to reduce this dehydration effect as much as possible passing through three different setup configurations, which are shown in Fig. 2.2: *Sponge*, *PBS* and *Teflon* setups. In all three cases, before *NMR* measures, the samples were first thawed for about 20 minutes inside the same *PBS* solution that has been used for the coring procedure (Section 2.1).

The initial approach was to simply insert the sample in the extremity of a cylindrical glass tube, which had a soaked sponge and a cap in the other extremity and put this tube directly over three slides resting on the radiofrequency coil of the *NMR-MOUSE*. It will be seen that this setup makes the sample particularly exposed to water molecules evaporation, especially for the cartilage superficial layer, which is in direct contact with the external environment. To improve this setup some thin layers of *Polytetrafluoroethylene (PTFE)*, commercially known as *Teflon*, were added in the glass tube extremity that is in direct contact with the cartilage superficial layer. The *Teflon* is a good insulator, so in this case, it was useful to reduce the dehydration effect. To further improve setup configuration it has been also tried to immerse the sample in the *PBS* solution inside the glass tube, but it will be seen that this setup has two main disadvantages. First, the presence of the *PBS* solution can affect some *NMR* measures; second, after several hours of immersion, the sample starts to interact with the *PBS* solution and the latter becomes visibly more turbid. For these reasons, the *Teflon* setup was chosen as the best one for this thesis work. To support

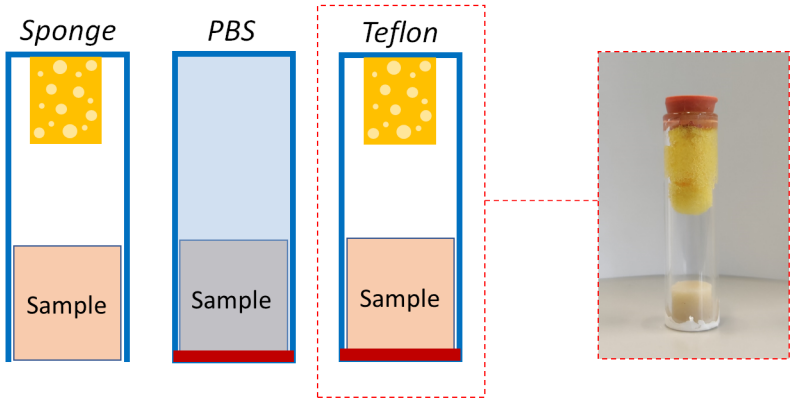

Figure 2.2: *Three different experimental setup configurations used in the preliminary NMR measures trying to reduce the dehydration effect as much as possible. They are shown in chronological order: from the left, the Sponge setup, PBS setup and Teflon setup. The two red lines at the bottom represent PTFE (Teflon) layers. As reported in the text, considering several factors, the Teflon setup was chosen as the best one (photo on the right).*

this choice, Chapter 5 will go through quantitative results of several degradation tests done with all three setups.

In this preliminary part, it is also needed to confirm that the *Teflon* didn't affect in any way the *NMR* measures of the cartilage. From the *NMR* theory that will be deepened in Section 3.1, it is known that when placed in a static magnetic field $\boldsymbol{B_0}$, a particle with a net spin can absorb a photon of energy $h\nu_0$ which satisfies the following resonance condition [24]:

$$\omega_0 = \gamma B_0 \tag{2.1}$$

where $\omega_0 = 2\pi\nu_0$ is the so called Larmor frequency, γ is the gyromagnetic ratio of the particle and B_0 is the amplitude of $\boldsymbol{B_0}$ field.

In this specific case, there is a focus on the hydrogen nuclei (^1H) of the cartilage: they have a gyromagnetic ratio of $42.58\,MHz/T$. The *Teflon* instead contains fluorine nuclei (^{19}F) which have a gyromagnetic ratio of $40.08\,MHz/T$, very close to the ^1H one [25]. So, ^1H and ^{19}F can absorb photons with similar Larmor frequencies (being subject to the same B_0 field). As it will be deepened in Section 3.2, in the *NMR-MOUSE* device there is a gradient of B_0 field inside the excited sample volume (i.e. sensitive volume), so to excite all this volume, photons in a certain frequency range have to be sent. In this preliminary part, it has been verified that the ^1H

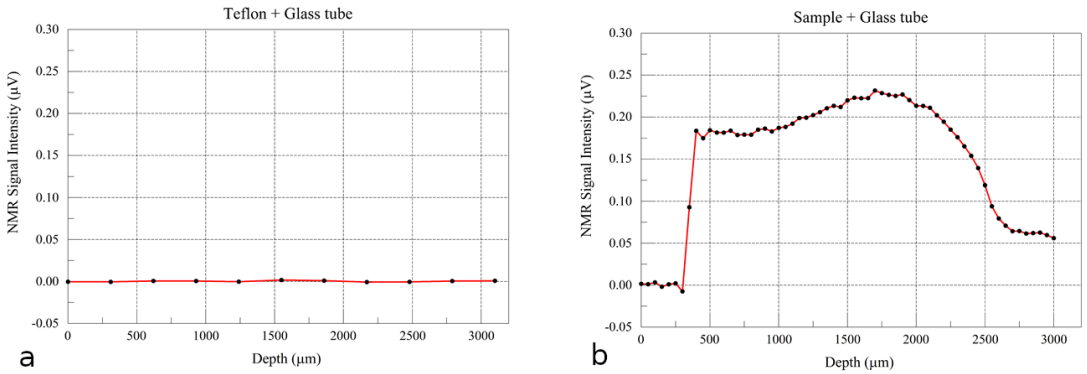

Figure 2.3: *NMR profile measures of the glass tube in two different cases: (a) with only Teflon layers in the tube extremity (11 profile steps); (b) with only the sample inside the tube, removing Teflon (61 profile steps). All the sample thickness under study has been considered: from the cartilage surface (about* 300 μm *of depth) to the trabecular bone (about* 3000 μm *of depth). There is no contribution of the Teflon to the NMR signal intensity in all the sample thickness.*

frequency range didn't excite *Teflon* ^{19}F nuclei along with all the sample thickness under study.

A *NMR* profile measure (see Section 3.3 for further details) of the glass tube in two different cases has been made: only with *Teflon* layers in the tube extremity (Fig. 2.3a) and only with the sample inside the tube, removing *Teflon* (Fig. 2.3b). By comparing the two graphs it could be seen that there is no contribution of the *Teflon* to the *NMR* signal intensity in all the sample thickness under study (i.e. from the cartilage surface to 3100 μm of depth). This was because ^{19}F didn't resonate in these particular conditions, or maybe the signal decay was too fast to see it. Anyway, this demonstration allowed us to choose the *Teflon* setup configuration as the best one for this work.

Chapter 3

NMR apparatus

In this Chapter, the Nuclear Magnetic Resonance (*NMR*) theory is illustrated starting from basic concepts and passing through relaxation, diffusion and multi-quantum phenomena. The *NMR-MOUSE* device and the Kea Prospa software which have been used in this work are presented in their operation. *NMR* pulse sequences and their role in a final automatized procedure are described.

3.1 A brief introduction to *NMR*

3.1.1 Basic concepts and relaxation phenomenon

The Nuclear Magnetic Resonance (*NMR*) is a physical phenomenon related to energy transitions of atomic nuclei with a nuclear magnetic moment $\boldsymbol{\mu}$, such that

$$\boldsymbol{\mu} = \gamma_n \Big(\frac{h}{2\pi} \Big) \boldsymbol{I} \tag{3.1}$$

where $\boldsymbol{I}$ is the spin and γ_n the gyromagnetic ratio of the nucleus n. The nuclei interact with a static magnetic field $\boldsymbol{B_0}$ of amplitude B_0 through the so called Zeeman interaction and the result is a splitting in the nuclei energy levels. Transitions between energy levels are only possible by sending electromagnetic waves with an energy which satisfies the resonance condition $\omega_0 = \gamma B_0$, as has been seen in Section 2.2 (eqn 2.1).

Since *NMR* phenomenon usually involves a huge number of nuclei, the ensemble behaviour can be characterized by a vector, called Nuclear Magnetization ($\boldsymbol{M}$), that is the macroscopic observable in *NMR* experiments. The Curie law states that the

Magnetization at the equilibrium ($\boldsymbol{M_0}$) is aligned along the magnetic field's direction. The Magnetization evolution is described by the following motion equation [24]:

$$\frac{d\boldsymbol{M}}{dt} = \gamma \boldsymbol{M} \times \boldsymbol{B_0}. \tag{3.2}$$

The solution to eqn (3.2) corresponds to a precession of the Magnetization about the $\boldsymbol{B_0}$ field (considering the latter along the z-axis direction) at rate $\omega_0 = \gamma B_0$, the Larmor frequency. The precession occurs only if $\boldsymbol{M}$ is not aligned with $\boldsymbol{B_0}$, and this $\boldsymbol{M}$ motion induces a current in a receiver coil allowing us to acquire *NMR* signal as an electric signal. This signal is an oscillating dumping function called *FID* (Free Induction Decay).

To generate this signal it is only necessary to tilt $\boldsymbol{M}$ by the application of a transverse (i.e. orthogonal to B_0) magnetic field $\boldsymbol{B_1}$ oscillating at ω_0: it means that the system acquires energy under the resonance condition. The spins respond to this energy pulse in such a way as to cause $\boldsymbol{M}$ to rotate about the direction of the applied $\boldsymbol{B_1}$ field. The rotation angle α depends on the length of time the field is on, t_p:

$$\alpha = \gamma B_1 t_p \tag{3.3}$$

The rotating field $\boldsymbol{B_1}$ consists in a radiofrequency (RF) pulse produced by a coil with the axis orthogonal to $\boldsymbol{B_0}$. The same coil is also used to reveal and acquire the *NMR* signal and, for this reason, it is called transceiver coil.

The effect of a resonant RF pulse is to disturb the spin system from its thermal equilibrium state. In due course that equilibrium will be restored by a process known as spin-lattice relaxation. As the name implies, the process involves an exchange of energy between the spin system and the surrounding thermal reservoir, the lattice, until $\boldsymbol{M_0}$ is again along the longitudinal direction, like $\boldsymbol{B_0}$ (i.e. equilibrium condition). The phenomenological description of this process is given by the equation [24]:

$$\frac{dM_z}{dt} = -\frac{(M_z - M_0)}{T_1} \tag{3.4}$$

with solution

$$M_z(t) = M_z(0) \cdot e^{-\frac{t}{T_1}} + M_0\left(1 - e^{-\frac{t}{T_1}}\right) \tag{3.5}$$

where T_1 is known as the spin-lattice or longitudinal relaxation time. This time constant can also describe the lifetime of transverse Magnetization resulting from the application of the same resonant RF pulse. Transverse relaxation, which is

characterized by the time constant T_2, is the process whereby nuclear spins come to thermal equilibrium among themselves. It is therefore known also as spin-spin relaxation in which a loss of phase coherence of the spin system is observed. The phenomenological description for transverse relaxation is written

$$\frac{dM_{x,y}}{dt} = -\frac{(M_{x,y})}{T_2} \tag{3.6}$$

with solution

$$M_{x,y}(t) = M_{x,y}(0) \cdot e^{-\frac{t}{T_2}}. \tag{3.7}$$

This approach works well for spins residing in liquid state molecules. However, for solids and macromolecules undergoing very slow motions, as will be seen in Section 3.3.5, the decay is more complicated than that represented by eqn (3.7) [24].

Summing up, the transverse relaxation is characterized by the loss of phase coherence of the spins system while the longitudinal one is a process of energy exchange between the spins system and the lattice, that also determines a loss of phase coherence. As a consequence, $T_2 \leq T_1$. In order to measure these time constants, which are characteristic of the material under study, some proper *NMR* sequences will be performed (see Sections 3.3.1 and 3.3.3).

3.1.2 Diffusion phenomenon

Diffusion is a spontaneous phenomenon in any fluid of temperature greater than absolute zero and it can be considered the macroscopic observable effect of the microscopic Brownian motion of particles. It is the random translational motion of molecules or ions driven by internal kinetic energy. In many systems molecular diffusion provides important information on molecular organization and interactions of mobile molecules with the environment. From a theoretical point of view, the trajectory of each molecule can be described by a random walk: the molecule stays in a particular place for a fixed time t before moving to a random, new location in space. In 1905 Einstein considered the mean square displacement of molecules from their starting point r_0 over the observation time t, averaged over all the molecules in the sample. For the 3-D space in free diffusion condition the mean square displacement varies linearly with time:

$$\left\langle (r - r_0)^2 \right\rangle = 6Dt \tag{3.8}$$

where D is the so called diffusion coefficient. Diffusion is also closely related to molecular size, as the Stokes-Einstein equation states:

$$D = \frac{kT}{f}, \tag{3.9}$$

where k is the Boltzmann constant, T is the temperature and f is the friction coefficient that depends on molecular shape. From the *NMR* point of view, a diffusion term is included in the macroscopic Nuclear Magnetization behaviour [26]:

$$\frac{d\boldsymbol{M}}{dt} = D\nabla^2\boldsymbol{M}. \tag{3.10}$$

Note that in Equation (3.10) only the diffusion of Magnetization term is reported. The total macroscopic Nuclear Magnetization trend is also composed by the terms of Equations (3.2), (3.4) and (3.6).

Nuclear Magnetic Resonance provides several pulse sequences to analyse molecular diffusion dynamics. The procedures that allow to study the translational diffusion are based on the attenuation of the spin echo due to the phase shift of the nuclear spins. This phase shift is caused by the diffusion phenomenon in presence of a magnetic field gradient. So, large gradients (as provided by the *NMR-MOUSE*, Section 3.2) simplify measurements of the diffusion coefficient D in heterogeneous materials like porous materials and biological systems. In general, in the presence of a gradient, the signal attenuation due to relaxation and the signal attenuation due to diffusion are independent, and so can be written [26]:

$$S(t) = S(0) \cdot e^{-\frac{t}{T_2}} \cdot f(t) \tag{3.11}$$

where $S(0)$ is the signal without attenuation due to relaxation and $f(t)$ is a function that represents the attenuation due to diffusion. In the specific case of a Stimulated Echo Sequence (*SSE*, Section 3.3.4), which has been used in this work to encode the effect of molecular diffusion, Equation (3.11) can be rewritten as follows:

$$\frac{S(t)}{S(0)} = e^{-\frac{t}{T_2}} \cdot e^{-\gamma^2 g^2 \delta^2 D(\Delta + \frac{2}{3}\delta)} \tag{3.12}$$

where γ is the gyromagnetic ratio, g is the magnetic field gradient, D is the diffusion coefficient, δ is the encoding time and Δ is the diffusion time (the role of these parameters will be better explored in Section 3.3.4). In free diffusion condition, the

measurement of D is independent of the chosen diffusion time Δ, as Equation (3.8) states. However, if the diffusion is restricted by barriers, the previous consideration is no longer valid. The displacement becomes a function of Δ, of D (that now is the apparent diffusion coefficient) and of the geometry of the confining space [26]:

$$R = \sqrt{D \cdot \Delta} \tag{3.13}$$

where the diffusion within a pore of radius R is considered. So, the measurement of D as a function of the diffusion time Δ offers the possibility to probe different length scales of restriction.

3.1.3 Multi-Quantum phenomenon

In comparison with their dimensions, the separation of atomic nuclei in condensed matter is enormous. Despite this, the intrinsic magnetic moment $\boldsymbol{\mu}$ associated with each nuclear spin dipole exerts a severe influence on its neighbours via the magnetic field produced by this dipole, acting on the dipole moments of remote spins. This is the so called magnetic dipole-dipole interaction [24]. To make a practical example, the magnetic attraction and repulsion of the two protons in a methylene group (CH_2) of an elastomer polymer chain can be considered. Since the applied magnetic field is typically much stronger than the magnetic field one spin experiences from its neighbor spin, it keeps the spins aligned along its direction. Then, as the methylene group rotates, the dipole-dipole interaction between the spins alternates between attraction and repulsion. Rapid isotropic motion of a free chain averages the dipole-dipole interaction to zero. Rapid anisotropic motion of a chain constrained between two cross links (i.e. knots to which elastomer chains are tied) leaves a residual dipole-dipole interaction, which accelerates the transverse relaxation rate $1/T_2$ [27]. The more constrained and slower the motion (i.e. increasing of the cross-link density), the stronger the residual dipole-dipole interaction and the faster the spins relax.

Multi-Quantum *NMR* phenomenon arise in solid and soft materials when two interacting spins are excited coherently by a RF pulse and the dominant interaction between them is the dipole-dipole interaction. This phenomenon concerns transitions in spin systems where magnetic spin states with coherence orders different from ± 1 are generated with the exception of longitudinal Magnetization [28]. For spins 1/2, such states require a coherent coupling, by direct dipole–dipole coupling. As explained in the above example, this is strong among protons but is averaged to

zero by isotropic molecular reorientation, so that it vanishes in liquids. Stronger residual dipolar couplings are found in anisotropic environments like soft matter (i.e. biological tissues and rubber). They provide information on the molecular dynamics in the solid state. In the last years ^1H residual dipolar couplings (ω_D) were measured by different *NMR* techniques performed in low magnetic fields [29]. For example, by using the Double-Quantum (DQ) build-up curve fitting in the initial regime of the excitation/reconversion periods (short τ). In the case of *NMR-MOUSE* this curve can be approximated as follows [30]:

$$\frac{S_{DQ}(\tau)}{S_{DQ}(0)} \propto \left(1 - \frac{3}{4} \cdot \left\langle \omega_D^2 \right\rangle \cdot \tau^2\right) \cdot \sin^4 \alpha \tag{3.14}$$

where the left term is the normalized Double-Quantum signal amplitude and α is the rotation angle. So, the value of residual dipole-dipole coupling ω_D can be extracted by performing a Double-Quantum *NMR* pulse sequence repeated for different values of τ.

As will be explained in Section 3.3.5, the behaviour of the DQ build-up pulse sequence in the case of long τ has been explored for the purposes of this work. Schneider et al. [31] explained this behaviour for elastomers through simulations using the following relationship with high τ values:

$$S_{DQ}(\tau) \approx \frac{1}{2}\left\langle\left\langle \sin^2\left[\sqrt{\frac{3}{2}} \cdot \omega_{D2} \cdot \tau\right]\right\rangle\right\rangle + \frac{3}{10}\left\langle\left\langle \sin^2\left[\sqrt{6} \cdot \omega_{D3} \cdot \tau\right]\right\rangle\right\rangle \tag{3.15}$$

where the symbol $\langle\langle\ \rangle\rangle$ represents the powder average of the angular part of the residual dipolar coupling in the disordered elastomer. Equation (3.15) represents the DQ signal amplitude (S_{DQ}) trend considering CH_2 (first term) and CH_3 (second term) groups. Simulations results showed that for sufficiently long τ the signal reaches a saturation maximum, after an initial increase. The increase rate before saturation will be considered as an indicator of the residual dipole-dipole coupling of the material under study (Section 3.3.5).

3.2 The *NMR-MOUSE*

A mobile *NMR* surface scanner has been used for the nondestructive investigation of the bovine samples. Because of its compactness and mobility, the device is named *NMR-MOUSE* for *mo*bile *u*niversal *s*urface *e*xplorer and it was developed for the

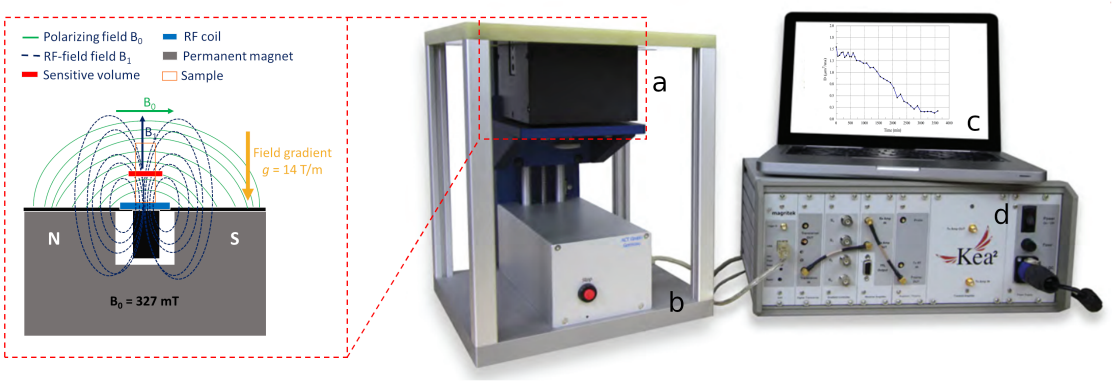

Figure 3.1: *(Left) Schematic representation of the probe system (permanent magnet + RF coil) that supports the sample. The B_1 RF field (dashed blue lines), the static B_0 polarization field (continuous green lines) and the sensitive volume (red region) are depicted. (Right) The single-sided Profile NMR-MOUSE PM10 (a) probe, (b) high-precision automatic lift, (c) PC console and (d) Kea2 spectrometer.*

first time in 1996 by Blumich et al. [13]. The single-sided Profile *NMR-MOUSE PM10* probe with the Kea2 spectrometer by Magritek has been used [32]. While radiofrequency (RF) generation and pulse programs are controlled by a PC-based *NMR* console, the probe provides not only the B_1 RF field but also the static B_0 polarization field. In particular, B_0 is generated by a U-shaped permanent magnet, while B_1 that is perpendicular to B_0, is created by a radiofrequency coil placed on top of the magnet, at the center of the system (see Fig. 3.1). These components dimensions are $12 \times 12\, cm$ and $15 \times 15\, mm$ for the magnet and coil bases, respectively.

The particular geometry of the magnet creates an intrinsic constant B_0 magnetic field gradient along the main direction (y) of the sample that is placed outside the magnet, on top of the setup. So, B_0 field amplitude decreases the further the distance from the magnet (Δy) increases. The value of this magnetic field gradient is

$$g = \frac{\Delta B_0}{\Delta y} = 14\,\frac{T}{m}. \tag{3.16}$$

The presence of a gradient makes a range of resonant frequencies to be available for the Nuclear Magnetic Resonance phenomenon. As explained in Section 3.1, this frequency range is related to B_0 field amplitude according to the resonance condition (eqn 2.1). The region where the resonance condition is satisfied is called sensitive volume (red region in Figure 3.1). So, all the ^1H particles that are inside this sensitive volume are excited and later detected. The sensitive volume related to all the *NMR*

experiments is created at a distance of $10\,mm$ from the magnet, where B_0 is equal to $0.327\,T$. The corresponding resonance frequency for ^1H particles is

$$\nu_0 = \frac{\omega_0}{2\pi} = \left(\frac{\gamma}{2\pi}\right) \cdot B_0 = 13.9\,MHz. \tag{3.17}$$

When the radiofrequency coil is switched on, it sends a pulse centered on ω_0 with a frequency bandwidth ($\Delta\omega$) which is inversely proportional to the time of the radiofrequency pulse, i.e. the pulse length t_p.

The distance between the RF-coil and the sensitive volume can be changed by inserting or removing four spacers between the magnet and the coil, each of them has $2\,mm$ of thickness. The choice of the spacer configuration is crucial to achieve the best Signal-to-Noise Ratio (*SNR*) for the experiments. The closer the coil is to the sensitive volume, the better will be the efficiency of the RF-pulse and the signal detection by the coil (that is transmitter and receiver at the same time). So, the more spacers are used, the better will be the sensitivity (at the cost of a reduced penetration depth), and thus the shorter will be the acquisition time. For all measures of this work, $8\,mm$ spacers configuration was chosen, providing the highest *SNR* and the lowest penetration depth. Using this setup the maximum sample measurable depth is $3\,mm$, more than enough to study the entire cartilage layer of the samples.

The *NMR-MOUSE* has been used in connection with a high-precision lift (Fig. 3.1b) for automatic up and down movement of the magnet. Moving the magnet means moving the sensitive volume too, because the same resonance frequency is used, detecting the signal at different depths within the sample. This type of measure is called *NMR* Profile. The *NMR-MOUSE PM10* system also includes a fully digital mobile spectrometer Kea2 (Fig. 3.1d) that processes the signal detected by the coil and sends the output to a PC console (Fig. 3.1c). Radiofrequency generation and pulse programs are controlled by the Kea Prospa software installed in that PC.

3.3 *NMR* pulse sequences

In this Section the *NMR* sequences that have been used in the experimental procedure are explained. *CPMG*, *SR* and *SSE* sequences were already present in the Prospa software, while *DQ* pulse sequence has been implemented on the occasion of this work directly using the same Prospa *MATLAB*-like language of the other three sequences.

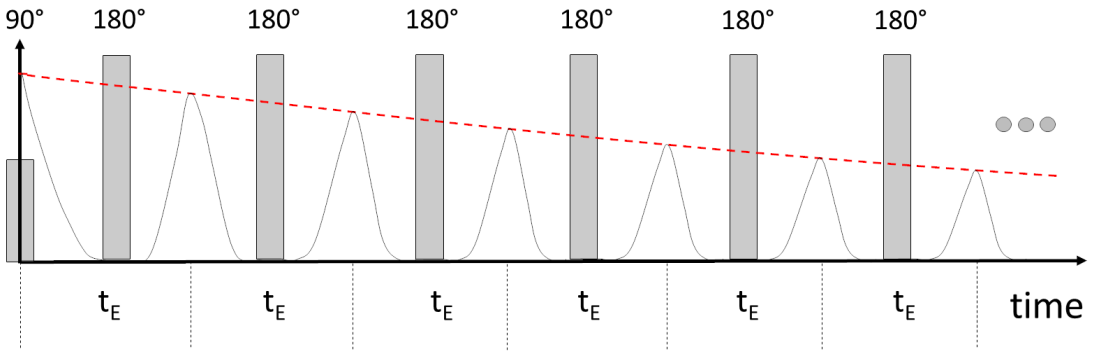

Figure 3.2: *A schematic diagram of a CPMG experiment. A series of echoes (black peaks) are formed by a series of 180° refocusing pulses. They decay in amplitude according to T_2 relaxation described in Equation (3.7) (dotted red line). The refocusing pulses are applied at times $t_E/2$, $(3t_E)/2$, $(5t_E)/2$, ... and echoes are seen at times t_E, $2t_E$, $3t_E$, ... , where t_E is the echo time.*

3.3.1 *CPMG* sequence

The Carr-Purcell-Meiboom-Gill (*CPMG*) is the basic pulse sequence to measure with the *NMR-MOUSE*. It minimizes the effects of inhomogeneity of B_0 and molecular diffusion in the magnetic field gradient. It consists of a 90° RF pulse followed by a train of n 180° refocusing pulses:

$$\left[90_x - \left(\frac{t_E}{2} - 180_y - \frac{t_E}{2} - Echo\ acquisition\right)_n - RT\right] \tag{3.18}$$

where t_E is the echo time, RT is the pulse repetition time, x and y are the phases of the pulses. After the 90° pulse the Nuclear Magnetization $\mathbf{M}$ is tilted on the transverse plane and the free induction decay (*FID*) is generated. Because of the selective excitation of the RF pulse and the dead time this signal cannot be acquired (it simply decays to zero before it can be detected). However, the *FID* signal can be refocused by a 180° pulse leading to the formation of an echo. The echo signal can be repeatedly refocused by applying the train of 180° pulses obtaining a train of echoes. By sampling the echo decay envelope as a function of the echo time t_E, the transverse relaxation time T_2 can be measured in a single experiment following the Equation (3.7). The refocusing pulses are applied at times $t_E/2$, $(3t_E)/2$, $(5t_E)/2$, ... and echoes are seen at times t_E, $2t_E$, $3t_E$, ... , as shown in Figure 3.2.

The production of multiple echoes suggests an obvious application in signal averaging. Co-addition of echoes within a train leads to Signal-to-Noise enhancement

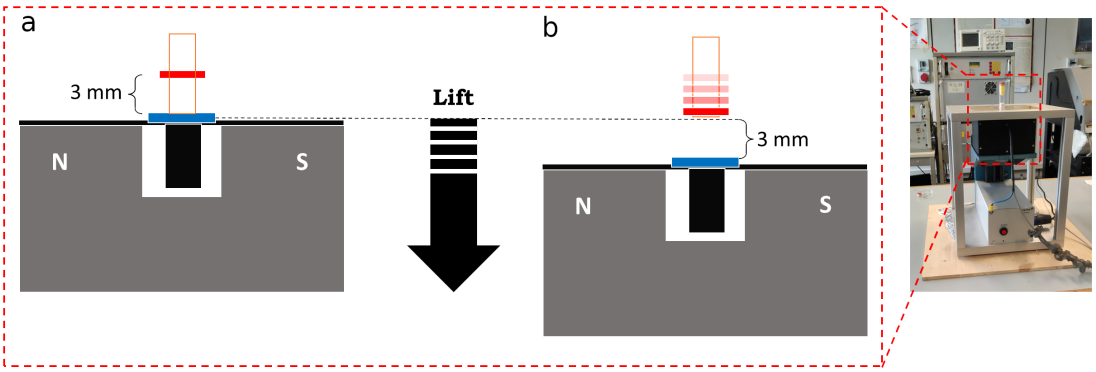

Figure 3.3: *A sketch of the functioning of the MOUSE apparatus to obtain NMR signal profiles at different depths inside the sample. By mechanically moving the probe system by the lift, the sensitive volume (red region) is stepped through the sample and the CPMG sequence is then applied at each position. (a) initial profile condition: maximum penetration depth of about* 3100 μm *from the plate (dashed black line). (b) final profile condition: the system went down through various steps and the sensitive volume is slightly above the plate at about* 0 μm *of depth. Dimensions are not in scale: the sample height is about* 10 mm *and also the distance between the magnet and the sensitive volume is always* 10 mm*, as explained in Section 3.2.*

in addition to that obtained by addition of the independent experiments separated by the T_1 recovery period, RT [24]. So, the *CPMG* pulse sequence is used either to measure effective T_2 or as the detection period of different sequences to increase the *SNR* by co-adding the complete echo train. The latter approach will be used in all the *NMR* pulse sequences of this work.

3.3.2 *CPMG* profile sequence

The *NMR* profile sequence runs a *CPMG* sequence and controls the position of the *MOUSE* to scan profiles. As explained, the sensor excites the sensitive volume at a fixed distance from the magnet surface. By mechanically moving the sensor by the lift (Fig. 3.1b), the sensitive volume is stepped through the sample and the *CPMG* sequence is then applied at each position. Figure 3.3 shows a sketch of the functioning of the apparatus to obtain signal profiles at different depths inside the samples. A set of parameters defines the range and step for scanning the object. The zero in position is set at the surface of the plate and the profiles are measured starting inside the object and going down in position. To cover the desired range an initial position is defined (the maximum value is defined by the chosen spacer configuration, 8 mm

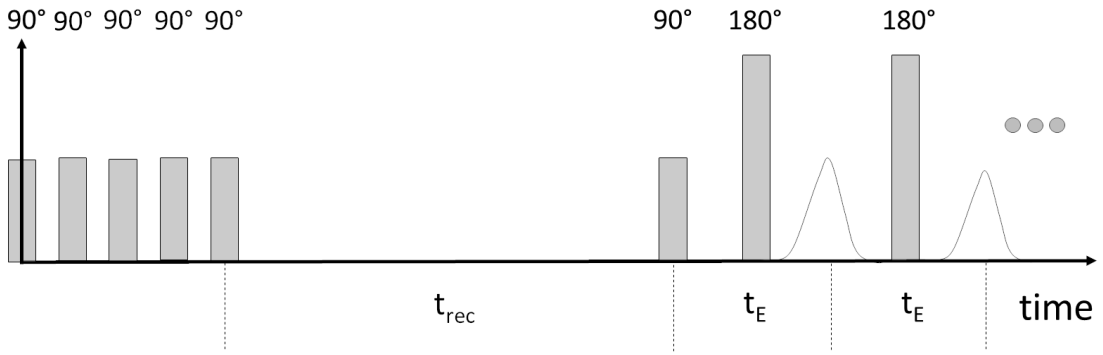

Figure 3.4: *A schematic diagram of a SR experiment to measure T_1 relaxation. A series of five saturation pulses are separated from a CPMG detection by the recovery time t_{rec}. Experiments with different recovery times are carried out to follow the recovery of the Magnetization.*

setup in this case, as explained in Section 3.2) and a step in position is given together with the number of points in the profile. As a reference position the system uses an optical sensor set on the plate. Each time a profile is measured the sensor is moved up to this position and then down to the initial position in the profile.

3.3.3 *SR* sequence

The Saturation Recovery (*SR*) is a standard pulse sequence to measure the longitudinal relaxation time T_1. In this case it is combined with a *CPMG*-train used in the detection period to increase the sensitivity:

$$\left[\left(90\right)_m - t_{rec} - 90_x - \left(\frac{t_E}{2} - 180_y - \frac{t_E}{2} - Echo\ acq\right)_n - RT\right] \tag{3.19}$$

where t_{rec} is the recovery time and m (equal to five in this case) is the number of 90° pulses sent at the beginning of the sequence, during the so called saturation period. These five saturation pulses are applied to destroy the z-Magnetization, M_z (more than one 90° pulse is applied because of the B_1 inhomogeneity) [33]. Then, after a recovering period, t_{rec}, a single 90° pulse is applied. As explained before, since the *FID* cannot be used, an echo must be generated. So, a *CPMG* train for detecting M_z at the end of the recovering period is used. Figure 3.4 shows a schematic representation of the *SR* pulse sequence just described.

During the recovery period the Magnetization is built up again with the characteristic time T_1. Experiments with different recovery times t_{rec} are carried out to

follow the recovery of the Magnetization and then build the full recovery curve that is given by:

$$M_z\left(t_{rec}\right) = M_0\left(1 - e^{-\frac{t_{rec}}{T_1}}\right) \tag{3.20}$$

where M_0 is the magnitude of the equilibrium Magnetization along the z-axis and $M(t_{rec})$ is the value at time t_{rec} after the initial string of saturation pulses. Equation (3.20) has been derived by the deletion of the first term of Equation (3.5), considering that M_z value is zero at time t_{rec} equal to zero.

3.3.4 *SSE* sequence

The Stimulated Spin Echo (*SSE*) pulse sequence can encode the effect of molecular diffusion through the amplitudes of stimulated echoes. The *NMR-MOUSE* takes advantage of the highly uniform and strong gradient generated to measure the self-diffusion coefficient D of molecules with high accuracy and in very short times. The sensitivity of these measurements is improved by applying a *CPMG* pulse sequence after the diffusion-encoding period:

$$\left[90_x - \delta - 90_x - \Delta - 90_x - \delta - Echo\ acq - \left(\frac{t_E}{2} - 180_y - \frac{t_E}{2} - Echo\ acq\right)_n - RT\right] \tag{3.21}$$

where δ is the encoding time and Δ is the diffusion time. The approach of this sequence is to monitor the transverse magnetization at a later time to see how far the molecules containing the *NMR* nuclei have moved [24]. A single 90° pulse applied after the encoding time δ has the effect of rotating the y-component of Magnetization into longitudinal polarization along the z-axis, a state in which only T_1 relaxation will occur. Of course any x-Magnetization will be unaffected so that only half the transverse Magnetization can be stored in this way. Recall is made after the diffusion period Δ using another 90° pulse. This leads to an echo (i.e. the Stimulated Echo) at time δ after this last RF pulse, before the application of the *CPMG* pulses. It should be noted that the *SSE* pulse sequence also generates two additional spin echoes. These are, respectively, the echo of the initial pulse *FID* caused by the second pulse, and the echo of the second pulse *FID* caused by the third pulse. Special care is needed to avoid interference between the Stimulated Echo and the two spin echoes. Figure 3.5 shows a schematic representation of the *SSE* pulse sequence just described.

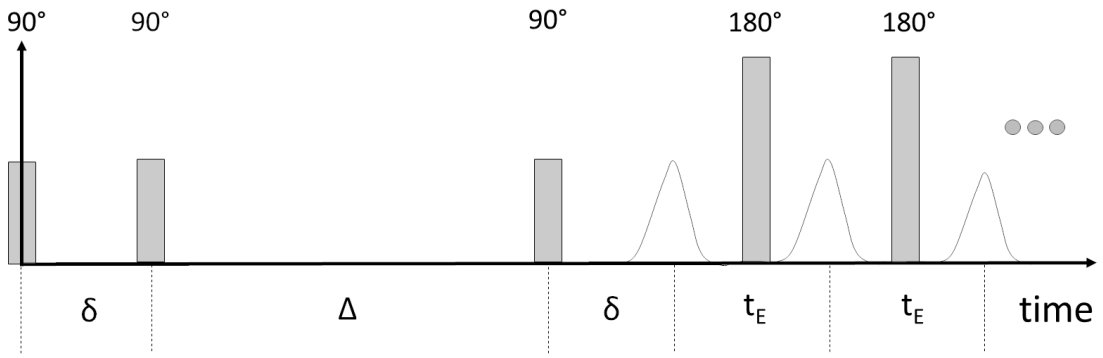

Figure 3.5: *A schematic diagram of a SSE experiment to obtain the diffusion coefficient D. The three 90° pulses are separated by the encoding time δ and the diffusion time Δ. A Stimulated Echo (first peak from the left) is created just before the CPMG detection. Experiments with different encoding times, keeping a constant diffusion time, are carried out.*

In general, the measurement of D as a function of the diffusion time Δ offers the possibility to probe different length scales of restriction (see Equation 3.13). In this case a constant value of Δ equal to $1\,ms$ was considered and only δ value was varied during experiments in order to obtain the diffusion coefficient D following this formula:

$$\ln \frac{S}{S_0} = -\gamma^2 \cdot g^2 \cdot D \cdot \delta^2 \cdot \left(\Delta + \frac{2}{3} \cdot \delta\right) \tag{3.22}$$

where S is the measured signal, S_0 is the observed signal immediately after the 90° pulse, γ is the gyromagnetic ratio and g is the magnetic field gradient. Equation (3.22) has been derived by Equation (3.12) only considering the signal attenuation due to the diffusion effect, neglecting the attenuation due to T_2 relaxation.

3.3.5 *DQ* sequence

The Double-Quantum (DQ) build-up pulse sequence can explore the Double-Quantum coherence in a dipolar-coupled system and measure ^1H residual dipolar couplings, that are correlated with the cross-link density, as explained in Section 3.1.3. Also in this case the sequence is combined with a *CPMG* sequence used in the detection

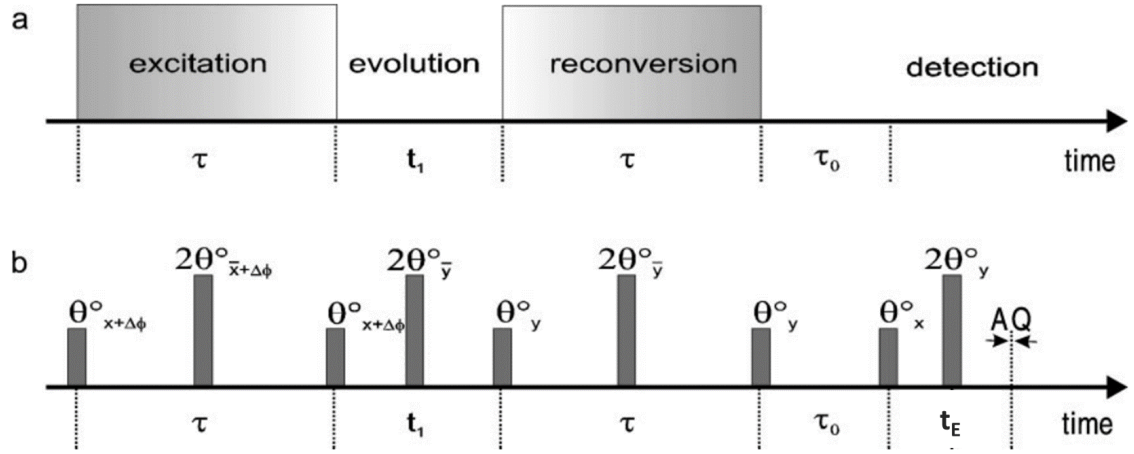

Figure 3.6: *A schematic diagram of a DQ build-up experiment taken from [34]. (a) General scheme for filtering NMR signals according to dipolar encoded Multi-Quantum coherences. Fixed evolution and filter times (t_1 and τ_0) and variable excitation/reconversion time τ are considered before the CPMG detection. (b) Pulses and timing of the DQ sequence that has been implemented on the occasion of this work ($\theta = 90°$).*

period to increase the sensitivity:

$$\left[90_{x+\Delta\phi} - \frac{\tau}{2} - 180_{-x+\Delta\phi} - \frac{\tau}{2} - 90_{x+\Delta\phi} - \frac{t_1}{2} - 180_{-y} - \frac{t_1}{2} - 90_y - \frac{\tau}{2} - 180_{-y} - \frac{\tau}{2} - \right.$$
$$\left. - 90_y - \tau_0 - 90_x - \left(\frac{t_E}{2} - 180_y - \frac{t_E}{2} - Echo\ acq\right)_n - RT\right] \quad (3.23)$$

where τ is the conversion time, t_1 is the evolution time, τ_0 is the filter time, t_E is the echo time, $\Delta\phi = 0°, 90°, 180°, 270°$ is the phase shift that changes value at each experiment (the experiment is repeated four times). There are several ways to perform a *DQ* build-up pulse sequence using the *NMR-MOUSE* device. The one reported by Wiesmath et al. in [34], that is the same of Blumich et al. in [27], was chosen (Fig. 3.6). Also the ones in [30] and [28] were tried, but excluded because of the worst results. Since the *DQ* pulse sequence did not exist in the Prospa software (unlike *CPMG*, *SR* and *SSE*), it has been implemented on the occasion of this work following the literature details and using the same Prospa *MATLAB*-like language of the other three pulse sequences.

The *DQ* sequence starts with the spin system in thermodynamic equilibrium. Then, three pulses are applied in a time τ that excite the coherent motion of a

magnetically coupled spin pair. After this excitation period, let the system evolve for an evolution time t_1. A 180° pulse midway during this time compensates for the effects of field inhomogeneity on this motion. The Double-Quantum coherence is then converted into longitudinal Magnetization by another series of three pulses during a reconversion period τ. Then, after waiting for a filter time τ_0, a *CPMG* pulse sequence is performed for the *NMR* signal detection. As suggested in [34], the experiment can be repeated for different values of τ to obtain the Double-Quantum build-up curve and extract the value of residual dipole-dipole coupling ω_D by fitting the initial part of experimental data (for short τ, smaller than $500\,\mu s$) to the quadratic function in Equation (3.14). Since the cited literature works are related to studies on elastomers, two different types of rubber were used in the preliminary DQ measures of this work. Unfortunately, is has not been possible to replicate these literature results for short τ probably because of the high sensitivity of the sequence parameters to the elastomer type and the experimental conditions. However, interesting results have been obtained trying to increase the conversion time τ up to $4000\,\mu s$. In Figure 3.7 the DQ *NMR* Signal magnitude trend as a function of τ for the two different rubbers is shown. Rubber 1 (red line) presents lower absolute signal values than rubber 2 (black line). Considering Equations (3.14) and (3.15), this difference can be related to a different value of the residual dipole-dipole coupling ω_D between the two rubbers. Another very important difference is the slope of the two lines: Rubber 1 has a less rapid increase than Rubber 2. This behaviour was also confirmed by using higher τ values. This means that probably also these slopes are indicators of the ω_D values because the experimental conditions for the two rubbers were equal: same room temperature and same DQ sequence parameters, so the difference can be only related to the composition and structure of the two rubbers.

Following the previous considerations, the behaviour of the DQ build-up pulse sequence for long τ was explored. As was seen in Section 3.1.3, literature simulations results on elastomers confirm that for sufficiently long τ the DQ signal reaches a saturation maximum, after an initial increase. This increase rate before saturation (i.e. the slope in Fig. 3.7) can be considered as an indicator of the cross-links density (ω_D) of the material under study.

Since the cartilage tissue structure is characterized by a collagen cross-links network (Section 1.1), the DQ pulse sequence was performed also on the sample cartilage layer. Even if Equation (3.15) is strictly related to elastomers, a simulation of it was performed with the *MATLAB* software. It was adapted to the cartilage tissue by

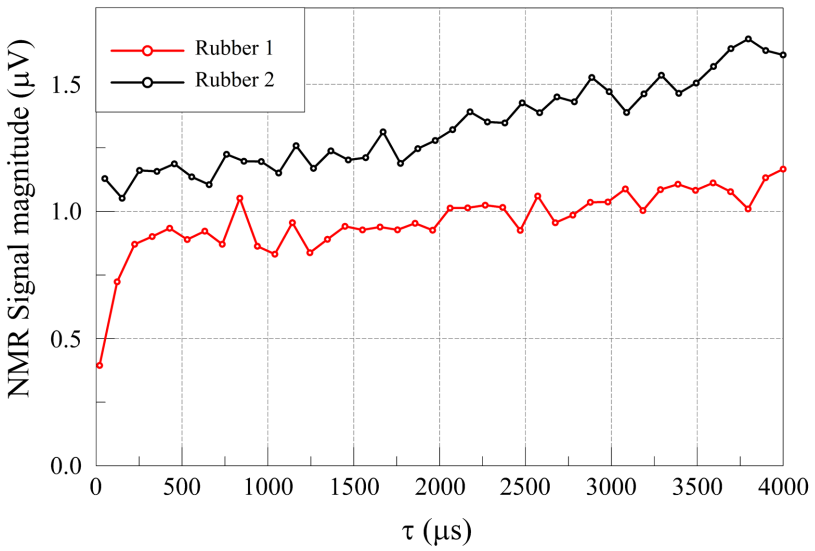

Figure 3.7: *Double-Quantum (DQ) build-up pulse sequence results on rubber samples: NMR Signal magnitude trend as a function of the conversion time τ. Two different types of rubber, Rubber 1 (red line) and Rubber 2 (black line), are investigated.*

exploring lower ω_D values and much higher τ values. The overall signal trend was confirmed and the *DQ* build-up pulse sequence in the long τ regime (hundreds of *ms*) was used for this work.

3.4 The automatized procedure

The *NMR* pulses sequences just described in the last Section have been collected in a unique procedure using the *NMR-MOUSE* device (Section 3.2). This procedure is divided in two main consequent steps: the profile analysis and the three-layer analysis, which are depicted respectively in left and right parts of the Figure 3.8.

The profile analysis is intended to indicate the depth and thickness of the three anatomical cartilage layers (see Section 1.1) of the sample. First of all, before *NMR* acquisitions, each sample was first thawed for about 20 minutes inside the *PBS* solution. After that, the sample was inserted in the *Teflon* experimental setup above the *NMR-MOUSE* device (see Section 2.2). Then, a *CPMG* profile pulse sequence (Section 3.3.2) was performed in about half an hour using profile steps of $50\,\mu m$. The acquired signal related to each *CPMG* was processed by a *MATLAB* script to obtain the Nuclear Magnetization amplitude $M_{x,y}$ at time $t = 0$ and the transverse

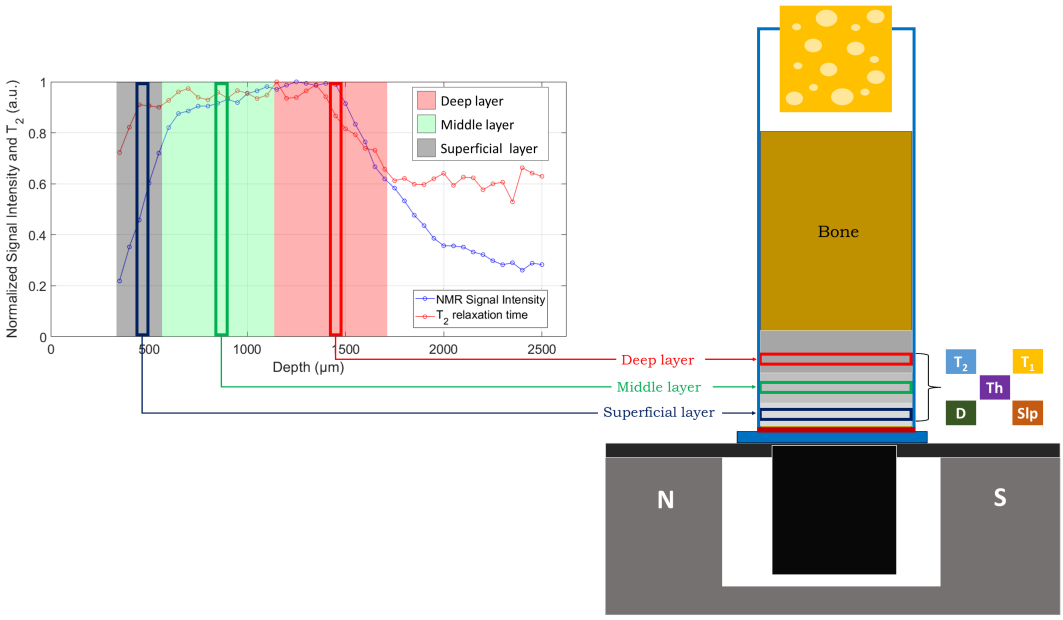

Figure 3.8: *A sketch of the automatized procedure steps: (left) the profile analysis and (right) the three-layer analysis. The first is intended to indicate the depths and thicknesses (Th) of the superficial (black), middle (green) and deep (red) cartilage layers of the sample. The second uses the information collected in the first to place the sensitive volume of the NMR-MOUSE in each cartilage layer performing CPMG, SR, SSE and DQ pulse sequences. From acquired data it is possible to obtain T_2, T_1, D and Slp values related to each layer, as it will be explained in Chapter 4.*

relaxation time T_2. The *fitnlm* function was used to perform an exponential fit of the data following Equation (3.7). So, $M_{x,y}$ and T_2 values along the entire sample profile were obtained. By normalizing $M_{x,y}$ and T_2 profiles by their maximum values and by representing them in the same plot (see Fig. 3.8), a method to identify the three cartilage layers was determined. In Chapter 6 this method will be described in detail and the profile analysis goodness will be verified. Following the just mentioned method, the superficial, middle and deep cartilage layers (black, green and red in Fig. 3.8) were identified. Then, approximately in the center of each of these layers, a depth value was established following a precise criterion (see Section 6.1). These three depth values were used as input of the three-layer analysis.

The three-layer analysis, that will be validated in Section 6.2, uses the three depth values collected in the profile analysis to place the sensitive volume of the *NMR-MOUSE* in each of these depths performing four different *NMR* pulse sequences. The Prospa software (Section 3.2) already contains a functionality that

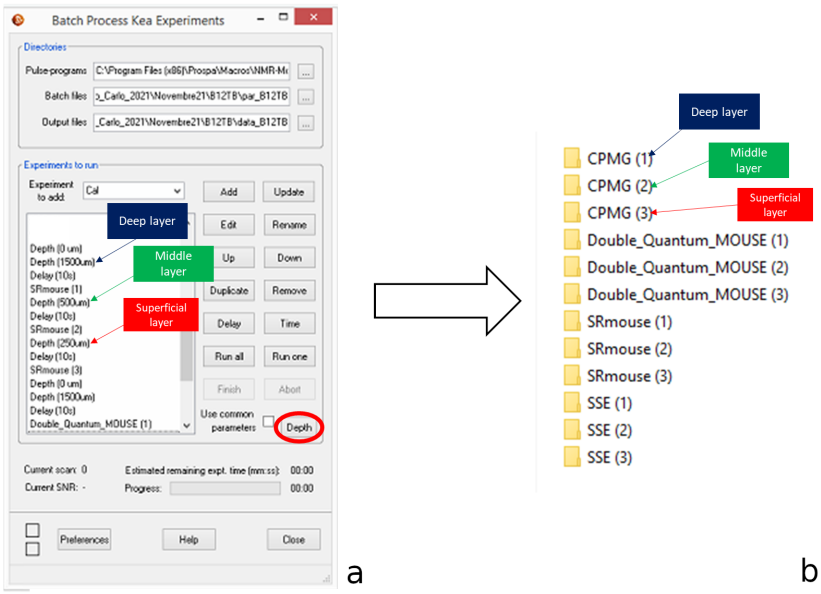

Figure 3.9: *(a) Prospa Kea Batch Process interface with the implementation of the Depth function button (red circle). The Kea Batch Process takes as input the NMR pulse sequences codes and their parameters files. (b) The output of the Process: 12 folders, each containing the acquired data of a certain NMR pulse sequence in a certain cartilage layer.*

allows to automatically perform different pulse sequences separated from each other by a certain delay. This is the so called *Kea Batch Process*. It takes as input only the *NMR* pulse sequences codes and their parameters files, where the parameters are specific for each sequence and they can be modified as desired. The main limitation of the *Kea Batch Process* is that the procedure is performed at the same sample depth: it is not possible to send a pulse sequence to two different depth in an automatized way. The only way is to perform the first, then move the probe through the lift using the *Service* functionality to reach another sample depth and repeat the pulse sequence for this new depth. But, since the use of the *Service* requires each time the user intervention, this can be a non-trivial problem if a huge number of measures has to be performed. Another drawback of the just mentioned approach is the possibility of mistakes made by the user during the procedure. To overcome these problems, a new function called *Depth* has been implemented inside the *Kea Batch Process*. This function can automatically move the probe to previously inserted depths. Figure 3.9a shows the Prospa *Kea Batch Process* interface, where the *Depth* button has been added (red circle).

So, at the beginning of the three-layer analysis the three depth values collected in the profile analysis are inserted in the *Kea Batch Process* through the *Depth* function. This allows to perform a procedure in which the sensitive volume of the *NMR-MOUSE* is automatically placed in each of these depths and four different *NMR* pulses sequences are automatically sent: *CPMG*, *SR*, *SSE* and *DQ* (see Section 3.3). After about 210 minutes of *NMR* measures, the final output of this automatized procedure is composed by 12 folders, each containing the acquired data of a certain pulse sequence in a certain cartilage layer, as shown in Figure 3.9b. In the next Chapter, it will be explained how T_2, T_1, D and Slp that are related to each layer are obtained from the data.

Chapter 4

Parameters acquisition and analysis

In this Chapter, the entire processing of the *NMR* data acquired with the automatized procedure is illustrated. By using a pipeline based on *UPENWin* and *MATLAB* software, T_2, T_1, D and Slp parameters are obtained for all the twenty bovine samples under study. The description of these samples' characteristics and the data analysis approach between them are reported. The statistical analysis (Kruskal-Wallis test) and the pattern recognition analysis (Principal Component Analysis, K-means, and *HDBSCAN* clustering) are briefly explained in the last Sections.

4.1 Data processing

In Section 3.4, the automatized procedure steps of profile and three-layer analyses were described. The *Kea Batch Process* final output is composed of 12 folders, each containing the acquired data (in '*.DAT*' format) of a certain pulse sequence in a certain cartilage layer (Fig. 3.9). These data are pre-processed by a script in the *MATLAB* software just before being processed by the *UPENWin* software. Then, a post-processing again with a *MATLAB* script is performed to directly obtain the T_2, T_1, D and Slp values related to each cartilage layer. These values are saved in a database that will contain information about all the samples under study. Finally, another script creates some plots for each measured sample highlighting the differences between the parameters among the three layers (some of these plots will be reported in Section 6.2). The just described pipeline will be illustrated with more details in Section 4.1.2.

4.1.1 The *UPENWin* software

The *UPENWin* software was developed in 2012 by the University of Bologna [35]. It is a software for inversion of multi-exponential decay data for Windows system based on the implementation of the *U*niform *PEN*alty (*UPEN*) inversion algorithm. This algorithm was designed by Borgia, Brown and Fantazzini in 1998 [36] to recognise the multi-exponential behaviour of the *NMR* relaxation curves (see Equations 3.7, 3.5 and 3.12). Depending on the nature of the sample under study, the relaxation assumes a proper behavior that is related to the complexity of the system. For bulk materials (e.g. water) the spins are in the same environment and the relaxation can be described by a mono-exponential function. This behavior has been observed in the cartilage tissue (Section 6.2). In some other biological tissues, like the trabecular bone (results not reported), the relaxation behavior is represented by a bi-exponential function. Generalizing for more than two components, the *NMR* signal can be modeled as a sum of a finite number of exponential functions with their amplitudes and relaxation time constants. Then, if a continuous distribution of relaxation times is considered, the *NMR* signal as function of time $S(t)$ can be written as follows [33]:

$$S(t) = \int p\big(T_{1,2}\big) \cdot e^{-\frac{t}{T_{1,2}}} \, dT_{1,2} + \epsilon(t) \tag{4.1}$$

where $T_{1,2}$ are the relaxation times, $p\left(T_{1,2}\right)$ is the relaxation time probability distribution function (i.e. the signal density function) and $\epsilon(t)$ is the experimental noise. From a theoretical point of view a mathematical operation, called Inverse Laplace Transform, can invert from the measured time scale t to the one of the relaxation times $T_{1,2}$ obtaining the signal density function $p\left(T_{1,2}\right)$. But in real conditions $S(t)$ has not an analytical expression: it is given by experimental discrete points affected by noise. So, the $\epsilon(t)$ term in Equation (4.1) makes the mathematical problem is known to be ill-posed (i.e. an infinite number of $p\left(T_{1,2}\right)$ exists). However, a unique solution can be found computing the so-called quasi-continuous distribution of relaxation times.

In the usual inversion algorithms a target function has to be minimized and a fixed smoothing coefficient is used to avoid the formation of isolated peaks in the distribution, that doesn't represent the real system. The *UPEN* algorithm introduced negative feedback in the smoothing of the computed distributions of relaxation times to maintain roughly the same smoothing penalty for each computed point in a dis-

tribution. Instead of using a uniform smoothing coefficient, the coefficient is varied with relaxation time to keep the smoothing penalty roughly uniform. This allows appropriate smoothing of both sharp peaks and broad features in the same distribution, allowing the sharp peaks without breaking broad features into multiple peaks not required by the data.

The *UPEN* inversion of the data made by *UPENWin* software requires first the so-called data windowing (T_2 or T_1 filter buttons) that is an average of the points, from the 16° point, in a increasing way (average of 2, 4, 8, ..., 100 data points). In this way, the noise and the numerosity of the dataset are reduced. After filtering the data, there are some inversion parameters to set: β_0 and *ND* are among the most relevant. The first is the smoothing coefficient, usually equal to 1 that is its default value. By increasing β_0, under-smoothing is obtained: there is the tendency to create peaks. On the other side, if a value between 0 and 1 is used, over-smoothing occurs and the distribution is more "softened". The second parameter, *ND*, is the number of data points that are rejected from the analysis. Usually, only the first point was rejected because an anomalous increase of the signal from the first to the second acquired point was observed (probably due to device or pulse sequence experimental limits), while an attenuation phenomenon would be expected. After the parameters setting, the *UPEN* inversion can be performed. Two output files are created: a *.DAT* file, which contains data columns and the fit of the data, and a *.TST* file, which contains all acquisition parameters. In the *.DAT* file the most relevant columns are T and Sig-Np, which correspond to the reconstructed relaxation axis ($T_{1,2}$) and to the signal density ($p\left(T_{1,2}\right)$), respectively. Some plots of these two quantities will be reported in Section 6.2. Another two important columns are SigT and Sig, which correspond to the "effective" time (echo time) and acquired signal after the data windowing (T_2 or T_1 filter), but before the *UPEN* inversion. In the *.TST* file the most relevant information are the geometric-mean relaxation time and the amplitude of the Nuclear Magnetization vector ($\boldsymbol{M}$) at zero time (see Section 5.1).

4.1.2 The *MATLAB* software pipeline

As mentioned before, the automatized procedure final output is composed by 12 folders, each containing the *CPMG*, *SR*, *SSE* and *DQ* acquired data for the three cartilage layers (Fig. 3.9). *CPMG* data file contains 2000 echo measures taken at regular intervals of $50\,\mu s$, that is the echo time t_E. *SR* data file has 48 signal

measures correspondent to 48 different t_{rec} values, ranging from 0 to 2500 ms. Also *SSE* data file contains 48 different δ values, ranging from 0.055 to 0.3 ms, and their correspondent signal measures. Finally, the *DQ* data file has 5 signal points related to 5 different τ values between 6 and 500 ms (more details about pulse sequences parameters have been illustrated in Section 3.3). All these data are pre-processed by a script in the *MATLAB* software that takes each file and converts the unit of measurement of the time column in milliseconds. This is because the *UPENWin* software wants time data expressed in milliseconds as input. Then, the new data files, except for the *DQ* file, are processed by the *UPENWin* software: a filter and a *UPEN* inversion are performed for each file (see Section 4.1.1).

After that, a post-processing procedure is done through another *MATLAB* script. In order to obtain the T_2, T_1, D and *Slp* values, the *NMR* theory is followed. Equations (3.7), (3.20) and (3.22) are used as model in the *fitnlm* MATLAB function that can fit nonlinear regression models. Figure 4.1 shows an example of the results of the four *NMR* pulses sequences data fit. *fitnlm* estimates model coefficients using an iterative procedure starting from provided initial values. As regards T_2 and T_1 (Fig. 4.1a and b), two *UPENWin* outputs are used for data fit: SigT and Sig, which correspond to the time and acquired signal after the data windowing (see Section 4.1.1). By using two exponential model functions of the type of Equations (3.7) and (3.20), four model coefficients (T_2, $M_{x,y}(0)$, T_1 and M_0) with their standard error are estimated by *fitnlm*. As regards D and *Slp* (Fig. 4.1c and d), pre-processed data files are used, even before the *UPENWin* windowing. Two linear model functions of the type of Equation (3.22) (that is linear in D) are considered. As seen in Section 3.1.3, there is not a unique model related to *DQ* data for long τ. Equation (3.15) is only referred to elastomers, so there should reasonably be some differences for the cartilage. Since no one in the literature has so far tried the *DQ* pulse sequence on the cartilage and having observed a roughly linear trend for τ values up to 500 ms, a simple linear model function is used for the data fit. By using these two linear model functions, four model coefficients (D, *Slp* and Signal amplitudes at zero time, i.e. fit intercepts) with their standard error are estimated by *fitnlm*. All the derived model coefficients and also the *UPEN* inversion outputs are automatically saved in a database that will contain information about all the samples under study. Finally, by using T and Sig-Np vectors, another script creates some distributions plots for each measured sample highlighting the differences between the parameters among the three layers (for *DQ* plots, linear fit are directly depicted, see Section 6.2).

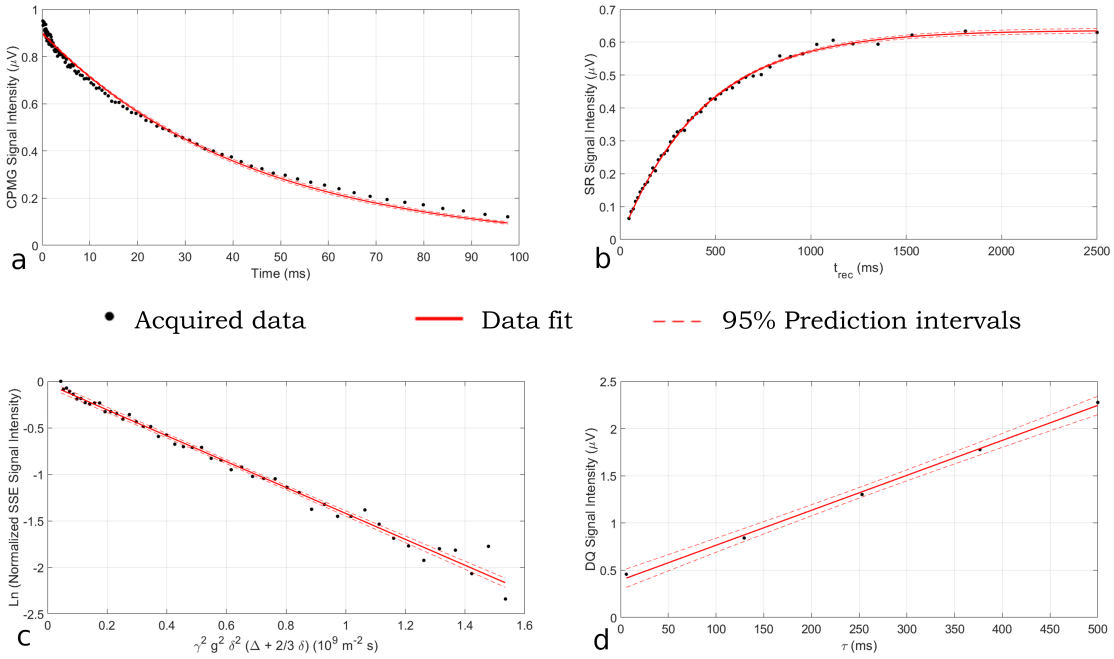

Figure 4.1: *Results of (a) CPMG, (b) SR, (c) SSE and (d) DQ pulse sequences performed on the deep cartilage layer of B20FA sample (cored from lateral bovine femoral condyle, see Section 4.2). Black points represent acquired data: in the CPMG and SR cases an additional UPENWin windowing is done to reduce the noise. The error on acquired data points is given by the instrumental uncertainty that can be roughly estimated through the Signal-to-Noise Ratio of the measure. This latter depends on the square root of the number of scans performed for each measure: 128 for CPMG and DQ, 16 for SSE and 8 for SR sequences. Red continuous lines are the data fits performed by fitnlm MATLAB function. Exponential model functions are used for (a) and (b) data, while in (c) and (d) linear functions are preferred. Red dashed lines are the 95% prediction intervals computed by predict MATLAB function that predicts confidence bounds for the fitted mean values of the fitnlm nonlinear regression model. Model coefficients like T_2, T_1, D and Slp with their standard error are estimated.*

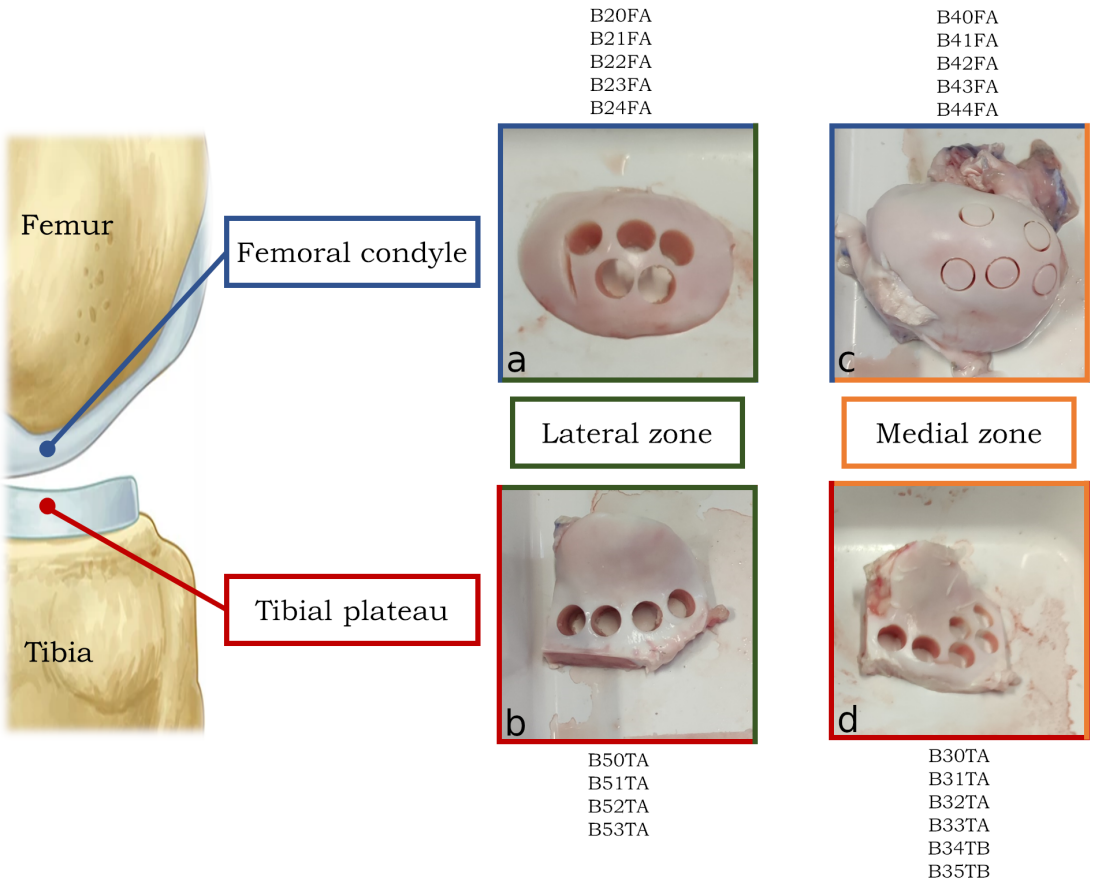

Figure 4.2: *Four different bovine knee joint pieces from which the twenty samples have been cored. (a) 5 samples from lateral femoral condyle, (b) 4 samples from lateral tibial plateau, (c) 5 samples from medial femoral condyle and (d) 6 samples from medial tibial plateau. The names of the twenty samples are reported above and below the four boxes.*

4.2 The samples

Twenty bovine samples were studied using the already illustrated *NMR* automatized procedure and data processing approaches. These samples have been cored in the Laboratory of Medical Technology of the Rizzoli Orthopedic Institute and they came from the same bovine knee joint. Through knee boning and sawing, four different bovine pieces were obtained: two tibial plateaus and two femoral condyles from lateral and medial zones (see Section 1.2). The coring procedure of the bovine knee joint and the treatment of the samples from coring to *NMR* tests have already been explained in Section 2.1. The characteristics of the twenty samples are summarized

in Figure 4.2. There are 5 samples from the lateral femur, 5 from the medial femur, 4 from the lateral tibia, and 6 from the medial tibia. These different numbers are the consequence of the different curvatures of cartilage surface among the bovine pieces. Since it is essential to obtain samples with cartilage layers perpendicular to the core axis (see Section 2.1), the coring positions in each bovine piece behave differently.

4.3 Data analysis

In Section 4.1 it has been seen how to obtain T_2, T_1, D, and Slp parameters and save them in a database that contains information about all the samples. The *NMR* automatized procedure has been performed on twenty bovine samples. The final database contains three values of each parameter for each sample, i.e. one for each cartilage layer, reaching a total of sixty values. Considering this database, statistical and pattern recognition data analyses were performed using Kruskal-Wallis test (KW), Principal Component Analysis (PCA), K-means and *HDBSCAN* clustering, which are briefly explained below.

4.3.1 Kruskal-Wallis test

A common problem in statistical analysis is to decide whether several samples should be regarded as coming from the same population. Since usually, the samples differ, the question is whether these differences are among the populations or are merely related to the chance variations to be expected among random samples from the same population. When this problem arises one may assume that the populations are approximate of the same form, in the sense that if they differ it is by a shift or translation. The usual technique for attacking such a problem is the analysis of variance ($ANOVA$) that is used to test the equality of more than two population means, considering them all equal to each other as the null hypothesis. The $ANOVA$ test requires some assumptions including that the data have to be normally distributed and that the population variances have to be equal [37]. So, when the populations are not normally distributed or do not have equal variances, the use of this test may yield inaccurate estimates of the p-value (i.e. the probability, under the assumption of the null hypothesis, of obtaining a result equal to or more extreme than what is observed).

The Kruskal-Wallis test (KW) has been introduced in 1952 by Kruskal and Wallis

[38] as a nonparametric alternative to the one-way *ANOVA* test. *KW* does not make normality assumptions and instead of comparing population means, it compares population mean ranks of the measurement observations (i.e. medians). The null hypothesis of the *KW* test states that the samples are from identical populations (i.e. the population medians are equal). The only assumptions of this method are that the observations come from populations having the same continuous distribution and that they are mutually independent [39]. The *KW* test starts by substituting the rank in the overall data set for each measurement value. The smallest value gets a rank of 1, the second smallest gets a rank of 2, etc, up to N. The sum of the ranks R_i is calculated for each group i ($i = 1, 2, ..., C$) of size n_i (i.e. the number of observations in the i^{th} group), then the test statistic H is computed [38]:

$$H = \frac{12}{N(N+1)} \sum_{i=1}^{C} \frac{R_i^2}{n_i} - 3(N+1) \tag{4.2}$$

where $N = \sum_{i=1}^{C} n_i$ is the number of observations in all groups combined. Equation (4.2) represents the variance of the ranks among groups: large values of H lead to rejection of the null hypothesis. H is approximately χ^2 distributed (with the degrees of freedom equal to the number of groups C minus 1), so the p-value measures the significance of the chi-square statistic.

When the Kruskal-Wallis test leads to significant results, then at least one of the groups is different from the other groups. The test does not identify where the differences occur or how many differences occur. Therefore, a test procedure for making pair-wise comparisons is needed. There is to consider that the probability of committing false statistical inferences would considerably increase when more than one hypothesis is simultaneously tested (namely the multiple comparisons), which therefore requires proper adjustment [40]. Bonferroni adjustment is one of the most commonly used approaches for multiple comparisons. This method computes the adjusted p-values by directly multiplying the number of simultaneously tested hypotheses. Bonferroni adjustment has been well acknowledged to be much conservative and it considers the populations as independent of each other. Another method is the False Discovery Rate (*FDR*) correction, which instead considers a dependence between populations and it estimates the positive false discovery rate for each p-value.

The Kruskal-Wallis test has been performed using the *kruskalwallis* MATLAB function and in the case of multiple comparisons, the *multcompare* and *mafdr* func-

tions (from Statistics and Machine Learning Toolbox) have been subsequently used with the proper adjustment method.

4.3.2 Principal Component Analysis

The Principal Component Analysis (*PCA*) is the most popular and the oldest multivariate statistical technique [41]. 'Multivariate' means that there are several variables that have been measured many times. Practically, *PCA* analyzes a matrix X containing these variables n as columns and their observations p as rows. Performing *PCA* on X can lead to obtaining a first look at the structure of the data, helping the identification of outliers, delineating classes, etc. However, when the objective is classification (i.e. pattern recognition, search for the natural structure inside data) or relating one set of variables to another, other ways are more efficient for these problems [42], as will be seen in the next Section. The idea of *PCA* is to transform the dataset of correlated variables into uncorrelated components through linear combinations of the original variables. This is practically done through a spectral decomposition of the matrix $\Sigma = X \cdot X^T$, i.e. the covariance matrix computed between the original variables. It can be easily proven that the diagonalization of Σ corresponds to a rotation in n dimension in the space of the original variables. In this way, the initial variables data space is transformed into a new space in which each new variable will be a linear combination of all the original variables. The eigenvectors of the new space are called Principal Components or also loadings because they contain the contribution (i.e the 'load') of the original variables. The eigenvalues correspond to the variances of the new variables. As regards the p measurements, they are transformed in the so-called scores, which are projections of the original data onto new axes.

Loadings, eigenvalues, and scores can help to understand and visualize *PCA* results. Two possible plots can be performed: the loading and the score plots. The first is a scatter plot of loadings vectors (one point in the plot for each variable) and it helps to understand the relation between original variables and the newly transformed space. The second is a scatter plot of score vector components (one point in the plot for each sample) and it characterizes the sample space structure. This last type of plot will be used in this work choosing a subset of two Principal Components for data visualization, plotting the new data in two dimensions. These new data are the projection of the original data onto these two components. The components are ordered by the amount of variance (i.e. eigenvalues) they account

for. The first component accounts for the largest possible variation. The second component accounts for the largest possible variance of the remaining variation (the variation not captured by component one), and so on. Most of the variation is captured within the first few principal components, as can be verified directly by looking at eigenvalues (see Section 7.1), making *PCA* a suitable method for reducing the dimensionality of data [41].

The Principal Component Analysis has been performed through the *pca* MATLAB function.

4.3.3 K-means and *HDBSCAN* clustering algorithms

A basic pattern recognition analysis was also performed through K-means and *HDBSCAN* clustering algorithms to search for the natural structure inside the data and to classify similar data items into clusters. K-means belongs to partitional clustering techniques, while *HDBSCAN* is a hierarchical clustering technique [43].

The K-means algorithm is based on a very simple idea to find K clusters between data: starting with K centroids (initial values for the centroids are randomly selected or derived from a priori information), each pattern in the data set is assigned to the closest cluster (i.e. closest centroid). So, distances between samples and centroids are calculated and each sample is assigned to a centroid based on minimum distance (i.e. minimizing the intra-cluster distance). Then, the centroids are recalculated according to an average of the associated patterns. This process is iteratively repeated until no changes occur. The K-means algorithm has the great advantage of being easy to implement, but it can also be really slow for large data set since in each step the sample distance has to be calculated. Another drawback is that this method is really sensitive to the provided initial clusters.

As has just been explained, partitional clustering algorithms (e.g. K-means) divide the data set into a specified number of clusters trying to minimize certain criteria (e.g. the distance) and they can therefore be treated as optimization problems. Hierarchical clustering algorithms, on the other hand, generate the so-called cluster tree (or dendrogram) by using heuristic splitting or merging techniques (i.e. divisive or agglomerative algorithms). Divisive algorithms start with all the patterns assigned to a single cluster. Then, splitting is applied to a cluster in each stage until each cluster consists of one pattern. Contrary to divisive algorithms, agglomerative algorithms start with each pattern assigned to one cluster. Then, the two most similar clusters are merged. This step is repeated until all the patterns are assigned to

a single cluster. *HDBSCAN* belongs to the latter category of hierarchical clustering algorithms. The idea is to generate a complete density-based clustering hierarchy from which a simplified hierarchy composed only of the most significant clusters can be easily extracted [44]. This is done by following some steps. First of all, the space is transformed according to the density/sparsity of the data by defining a new distance metric between points, the so-called mutual reachability distance. Under this metric dense points remain the same distance from each other but sparser points are pushed away. Then, a minimum spanning tree based on mutual reachability distance values is constructed. Given the minimum spanning tree, the next steps are to convert that into the hierarchy of connected components and to condense them (i.e. agglomerate), based on the minimum cluster size parameter that is provided at the beginning. Finally, there is the extraction of the stable clusters from the condensed tree.

The K-means clustering has been performed through the *kmeans* MATLAB function, while *HDBSCAN* clustering was implemented through the *HDBSCAN()* Python function from the *hdbscan* library [45].

Results and discussion

Chapter 5

Degradation tests

In this Chapter, the most significant results of several degradation tests in three experimental setups (see Section 2.2) are illustrated. Degradation is the exposition at room temperature of the sample in which it is subjected to dehydration with a consequent structural change. As explained in Section 2.2, parameters stability was conditioned by degradation of the cartilage tissue. Degradation test means the study of a certain *NMR* parameter trend during the time which starts immediately after the sample thawing (usually tens of hours were tested). These initial tests aimed to determine the changes during time of *NMR* parameters that would later be used in the final automatized procedure (T_2, T_1, D and Slp, see Section 4.1).

The results of the degradation test allowed the optimization of the automatized procedure by:

- definition of the best experimental setup to preserve the sample during measurements;
- determination of *NMR* pulses sequences timing and the maximum duration of the procedure.

5.1 Signal Intensity and T_2 degradation tests

The sensitive volume of the *NMR-MOUSE* was placed inside the sample cartilage layer (usually about $1000\,\mu m$ from the cartilage surface, depending on sample cartilage layer thickness) and performed the same *NMR* sequence repeatedly over time. The first was the *CPMG* sequence (Section 3.3.1). Each *CPMG* took about 30 minutes, so two of them have been acquired each hour for tens of hours. Then the signal

of each *CPMG* was processed by *UPENWin* software (Section 4.1.1). As output, for each *CPMG* the T_2 distribution, its geometric-mean relaxation time T_2 and the amplitude of the Nuclear Magnetization at $t = 0$ (i.e. the signal intensity) were obtained. The trend during time of the latter is represented in Fig. 5.1 for the three experimental setups. Considering the first hours *NMR* signal intensity with *Sponge* setup shows a decrease during time (Fig. 5.1a). While with *Teflon* setup (that in addition to the sponge contains some layers of Teflon, see Fig. 2.2) and *PBS* setup the trend remains more constant (Fig. 5.1c and b). In Section 2.2 it has been seen that the *Sponge* setup makes the sample particularly exposed to water molecules evaporation. This fact can be considered as the main cause of the signal intensity decrease because this quantity is closely related to the number of water molecules in the sample. The initial constant trend (i.e. up to 600 minutes) in *Teflon* setup can be attributed to the Teflon layers' presence: they insulate the sample from the external environment, considerably reducing water molecules evaporation. In *PBS* setup the sample is not affected by evaporation phenomena because it is immersed. For times bigger than about 600 minutes the signal intensity decrease starts to be evident also in *Teflon* setup, while in *PBS* setup the trend remains still constant for about 30 hours, then it starts to slowly increase. As explained, the first behavior can be attributed to sample dehydration. As regards the second, the interpretation is less obvious. One possible explanation can be that *PBS* starts to interact in some way with the sample. This hypothesis is supported by Figure 5.2a and b, which reports photos of the *PBS* setup at the beginning (a) and the end (b) of *CPMG* measures (about 60 hours later). After this long period, *PBS* solution becomes visibly more turbid compared to the beginning, a sign of the fact that *PBS* interacted with the sample. By evaluating the signal intensity values it can be also supposed that the *PBS* infiltrates in some spaces between the sample and the glass tube and it contributes to enhancing the signal only in *PBS* configuration.

In Fig. 5.3 some T_2 distributions are reported. For the first 24 hours, they are all unimodal distributions in all setups. In *Teflon* setup (Fig. 5.3c) distributions shape starts to change for times bigger than 24 hours: peaks move toward shorter relaxation times and distributions are no longer unimodal (blue and gray lines in the graph). In *Sponge* (up to 29 hours) and *PBS* setups (Fig. 5.3a and b) this phenomenon is not observed. This behavior is probably due to a structural change in the cartilage layer. The evidence of this hypothesis is shown in Figure 5.2c and d, which reports photos of the same sample immediately after thawing (c) and after 60

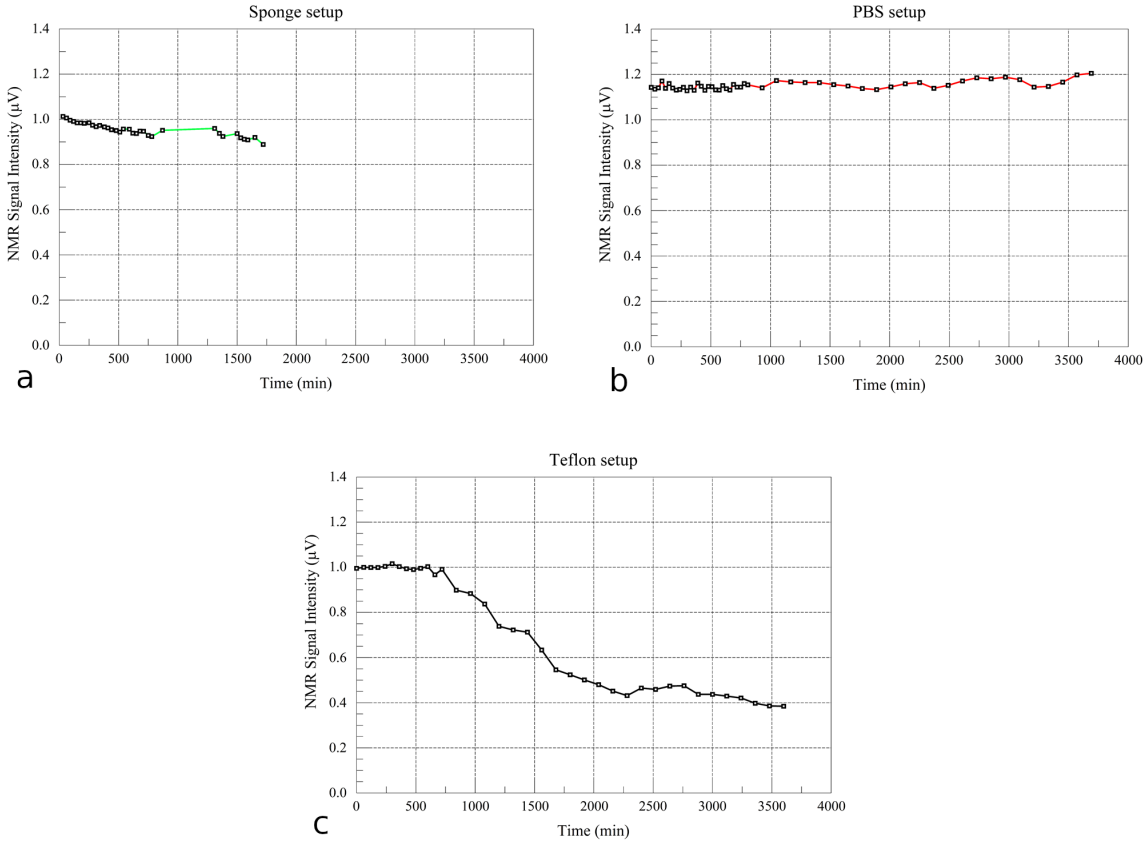

Figure 5.1: *NMR signal intensity trend during time for the three experimental setups measured with a CPMG sequence. The extrapolated signal value at $t = 0$ on the UPEN data fit was considered. (a) B40B sample results with Sponge setup; (b) B39A sample results with PBS setup; (c) B5FB sample results with Teflon setup.*

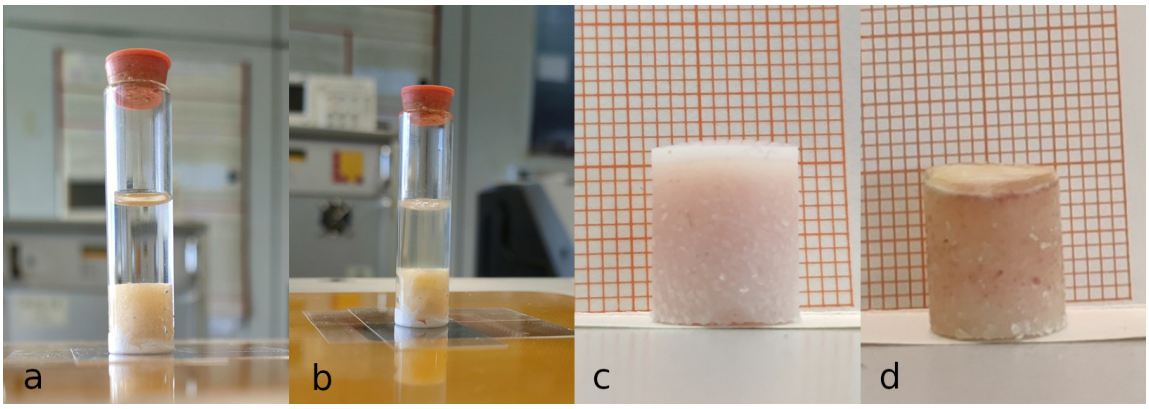

Figure 5.2: *Photos of two different samples used in two setups: B39A sample in PBS setup (a, b) and B5FB sample in Teflon setup (c, d). Two different degradation conditions are also shown: one at the beginning (a and c) and one at the end (b and d) of all CPMG measures, about 60 hours later than sample thawing.*

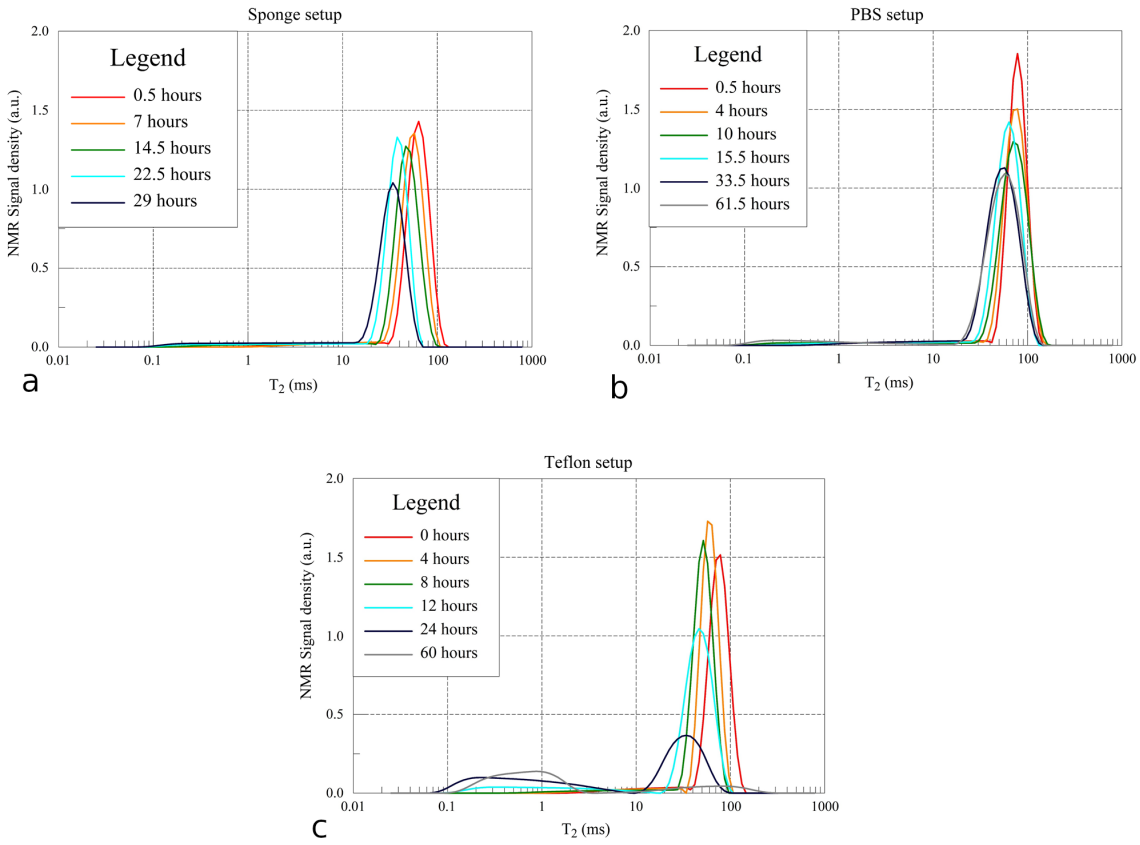

Figure 5.3: *T_2 distributions computed with a CPMG signal inversion made by UPEN algorithm. (a) B40B sample results with Sponge setup; (b) B39A sample results with PBS setup; (c) B5FB sample results with Teflon setup. For questions of space not all the distributions have been represented, but the overall trend towards shorter relaxation times for all three setups is unmistakable.*

hours of *CPMG* measures at room temperature using *Teflon* setup. The color and shape of the cartilage layer are deeply changed over time. Since this phenomenon is not present in *PBS* setup for the entire 60 hours range, the above described structural change can be mainly attributable to the dehydration phenomenon that, as explained before, does not affect *PBS* configuration. For this reason, it can be deduced that the structural change probably affects also measures in *Sponge* setup after 29 hours, even though there is no measure to prove it. Moreover from Figure 5.3, a similar behavior during the time between the three setups can be noted: there is a shift of the distributions on the left, so a decrease of the average T_2 of the system. By observing this result it can be inferred that T_2 relaxation time is widely affected by cartilage degradation. Now it is immediately clear that analyzing the cartilage in a time range of a few hours after thawing is fundamental.

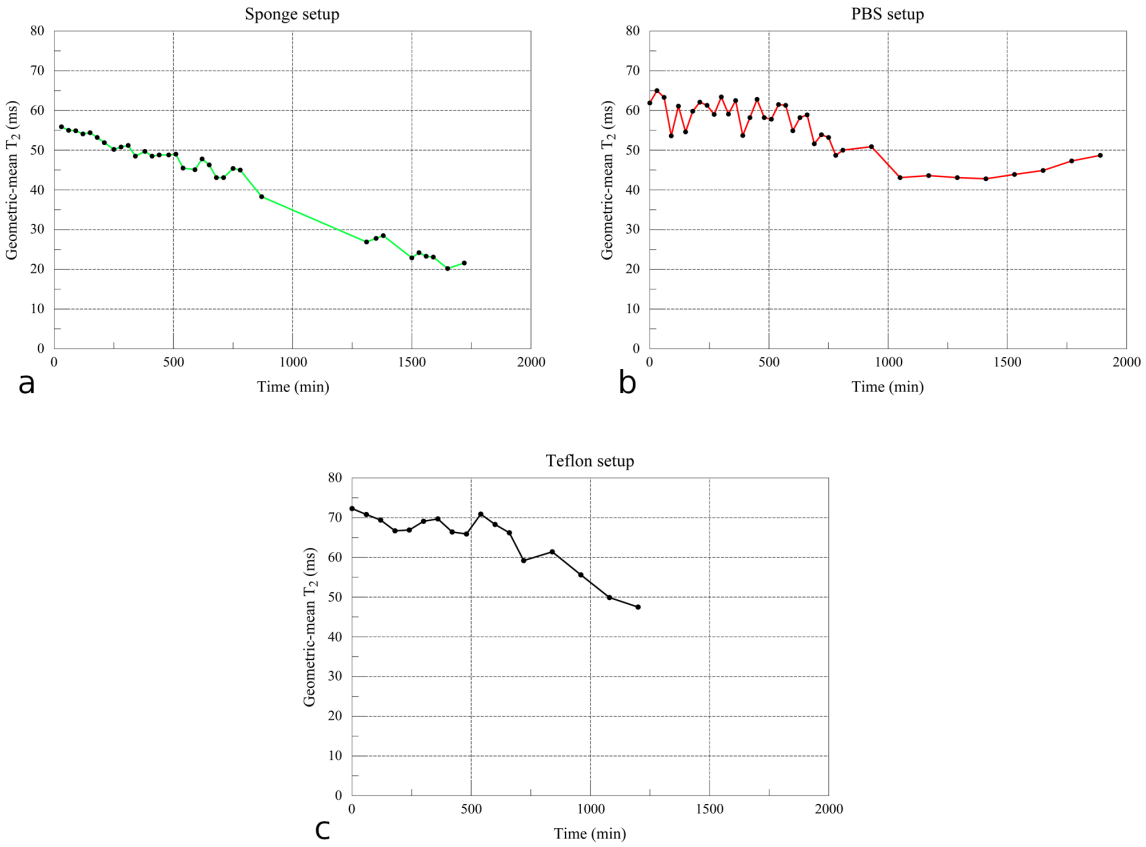

Figure 5.4: *Geometric-mean T_2 relaxation time trend during the time computed from the previous UPEN distributions for the three experimental setups. (a) B40B sample results with Sponge setup; (b) B39A sample results with PBS setup; (c) B39C sample results with Teflon setup.*

Along with the signal intensity analysis, the trend of transverse relaxation time was investigated. Since unimodal T_2 distributions were observed, a single value of relaxation time (i.e. the geometric-mean T_2) was considered. The results are reported in Figure 5.4. The trend in all three setups is the same it has been found in Fig. 5.3: T_2 relaxation time is widely affected by degradation for long times. This decreasing trend will be quantified in the next Section.

5.2 The choice of the best setup

As has been seen in the last Section, a general decrease of *NMR* signal intensity and T_2 was monitored during degradation. Other parameters were excluded from this analysis because the signal intensity and T_2 are known to be the most sensitive parameters to structural changes. To choose the best between the three setups the

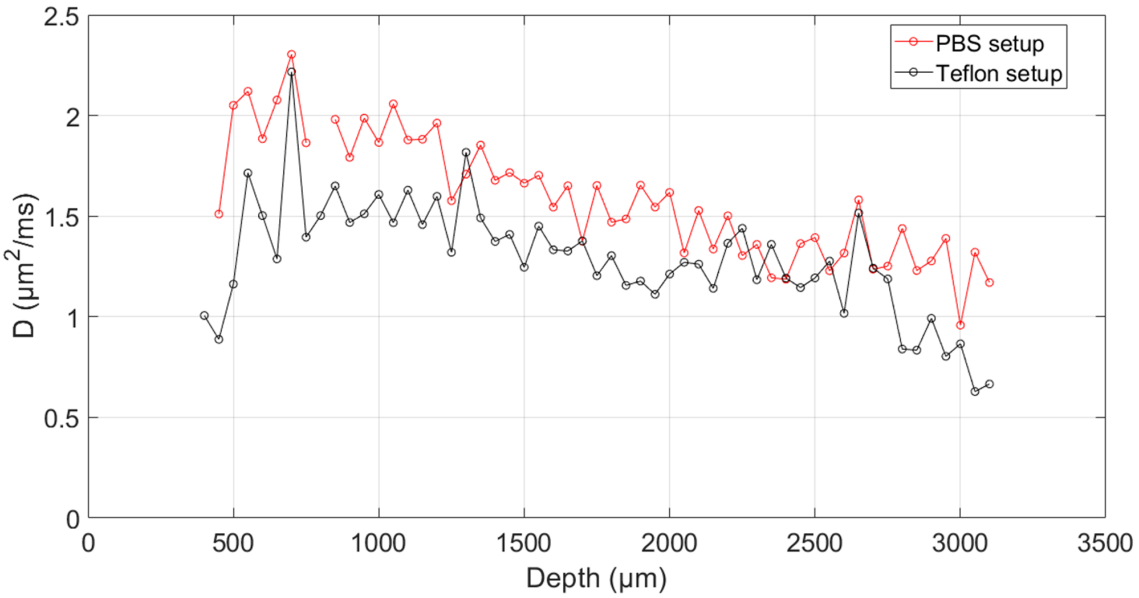

Figure 5.5: *Diffusion coefficient trends as a function of the sample cartilage depth (from the cartilage surface towards the bone layer). Red points are related to B43C sample with PBS setup and black points to B44A sample with Teflon setup. The duration of measures was about 9 hours, so the last measures (i.e. near the bone layer) could be influenced by degradation of the sample.*

percentage decrease rates of the two parameters for the three setups were computed. The first 10 hours were considered as a time range. The highest decrease rate was for *Sponge* setup (B40B sample), both for signal intensity and T_2 trends (0.8 %/h and 2 %/h, respectively). *PBS* and *Teflon* setups (B39A and B39C samples) achieved the best performance for preserving the initial state of the two parameters with *PBS* setup ahead (0.05 %/h and 0.5 %/h for signal intensity; 0.6 %/h and 0.8 %/h for T_2, respectively).

Diffusion profile measures on B43C sample with *PBS* setup and on B44A sample with *Teflon* setup were performed. A comparison between the two diffusion coefficient trends with the cartilage depth is reported in Figure 5.5.

PBS setup shows an increase of the absolute value of D (26%) compared with *Teflon* setup. As explained before, *PBS* setup minimized the dehydration of the sample but significantly influenced the measured D values due to interactions of *PBS* solution with the *NMR* signal. After several hours of immersion, the sample starts to interact with the *PBS* solution and the latter becomes visibly more turbid. For these reasons, the *Teflon* setup was preferred as shown in the last Section.

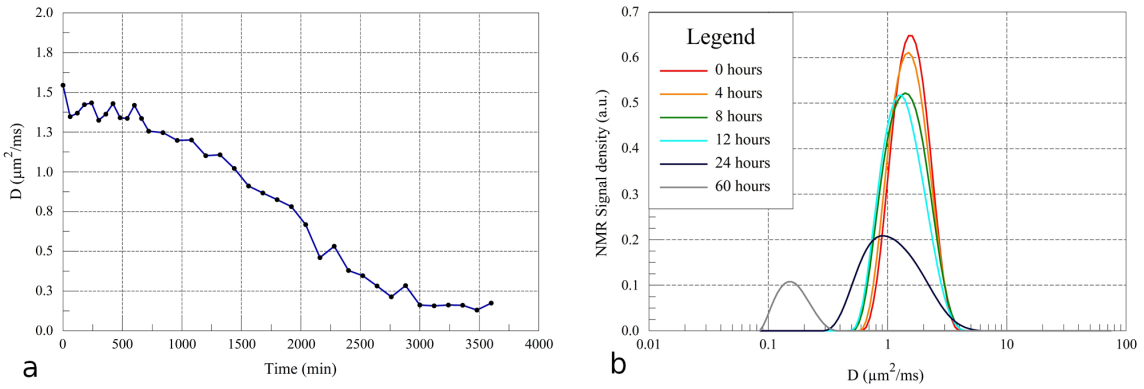

Figure 5.6: *(a) Diffusion coefficient trend during time for B5FB sample in Teflon setup obtained from the MATLAB linear fit of SSE sequence data. (b) D distributions for B5FB sample in Teflon setup computed with a SSE signal inversion made by the UPEN algorithm. For questions of space not all the distributions were represented, but the overall decrease trend is unmistakable.*

5.3 D, T_1 and Slp degradation tests with *Teflon* setup

Once it has been chosen to use the *Teflon* setup (Fig. 2.2), degradation tests for all the remaining parameters (D, T_1 and Slp) were performed using this experimental configuration. The approach was the same it was described in Section 5.1, by replacing *CPMG* with others ad-hoc *NMR* sequences.

A Stimulated Spin-Echo sequence (see Section 3.3.4) was performed to monitor the D trend over time. Results are reported in Figure 5.6. For about 10 hours D trend is quite stable, then there is a rapid decrease during time (Fig. 5.6a). The same information can be extracted from the D distributions in Figure 5.6b: there is a shift on the left for green and light blue lines with respect to red and orange ones, so a decrease of the average D of the system. This behavior is probably due to cartilage structural changes which make diffusion more restricted the more time passes. Moreover, distributions shape starts to change for times bigger than 24 hours: peaks move toward lower values (blue and gray lines in the graph) as described for the T_2 relaxation time (Section 5.1). Also, this behavior could be related to structural changes of the cartilage layer.

A Saturation Recovery sequence (see Section 3.3.3) was performed to monitor the T_1 trend over time. Results are reported in Figure 5.7. For about 20 hours T_1 trend is quite stable, then there is a rapid decrease during time (Fig. 5.7a).

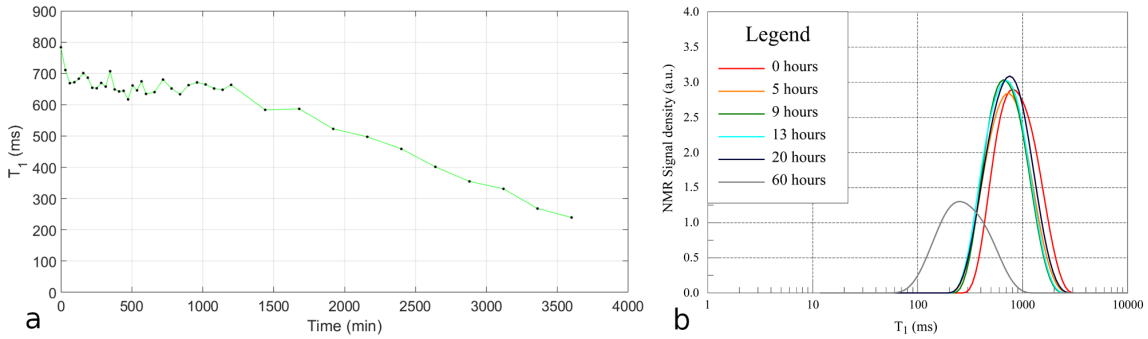

Figure 5.7: *(a) T_1 relaxation time trend during time for B39B sample in Teflon setup obtained from the MATLAB exponential fit of SR sequence data. (b) T_1 distributions for B39B sample in Teflon setup computed with a SR signal inversion made by the UPEN algorithm. For questions of space not all the distributions were represented, but the overall decrease trend is unmistakable.*

The same information can be extracted from the distributions in Figure 5.7b: up to 20 hours they are quite superimposed, then there is a consistent shift on the left (represented by the gray line), so a decrease of the average T_1 of the system. By observing this result it can be inferred that also T_1 relaxation time is affected by cartilage degradation.

Finally, a Double Quantum Build-up sequence (see Section 3.3.5) was performed to monitor the *Slp* trend over time: this is a parameter sensitive to low mobility ^1H. Results are reported in Figure 5.8. For about 10-15 hours *Slp* trend is quite constant, then there is a slow increase during the time. This is probably due to the structural changes of the cartilage which determine an increase of ^1H density and/or an increase of the ratio of low-high mobility ^1H.

In Figure 5.9 the degradation trends showed in this Chapter for the four main parameters of this work are summarized: T_2, T_1, D and *Slp*. There is a focus on the first degradation period (up to 10 hours) to follow the stability of the parameters during the automatized procedure time range. The general trend of the parameters can be considered approximately constant, taking into account experimental errors. So degradation factors have a negligible effect on *NMR* measures for the first 10 hours after thawing. According to these degradation tests results, as explained in Section 3.4, the total duration of the procedure was organized within 4 hours after thawing trying to minimize as much as possible the total acquisition time.

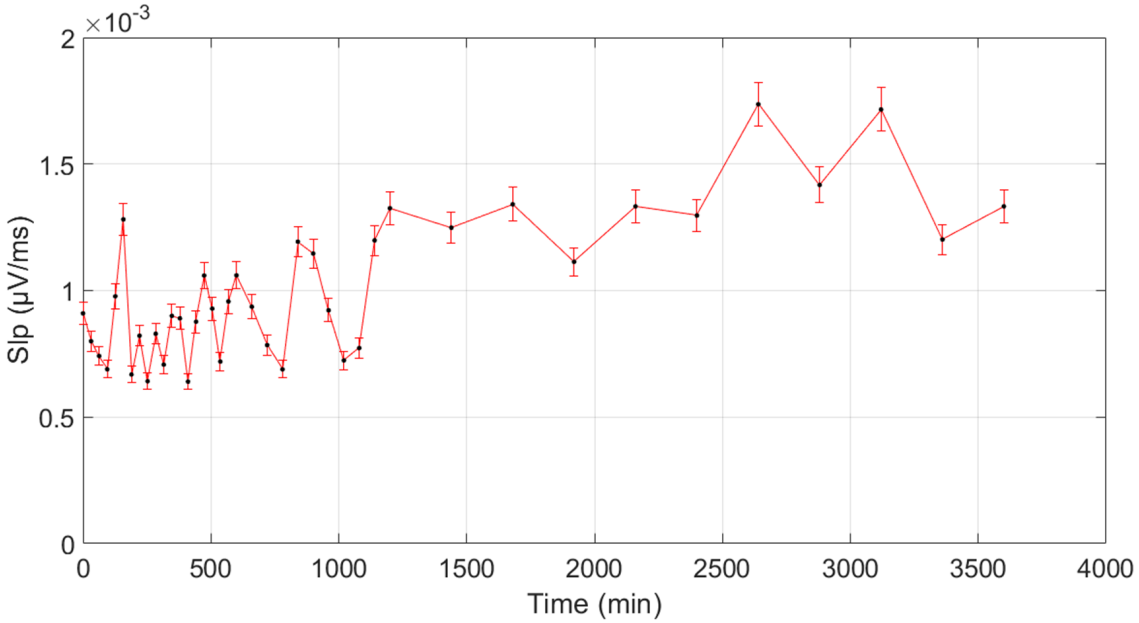

Figure 5.8: *Slp trend during time for B39B sample in Teflon setup obtained from the MATLAB linear fit of DQ sequence data.*

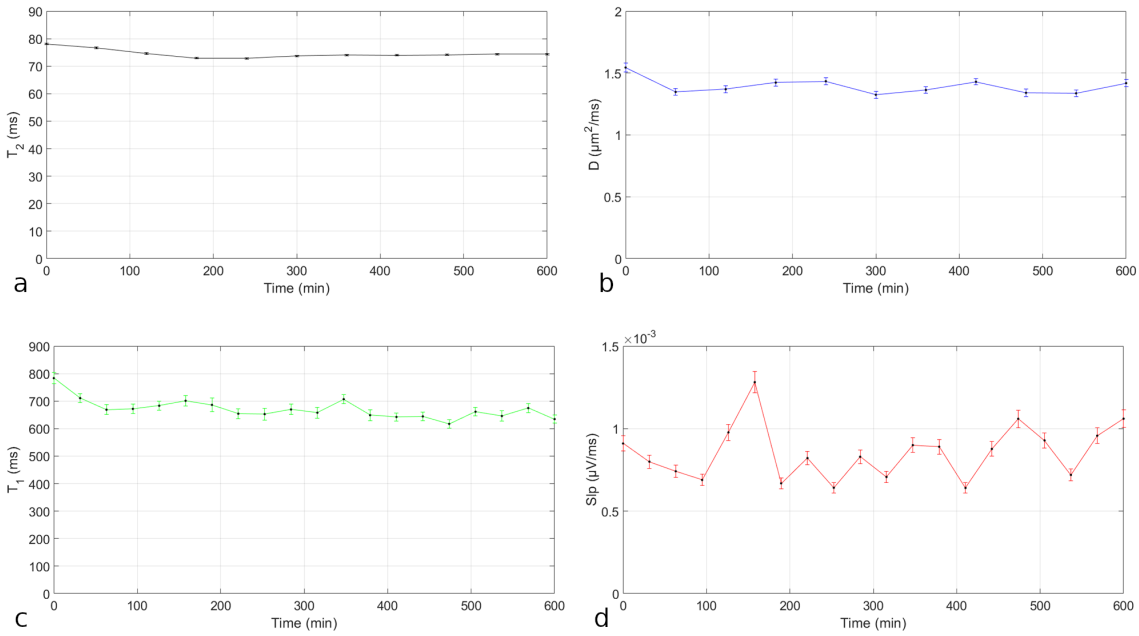

Figure 5.9: *(a) T_2, (b) D, (c) T_1 and (d) Slp degradation trends with Teflon setup for B39C, B5FB, B39B and B39B samples, respectively. Values and error bars were computed by the MATLAB data fit.*

Chapter 6

Procedure validation tests

In this Chapter, the most significant results of several validation tests with *Teflon* setup are illustrated. These tests aimed to check the validity of the final automatized procedure. As explained in Section 3.4, the automatized procedure is divided into two main consequent steps: the initial profile measure and the three-layer analysis. The first is intended to indicate the depth and thickness of the three anatomical cartilage layers (see Section 1.1) of the sample. The second uses the information collected in the first to place the sensitive volume of the *NMR-MOUSE* in each cartilage layer performing several *NMR* pulses sequences.

The results of the validation test allowed the optimization of the automatized procedure by:

- determination of a method to identify the three cartilage layers starting from *NMR* profile measure;
- improvement of the parameters setting of *NMR* pulses sequences;
- verification of the procedure goodness checking the repeatability of measure trends between different samples.

6.1 Profile validation

A *CPMG* profile sequence (see Section 3.3.2) was performed on several samples. B3FA sample results are shown in Figure 6.1. The dependence of the Nuclear Magnetization amplitude, i.e. the *NMR* signal intensity, on sample depth is depicted in Figure 6.1a. The signal starts from about $350\,\mu m$ because before that depth there

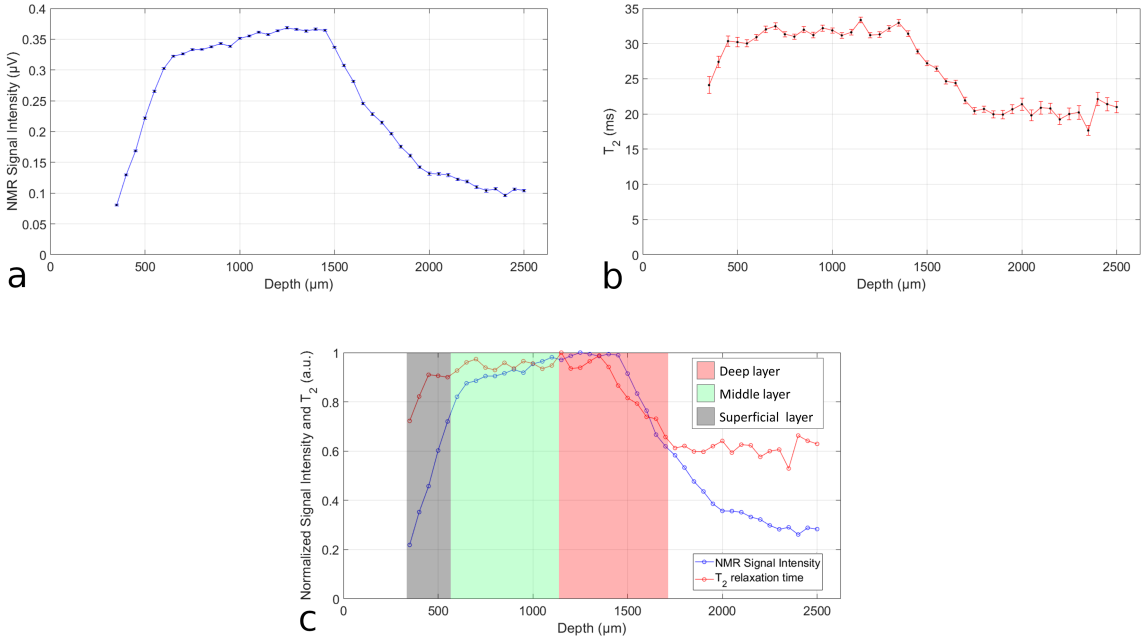

Figure 6.1: *CPMG profile sequence results on B3FA sample. (a) The Nuclear Magnetization amplitude and (b) the transverse relaxation time trends as a function of the sample depth. Values and error bars were computed by the MATLAB exponential data fit. (c) Overlap of the two trends obtained by a normalization of the previous profiles by their maximum value. Superficial (black), middle (green), and deep (red) cartilage layers are assumed to be distributed as the colors indicate.* 500, 850, *and* 1300 μm *were chosen as centers of the sensitive volumes for the three layers. A similar profile behavior was also observed in other samples, the results of which are reported in Appendix A.*

are the glass slides that support the sample. Then, from the cartilage surface towards the bone, the trend shows a first rapid increase followed by a much slower increase between about 600 and 1450 μm, up to a maximum value. The signal intensity then decreases towards a plateau that reaches values similar to the initial ones. In other samples, a slight increase after this plateau zone was also observed, up to about half the signal intensity of that in the maximum.

The signal intensity trend that has just been described is in accordance with a result of the literature in which bovine cartilage was studied using *NMR-MOUSE* device (Rossler et al. [14]). Following some deductions of that work, the *NMR* signal intensity profile can be explained as follows. The initial rapid increase is mainly due to three experimental reasons. First, the leftmost point in Figure 6.1a can be affected by a possible mismatch of the *MOUSE* sensitive volume with the sample surface, resulting in reduced signal intensity. Second, as explained in Section 2.1,

the cartilage surface is not perfectly perpendicular to the core axis due to technical reasons related to the coring procedure. For this reason, during initial measures the sensitive volume intercepts only a part of the sample, resulting in reduced signal intensity. The more the cartilage surface is perpendicular to the core axis, the more the initial increase is rapid. In Appendix A signal intensity profiles of other samples are reported and this initial increase changes between samples, depending on the angle between the cartilage surface and the coring axis of each sample. Third, the reduced signal intensity can possibly indicate drying of the sample, especially for the more exposed cartilage surface. The following slow increase up to the maximum of the profile is related to cartilage layers detection in which the protons of water and proteoglycans constitute the majority of the overall *NMR* signal. The subsequent decrease includes the end of the cartilage deep layer and the beginning of the calcified cartilage zone. In this zone, the signal is low because the cell population is scarce with a consequent smaller content of water and proteoglycans than cartilage layers. The minimum of the signal is probably related to the subchondral bone region detection and the subsequent slight increase (not present in Fig. 6.1) represents the beginning of the trabecular bone region.

The dependence of the transverse relaxation time T_2, on depth is shown in Figure 6.1b. A short T_2 value is identified at the cartilage surface, but now it is no longer related to experimental reasons: these T_2 values are typical of the superficial layer. Then, there is an increase towards maximum values forming a kind of plateau at a depth of approximately $700\,\mu m$, before decreasing again towards a second minimum. As reported in [14], this minimum corresponds to the calcified zone characterized by a smaller concentration of water also more restricted in mobility. After this minimum, as for the signal intensity profile, a slight T_2 increase was observed relating to the trabecular region. The overall T_2 trend from the surface towards the calcified zone has repeatedly been reported in the literature. In particular, the increase in T_2, maximum of T_2, and its subsequent decrease towards the calcified zone have been interpreted as superficial, middle, and deep layers, respectively [14]. Although no sharp boundaries are to be expected and the size of each layer depends on the cartilage thickness as well as the location it was taken from, the transition between the three cartilage layers can be determined.

Starting from the previous *NMR* signal intensity and T_2 profile measures, a method to identify the three cartilage layers was determined. Figure 6.1c shows the signal intensity and T_2 profiles normalized by their maximum values to be repre-

sented in the same plot. Then following the above-mentioned information the three cartilage layers were identified and the sensitive volume of the *NMR-MOUSE* was centered approximately in the middle of each of them (colored areas indicate the three layers). In the B3FA sample (Fig. 6.1c), 500, 850, and 1300 μm were chosen as centers of the sensitive volumes for superficial, middle, and deep layers, respectively. In general, a rule to choose these three depth values from the graph was established. For superficial layer, T_2 has to be shorter than plateau values, corresponding to the third or fourth signal intensity point. For the middle layer, the point was taken in the center of the T_2 plateau and in the first part of the signal slow increase. For the deep layer, the region around the signal peak and the rapid T_2 decrease was considered. This approach and these rules have been determined because similar profile behaviours were observed in all samples; the results are reported in Appendix A (Fig. A.2, A.4 and A.6). This repeatability of measure trends between different samples can be also considered as a validation of the procedure.

6.2 Three-layer analysis validation

The validity of the three-layer analysis approach was also tested. By using the information previously collected with the profile, the sensitive volume of the *NMR-MOUSE* was automatically centered in each cartilage layer performing several *NMR* pulses sequences: *CPMG*, *SR*, *SSE* and *DQ* (see Section 3.3). T_2, T_1, D distributions, and a Double Quantum linear data fit were computed for each of the three cartilage layers. This entire process was repeated on several samples. B3FA sample results are shown in Figure 6.2, in which 500, 850, and 1300 μm were chosen as centers of the sensitive volumes for superficial, middle, and deep layers, respectively. First of all, since only unimodal distributions were observed, a single value of T_2, T_1, and D was considered for the subsequent analysis (see Section 4.1). In Figure 6.2a T_2 distributions related to the three cartilage layers are shown. The average T_2 value is similar between layers, slightly larger for the middle layer. Similar behavior is also present in D distributions (Fig. 6.2b), with the D value of the deep layer different from the other two. T_1 distributions (Fig. 6.2c) are more distinct between layers and the average T_1 is the greatest in the superficial layer, followed by the middle and, last, the deep layer. The signal intensity value (i.e. the Magnetization) measured in these three sequences is half for the superficial layer concerning the other two. This is because the cartilage surface is not perfectly perpendicular to the core axis,

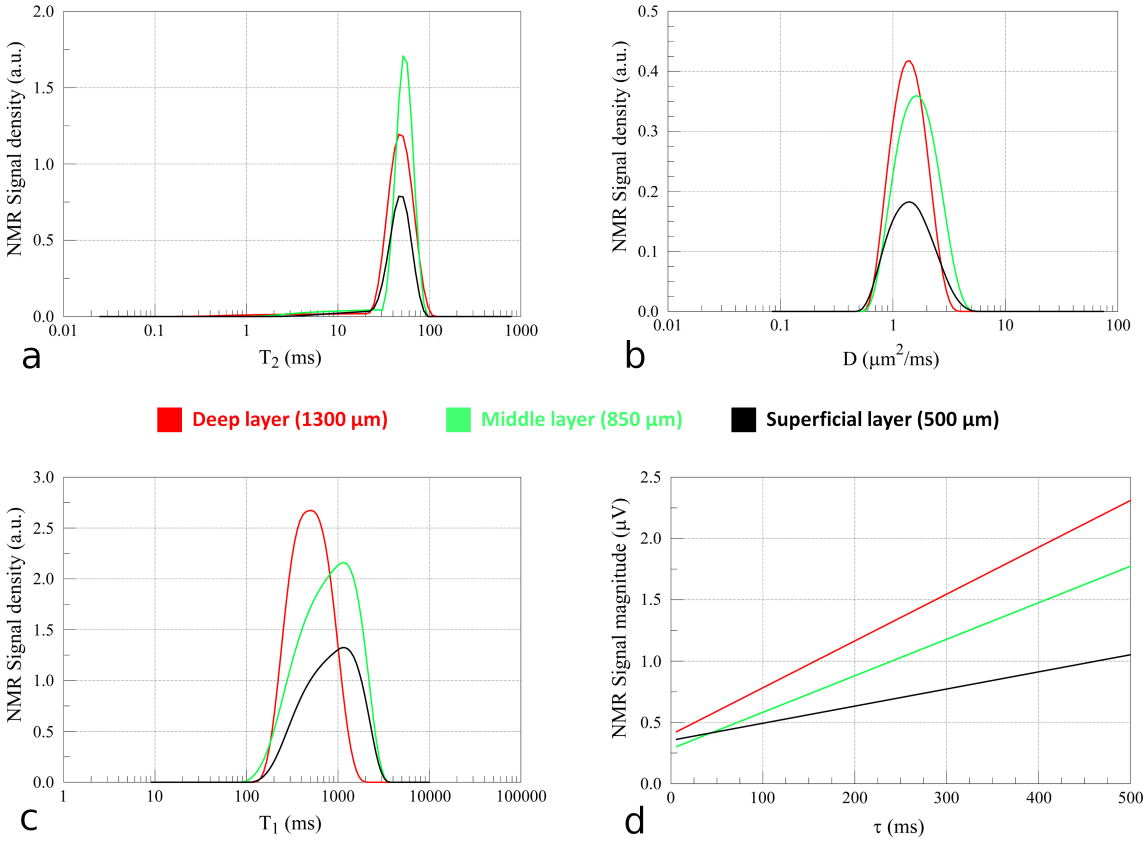

Figure 6.2: *(a) T_2, (b) D, (c) T_1 distributions computed with CPMG, SSE and SR signals inversion made by the UPEN algorithm for the three cartilage layers of the B3FA sample. (d) DQ sequence linear data fit for each cartilage layer. Results were obtained with the automatized three-layer analysis on B3FA sample using* 500, 850 *and* 1300 *µm as centers of the sensitive volumes for superficial, middle and deep layers, respectively. The same parameters behaviour was also observed in other samples, the results of which are reported in Appendix A.*

as explained in Section 6.1. In Figure 6.2d the *DQ* sequence linear data fit for each layer is shown. From these lines, the *Slp* parameters (i.e. the slopes of the lines) were obtained. *Slp* values can clearly distinguish the layers: deep value is the greatest, followed by middle and superficial ones.

The same parameters behavior was also observed in other samples, the results of which are reported in Appendix A (Fig. A.1, A.3 and A.5). The repeatability of measure trends among different samples validates the three-layer analysis.

Chapter 7

Cartilage *NMR* parameters: final results

In this Chapter, the most significant results of the cartilage *NMR* parameters analysis are illustrated. As described in Chapters 3 and 4, T_2, T_1, D and Slp parameters have been obtained from the cartilage of twenty bovine samples. These parameters have been saved in a database containing three values for each parameter for each sample, i.e. one for each cartilage layer, reaching a total of sixty values. Considering this database, statistical and pattern recognition analyses are performed. The approach behind this analysis is to determine whether and which *NMR* parameter can significantly discriminate the differences in the cartilage structure among the three layers (in Section 7.1) and among the four coring zones of the knee (in Section 7.2). The aim is to correlate the anatomical characteristics (that have been illustrated in Chapter 1) with the *NMR* measures results. The last step will be to correlate these two with the results of the mechanical tests.

7.1 Cartilage layers comparison

The most relevant and promising results are related to the discrimination of superficial, middle, and deep cartilage layers. Database in hand, a first approach was to plot the measured T_2, T_1, D, and Slp values of the twenty samples considering the samples' depths in which measures were performed. Figure 7.1 shows T_2 values as function of the samples depths. Each sample is represented by three points in the plot, i.e. one for each cartilage layer. The same plot has been colored considering two different samples information: the three cartilage layers, Fig. 7.1a, and the four

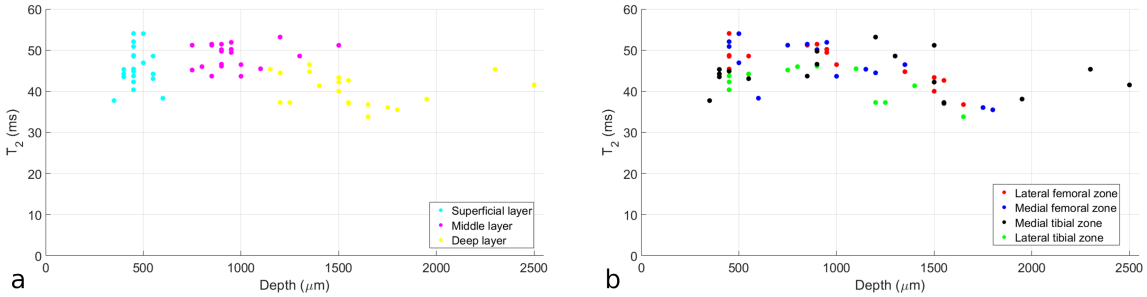

Figure 7.1: *T_2 values as function of the samples depths. The same plot has been colored considering two different samples information: (a) the three cartilage layers and (b) the four knee zones. Each sample is represented by three points in each of the two plots, i.e. one for each cartilage layer. The T_2 uncertainties computed by the MATLAB data fits have not been represented because almost all the bars have a length similar to the circles' diameter. Analogous trends for T_1, D and Slp are reported in Appendix B.*

knee zones, Fig. 7.1b (see Section 4.2).

In the first case, the three layers are visibly divided by each other along with the depth. This is expected because the layers are anatomically located at different cartilage depths (see Section 1.1). Looking at the plot, the overlapping of middle and deep layers depths is related to the different overall cartilage thickness among samples. As mentioned in Chapter 6, the sample depths that have been chosen by the profile analysis are strictly related to the overall cartilage thickness of the sample. However, the profile analysis still manages to place the sensitive volume approximately in the center of the three cartilage layers of different samples. Considering this fact, for simplicity of representation all the samples depths values from now on will be grouped into three main groups corresponding to superficial, middle, and deep cartilage layers. As regards T_2, superficial and middle layers seem to have similar values, while the deep layer has shorter T_2 values than the other two. A similar behaviour has been also observed for D and T_1 values, as shown in Appendix B (Fig. B.1 and B.2). In the *Slp* trend, however, superficial and middle layers values differ more (Fig. B.3).

In the case of the knee zone plot (Fig. 7.1b), the samples appear more mixed and no longer grouped as for layers. Only a fact can be noted: the samples from the lateral tibial zone (green points) have in general shorter T_2 values than samples from other zones. This has been also observed for D and T_1 trends (Fig. B.1 and B.2), but not for *Slp* trend (Fig. B.3).

More detailed results about *NMR* parameters trends between layers are reported

in Figure 7.2. Following the reasoning done above, samples depths values have been grouped into three main groups corresponding to superficial, middle, and deep cartilage layers. A box plot representation was chosen for each group by using the *boxchart* MATLAB function that provides a visual representation of summary statistics for the samples. Each box plot displays the following information: the median, the lower and upper quartiles, any outliers, and the minimum and maximum values that are not outliers. The first thing to notice is that samples are not normally distributed. Moreover, by comparing the medians of the distributions for the three cartilage layers the previous reasoning about Figure 7.1 is confirmed: superficial and middle layers medians are close to each other and both farther from deep layer median for T_2, D and T_1 parameters (Fig. 7.2a, b and c). Slp parameter is the only one in which the three medians are separated (Fig. 7.2d). For completeness, in these plots, the samples have also been divided into the four knee zones, even if a more detailed and clear analysis on this will be carried out in Section 7.2.

Since the samples are not normally distributed, a statistical analysis based on the Kruskal-Wallis test has been performed. As mentioned in Section 4.3.1, this test does not make normality assumptions and instead of comparing population means, it compares population medians. Its null hypothesis states that the samples are from identical populations (i.e. the population medians are equal). Kruskal-Wallis test results are shown in Table 7.1. P-values represent the probability, under the assumption of the null hypothesis, of obtaining a result equal to or more extreme than what is observed. The critical value for statistical significance is chosen as $P < 0.05$ (bold numbers in the Table). A comparison of the medians of samples distributions among the three cartilage layers for the four *NMR* parameters is reported. Initially, the KW test has been performed considering the three layers together. As expected, p-values are very small because it is very likely that among the three populations there is at least one different from the others. Then, a comparison in pairs between layers was done. For T_2, D and Slp all comparisons underline a statistically significant difference between cartilage layers. Only T_1 does not show significant differences in the Superficial-Middle layers comparison. However, these results are not completely accurate from a statistical point of view. As explained in Section 4.3.1, since three different hypotheses are tested at the same time (i.e. multiple testing), p-values should be adjusted. Two different corrections are proposed: Bonferroni correction, which considers the layers populations as independent of each other, and False Discovery Rate (FDR) correction, which considers a dependence between lay-

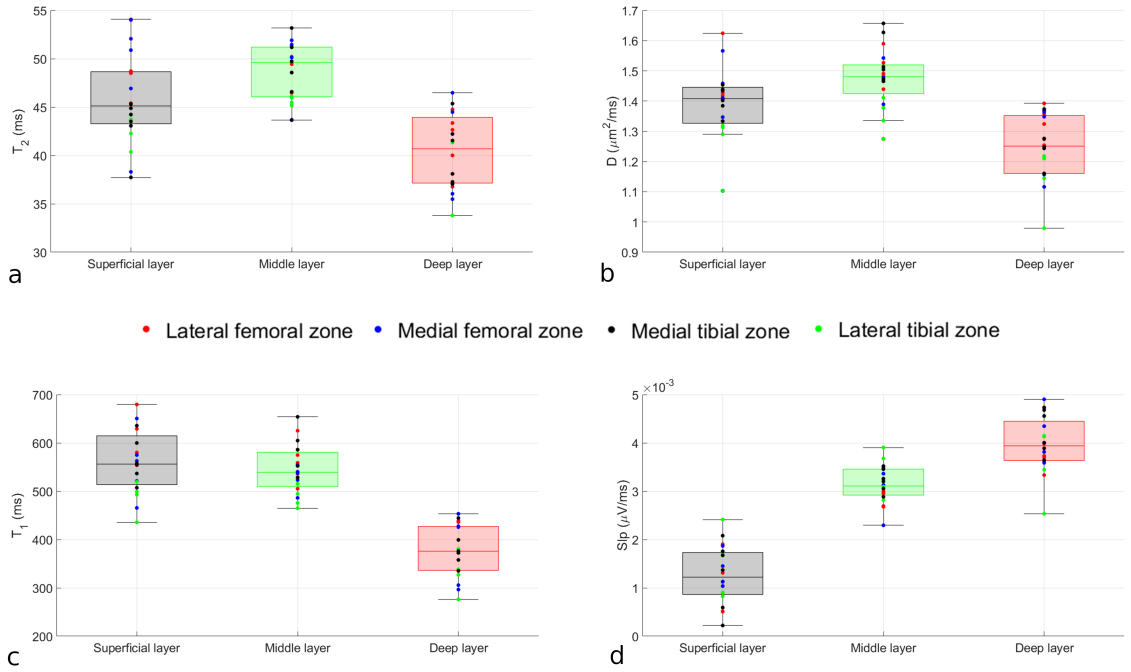

Figure 7.2: *(a) T_2, (b) D, (c) T_1 and (d) Slp parameters trends among cartilage layers. For simplicity of representation all the samples depths values were grouped into three main groups corresponding to superficial, middle, and deep layers. A box plot (by boxchart MATLAB function) representation is shown for each group. Each box plot displays the following information: the median (i.e. the line inside each box), the lower and upper quartiles (i.e. bottom and top edges of each box), any outliers, and the minimum and maximum values above and below each box that are not outliers (i.e. the whiskers). The distance between the top and bottom edges is the interquartile range (IQR), which by definition contains 50% of the samples, while the two edges are 75^{th} and 25^{th} percentiles, respectively. Outliers are values that are more than $1.5 \cdot IQR$ away from the top or bottom of the box. In T_1 plot, some upper outliers have been removed from the graphical representation for space reasons. The samples have also been divided into four colors representing the four different knee zones. The parameters uncertainties computed by the MATLAB data fits have not been represented because almost all the bars have a length similar to the circles' diameter.*

Parameter	*Layers*	*Kruskal-Wallis p-values*	*Bonferroni correction*	*FDR correction*
T_2	Sup-Mid-Deep	**< .0001**		
	Sup-Mid	**0.0284**	0.1453	**0.0284**
	Sup-Deep	**0.0006**	**0.0038**	**0.0009**
	Mid-Deep	**< .0001**	**< .0001**	**< .0001**
T_1	Sup-Mid-Deep	**< .0001**		
	Sup-Mid	0.4989	1.0000	0.4989
	Sup-Deep	**< .0001**	**< .0001**	**< .0001**
	Mid-Deep	**< .0001**	**< .0001**	**< .0001**
D	Sup-Mid-Deep	**< .0001**		
	Sup-Mid	**0.0045**	0.0644	**0.0045**
	Sup-Deep	**0.0002**	**0.0035**	**0.0002**
	Mid-Deep	**< .0001**	**< .0001**	**< .0001**
Slp	Sup-Mid-Deep	**< .0001**		
	Sup-Mid	**< .0001**	**0.0002**	**< .0001**
	Sup-Deep	**< .0001**	**< .0001**	**< .0001**
	Mid-Deep	**< .0001**	**0.0123**	**< .0001**

Table 7.1: *Results of statistical analysis based on the Kruskal-Wallis (KW) test. T_2, T_1, D and Slp parameters distributions among cartilage layers are considered. The KW test has been performed both considering the three layers together and in pairs. The p-values related to multiple testing are adjusted through Bonferroni and False Discovery Rate (FDR) corrections. The critical value for statistical significance is chosen as $P < 0.05$ (bold numbers). Abbreviations: Sup = Superficial layer, Mid = Middle layer, Deep = Deep layer.*

ers populations. Both corrections are reported in Table 7.1. As expected, Bonferroni correction is more conservative and the only parameter that can significantly distinguish the three layers is *Slp*. If instead *FDR* correction is considered, Kruskal-Wallis p-values remain all statistically significant, even after correction. Since layers are biological zones close to each other, layers populations are probably not independent of each other. So, the *FDR* correction could be more appropriate for this particular case.

The results achieved from this analysis are very promising: T_2, D and *Slp* parameters measured with the *NMR-MOUSE* device can catch the main structural differences between the three cartilage layers. T_1 also manages to find differences, except for the comparison between superficial and middle layers. So, in general, the discrimination of the three cartilage layers shows very good results in terms of signif-

icance. These results are strictly correlated to the anatomical characteristics of the cartilage layers, which have been illustrated in Chapter 1. In particular, *NMR* can detect protons belonging to different cartilage components like water and macromolecules (i.e. proteoglycans and collagen amide groups) [14]. Considering some interpretations reported in the literature, the four *NMR* parameters trend among the three cartilage layers can be explained as follows. T_2 and T_1 relaxation times trends mainly depend on the concentration and mobility of the water. Water relaxation depends not only on water content but also on the kind of interaction with existing interfaces [10]. The maximum of relaxation times occurs in the middle cartilage layer and it is connected to the highest anisotropy of collagen fibrils and to the highest water concentration in this layer (see Chapter 1). The minimum in the deep layer is because this layer is very close to the calcified cartilage in which there is the lowest water content and the mobility is very low. Also the diffusion coefficient D is related to the collagen fibrils structures and proteoglycans organization, which define the geometry of the confining space. The level of restriction of the water in this space strongly influences the measure of D (see Equation 3.13). So, the different organization of proteoglycans and collagen fibrils among the cartilage layers leads to different values of the diffusion coefficient. Finally, Slp is a parameter sensitive especially to low mobility protons like those of the proteoglycans or collagen amide groups. The rapid increase of Slp values passing from the superficial to the deep layers is related to the increase of collagen and proteoglycans content correspondent to the increasing of the cartilage depth [46].

It has been widely demonstrated in the literature that the mobility and content of water, the content of proteoglycans, and the collagen structure in the cartilage tissue are suitable indicators for *OA* severity. So, identifying these components through *NMR* parameters can help in deepening the knowledge about the cartilage changes occurring in this disease. Future developments will concern the assessment of correlations between *NMR* parameters and tissue mechanics, thus applying such an integrated framework in evaluating cartilage changes throughout osteoarthritis.

Multivariate statistical analysis has been also performed by using the Principal Component Analysis (*PCA*), see Section 4.3.2. The first two components (i.e. eigenvectors) have been considered because they contain the highest contribution of the original variables. In other words, the first two eigenvalues of the covariance matrix (i.e. the variances of the new transformed variables) together contain more than 90% of the total variance. The percentage of the total variance 'explained' by each

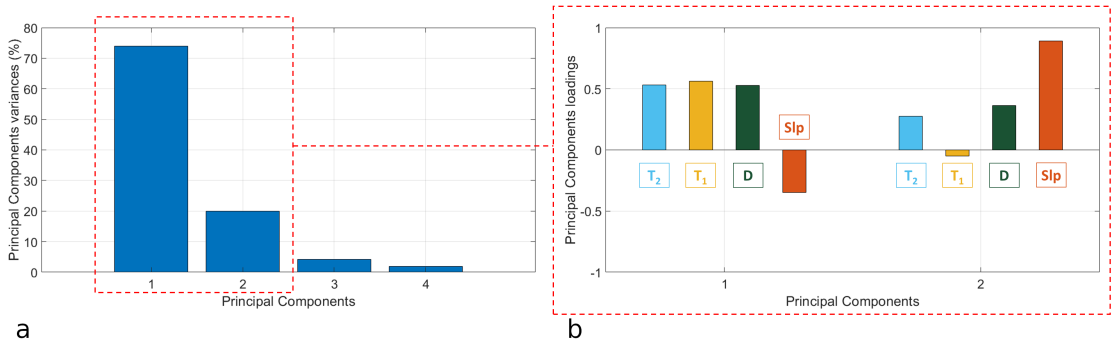

Figure 7.3: *Principal Component Analysis (PCA) results: (a) percentage of the total variance 'explained' by each component (i.e. eigenvalues of the covariance matrix); (b) loadings for the first two selected components (i.e. the contribution of each original variable). PCA has been performed through the pca MATLAB function.*

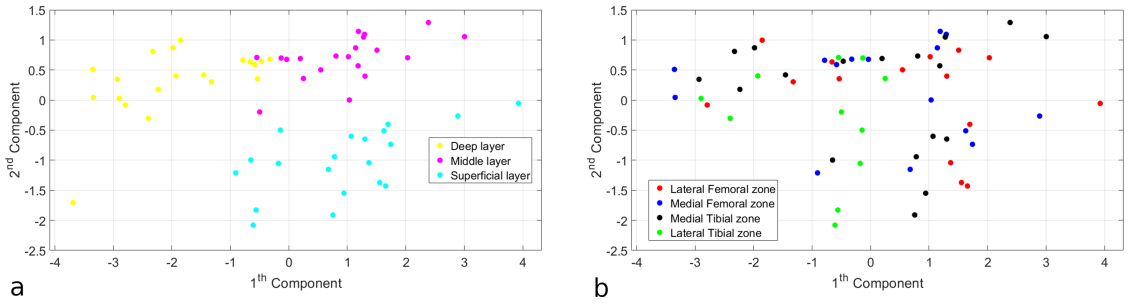

Figure 7.4: *Principal Component Analysis (PCA) results: the score plot of the first two components colored according to (a) the three cartilage layers and (b) the four knee zones. Each sample is represented by three points in each of the two plots, i.e. one for each cartilage layer.*

component is shown in Figure 7.3a. Moreover, the loadings for the first two selected components are reported (Fig. 7.3b): they represent the contribution (i.e the 'load') of each original variable. The first component contains high and similar contributions from T_2, T_1 and D variables, while from Slp is a bit lower. The second component instead contains a very high contribution from the Slp variable.

PCA results are visualized by making a two dimensions score plot, that is a scatter plot of score vector components (i.e. one point in the plot for each sample). In Figure 7.4 the score plot of the first two components has been colored according to both the three cartilage layers (a) and the four knee zones (b). The fact that performing this multivariate analysis the three layers appear clustered together confirm the Kruskal-Wallis test results. The chosen *NMR* parameters can discriminate very well among the three cartilage layers. However, looking at Figure 7.4b, they do not seem to have

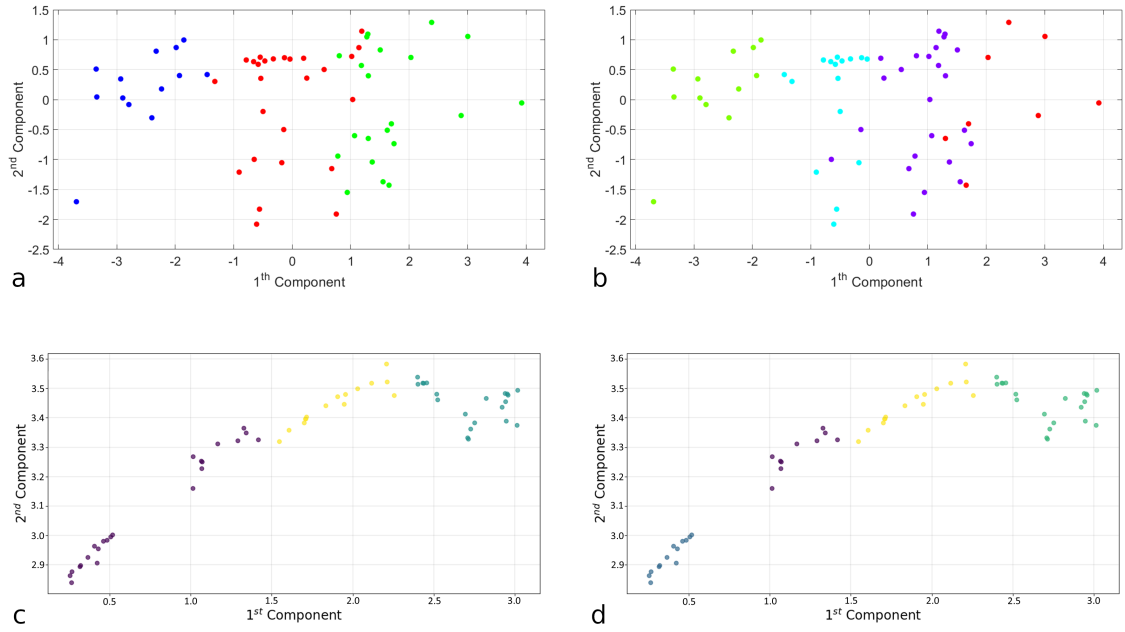

Figure 7.5: *Pattern recognition analysis results of K-means and HDBSCAN clustering algorithms. K-means algorithm has been repeated two times considering (a) $K = 3$ and (b) $K = 4$. The constructed clusters are represented on the score plot of the first two components of the previous PCA. Also HDBSCAN algorithm has been repeated two times considering minClusterSize parameter equal to (c) 11 and (d) 10. The constructed clusters are represented on a space obtained by performing the UMAP algorithm, which is a dimensionality reduction algorithm. Each sample is represented by three points in each of the four plot, i.e. one for each cartilage layer. Be careful not to confuse the points colors of these plots (which have been randomly selected) with those of the previous plots: using these two cluster algorithms, all the samples are reclassified and recolored without any a priori knowledge.*

the same ability to discriminate among the four knee zones because points are no longer clustered. These considerations will be deepened in Section 7.2.

A basic pattern recognition analysis has been also performed through K-means and *HDBSCAN* clustering algorithms to search for the natural structure inside the data and to classify similar data items into clusters, see Section 4.3.3. Results are shown in Figure 7.5. K-means algorithm has been repeated two times considering $K = 3$ and $K = 4$ (Fig. 7.5a and b, respectively) to detect possible clustering phenomena attributable to the 3 cartilage layers and the 4 knee zones peculiarity. The clusters constructed by the K-means algorithm are represented on the same previous space of the *PCA* (i.e. the score plot of the first two components). In both cases of $K = 3$ and $K = 4$, the clusters result well separated from each other. This

means that the *NMR* parameters dataset is predisposed to be grouped in 3 or 4 clusters that can be assumed as the cartilage layers and the knee zones, respectively. However, since some of these clusters are more populous than others, it is clear that there are clusters that contain more than one type of layer or zone. Similar behavior is also observed by performing the *HDBSCAN* algorithm on the parameters dataset. Similar to K-means, this algorithm has been repeated two times considering two different values of the $minClusterSize$ parameter, 10 and 11 (Fig. 7.5d and c, respectively), that defines the smallest size grouping that is considered as a cluster. By considering these two specific values, *HDBSCAN* algorithm can detect 3 and 4 well-separated clusters within the dataset, which could be attributed to the 3 cartilage layers and the 4 knee zones. However, as for K-means, it is evident that some of these clusters contain more than one type of layer or zone.

7.2 Knee zones comparison

From the results presented in the last Section, the four *NMR* parameters can almost always significantly discriminate the differences in the cartilage structure among the three layers. It has also been seen that these parameters seem to fail in discriminating the differences in the structure among the four knee zones. Now, a more detailed analysis related to the four coring zones of the knee will be carried out. The *NMR* parameters trends between layers reported through a box plot representation in Figure 7.2 have been divided by the four knee zones. T_2 trends are shown in Figure 7.6, while D, T_1 and Slp trends are reported in Appendix B (Fig. B.4, B.5 and B.6).

By comparing the medians of the distributions for the three cartilage layers among knee zones the observations made in the last Section are confirmed: superficial and middle layers medians are close to each other and both farther from deep layer median for T_2, D and T_1 parameters for all four knee zones. Slp parameter is the only one in which the three medians are separated. T_2 trends among knee zones are particularly interesting. Looking at Figure 7.6 a difference between femoral (a and b) and tibial (c and d) zones can be noted: in tibial zones, superficial and middle layers distributions are separated from each other, contrary to what happens for femoral zones. This zone distinction is also present in the D trends among knee zones (see Fig. B.4). This peculiarity is supported by the statistical analysis based on the Kruskal-Wallis test. Results are shown in Table 7.2. As for layer analysis (Section 7.1), the critical value for statistical significance is chosen as $P < 0.05$ (bold numbers in the Table).

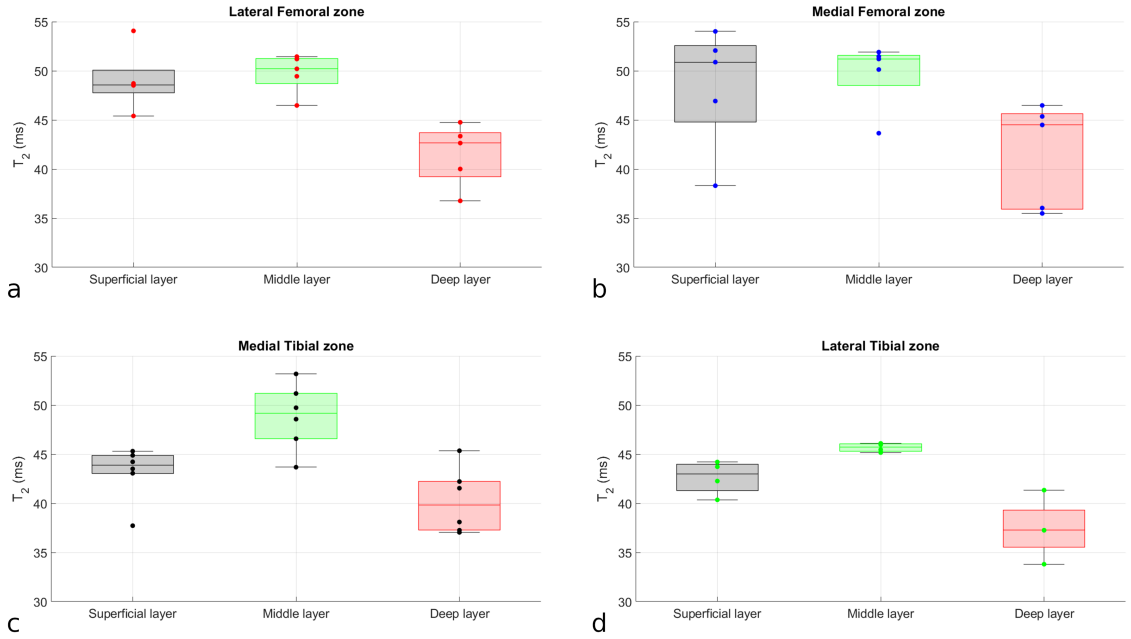

Figure 7.6: *T_2 trend among cartilage layers for the four knee zones: (a) Lateral femoral zone, (b) Medial femoral zone, (c) Medial tibial zone and (d) Lateral tibial zone. A box plot (by boxchart MATLAB function) representation is shown for each layer. The parameters uncertainties computed by the MATLAB data fits have not been represented because almost all the bars have a length similar to the circles' diameter. Analogous trends for T_1, D and Slp are reported in Appendix B.*

In support of the above considerations, for T_2 and D the Tibia-Femur comparison shows a statistically significant difference. For these two parameters also the four zones comparison underlines a significant difference and this means that among the four populations there is at least one different from the others. But if a comparison in pairs between zones is considered (i.e. multiple hypothesis testing), by considering *FDR* correction only D shows significant results as regards Lateral Femur-Lateral Tibia, Medial Femur-Lateral Tibia, and Medial tibia-Lateral tibia comparisons. Finally, the Lateral-Medial comparison does not show a significant difference for any parameter.

From results of the Principal Component Analysis (*PCA*) performed on the parameters dataset (see Section 7.1), *NMR* parameters do not seem to have the ability to discriminate among the four knee zones because points are not clustered (Fig.7.4). Then, three subsets of the data have been considered, avoiding the dependence on the three cartilage layers. Each subset contains twenty measures related to one of the layers. By performing the *PCA* on each of these subsets separately, only in the superficial layer case, a very interesting result is achieved. By considering the first and third components (in which the third contains very high contributions from T_2 and D parameters), discrimination among the four knee zones is achieved. Figure 7.7 shows the clustering phenomenon between the twenty samples based on the four zones separation and also on Tibia-Femur separation. The fact that this phenomenon has been observed only for cartilage superficial layer measures may be an indicator that this layer is more sensitive than the other two to the knee zone taken into consideration. This aspect is promising because the mechanical tests will be performed on the cartilage superficial layer, so the measured elastic modulus will be influenced mainly by the contribution of this layer.

Despite this last interesting result, the discrimination of the four cartilage knee zones made by *NMR* parameters does not show good results in terms of significance, as has been illustrated in this Section. However, this may not be considered as a negative aspect. Since all the twenty samples came from the same knee joint of the same bovine, the cartilage structural changes between one knee zone and another may not be so significant. Moreover, the studied bovine was certainly very young since the knee was taken from a butcher shop. From the literature, it is recognized that in cases of osteoarthritis (*OA*) or simply older subjects the cartilage structural changes between knee zones become more evident [22]. So, if in the future this study will be repeated on an older bovine or suffering from osteoarthritis, the distinctions

Parameter	*Zones*	*Kruskal-Wallis*	*Bonferroni corr.*	*FDR corr.*
	LF-MF-MT-LT	**0.0364**		
	Tibia-Femur	**0.0060**		
	Lateral-Medial	0.6292		
	LF-MF	0.7557	1.0000	0.7557
T_2	LF-MT	0.1116	0.7183	0.1675
	LF-LT	**0.0128**	0.1154	0.0744
	MF-MT	0.1037	0.5623	0.1675
	MF-LT	**0.0248**	0.0859	0.0744
	MT-LT	0.3302	1.0000	0.3963
	LF-MF-MT-LT	0.0606		
	Tibia-Femur	0.3366		
	Lateral-Medial	0.4266		
	LF-MF	0.2902	1.0000	0.4353
T_1	LF-MT	0.7449	1.0000	0.7449
	LF-LT	**0.0218**	0.0819	0.0668
	MF-MT	0.3661	1.0000	0.4393
	MF-LT	0.0971	0.8007	0.1942
	MT-LT	**0.0223**	0.1201	0.0668
	LF-MF-MT-LT	**0.0056**		
	Tibia-Femur	**0.0493**		
	Lateral-Medial	0.1836		
	LF-MF	0.4429	1.0000	0.6643
D	LF-MT	0.6383	1.0000	0.7660
	LF-LT	**0.0011**	**0.0061**	**0.0065**
	MF-MT	0.9136	1.0000	0.9136
	MF-LT	**0.0063**	**0.0474**	**0.0126**
	MT-LT	**0.0059**	**0.0241**	**0.0126**
	LF-MF-MT-LT	0.8614		
	Tibia-Femur	0.5266		
	Lateral-Medial	0.4711		
	LF-MF	0.4937	1.0000	0.8836
Slp	LF-MT	0.4264	1.0000	0.8836
	LF-LT	0.6605	1.0000	0.8836
	MF-MT	0.8565	1.0000	0.8836
	MF-LT	0.8836	1.0000	0.8836
	MT-LT	0.7670	1.0000	0.8836

Table 7.2: *Statistical analysis results of T_2, T_1, D and Slp parameters distributions among the knee zones. The four zones together and in pairs are considered for KW test. Bonferroni and FDR corrections are used for multiple testing. The critical value for statistical significance is chosen as $P < 0.05$ (bold numbers). Abbreviations: LF=Lateral femoral zone, MT=Medial tibial zone.*

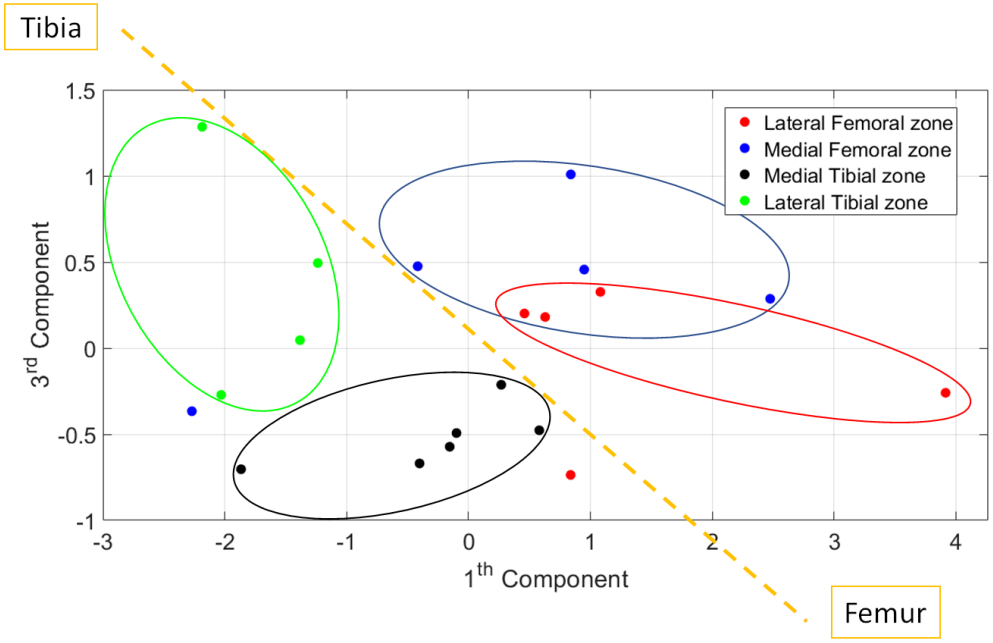

Figure 7.7: *Principal Component Analysis (PCA) results related to the superficial layer subset: the score plot of the first and third components colored according to the four knee zones. Each sample is represented by one point in the plot that is related to the measurements performed on the cartilage superficial layer. The samples from the same zone are circled and the Tibia-Femur separation is made by the dashed yellow line.*

made by *NMR* parameters between the medial and lateral zones of the tibia and the femur are expected to be more significant.

Conclusions

Studies of cartilage degradation as a function of three different experimental setups have been carried out, performing several tests with the *NMR-MOUSE*. Since *NMR* parameters were conditioned by degradation of the cartilage tissue, their trends during the time after the sample thawing have been measured to establish the best experimental setup. The changes during the time of the four *NMR* parameters under study (i.e. T_2, T_1, D and Slp) were determined before testing the final acquisition procedure. This *NMR* procedure based on the acquisition of these parameters has been implemented. The procedure has been made automatic to have a standardized protocol that can be used by others. Quantitative *NMR* parameters from the three cartilage layers of twenty bovine knee samples were obtained. Statistical and pattern recognition analyses on these parameters have been performed. It has been determined whether and which *NMR* parameter can significantly discriminate the differences on the cartilage structure among the three layers (i.e. superficial, middle and deep layers) and among four different coring zones of the knee (i.e. lateral/medial tibial and femoral zones).

The results achieved from this analysis are very promising: T_2, D, and Slp parameters can catch the main structural differences between the three cartilage layers. T_1 also manages to find differences, except for the comparison between superficial and middle layers. So, in general, the discrimination of the three cartilage layers shows very good results in terms of significance ($p < 0.0001$ in the Middle-Deep layers comparison and $p < 0.0009$ in the Superficial-Deep layers comparison for all the parameters; and $p < 0.005$ in the Superficial-Middle layers comparison for D and Slp parameters). These results are strictly correlated to the anatomical characteristics of the cartilage layers. In particular, it has been verified that *NMR* can detect protons belonging to different cartilage components like water and macromolecules and differences in the structural physical/chemical environment. Instead, the discrimination of the four cartilage knee zones does not show good results in terms of significance. Since all the twenty samples came from the same knee joint of the same bovine, the cartilage structural changes between one knee zone and another may not be so significant. Moreover, the studied bovine was certainly very young and it is known that in cases of osteoarthritis (*OA*) or simply older subjects the cartilage structural changes between knee zones become more evident.

In the future, these studies will be repeated on an older bovine or suffering from *OA*, and the distinctions made by *NMR* parameters between knee zones are expected to be more significant.

It has been widely demonstrated in the literature that the mobility and content of water, the content of proteoglycans, and the collagen structure in the cartilage tissue are suitable indicators for osteoarthritis severity. The original contribution of this work has concerned the determination of a multi-parametric set that can fully characterize the cartilage/subchondral tissue and this approach will help in deepening the knowledge about the cartilage changes occurring in *OA* disease. A further extension of these studies to pre-clinical cases could pave the way for extensive use of *NMR* single-sided devices for biomedical applications.

Another future step will concern the assessment of correlations between *NMR* parameters and tissue mechanics, thus applying such an integrated procedure in evaluating cartilage changes throughout osteoarthritis.

Finally, future further development of the *NMR* single-sided devices towards clinical use could concern the screening of the diseases related to cartilage tissue. This could have a positive impact both economically (including for underdeveloped countries) and socially, providing screening possibilities to a large part of the population. These desirable developments will meet many of the Sustainable Development Goals (*SDG*s) of the European Union: end poverty everywhere, ensure good health and promote well-being, ensure affordable energy, reduce inequalities within and among countries, ensure responsible consumption and production and take action to climate changes.

Appendix

Appendix A

Procedure validation results

Here the results of the three-layer analysis and the *CPMG* profile sequence on B1FA, B2FA, and B12TB bovine samples are reported. B3FA sample results are shown in Chapter 6.

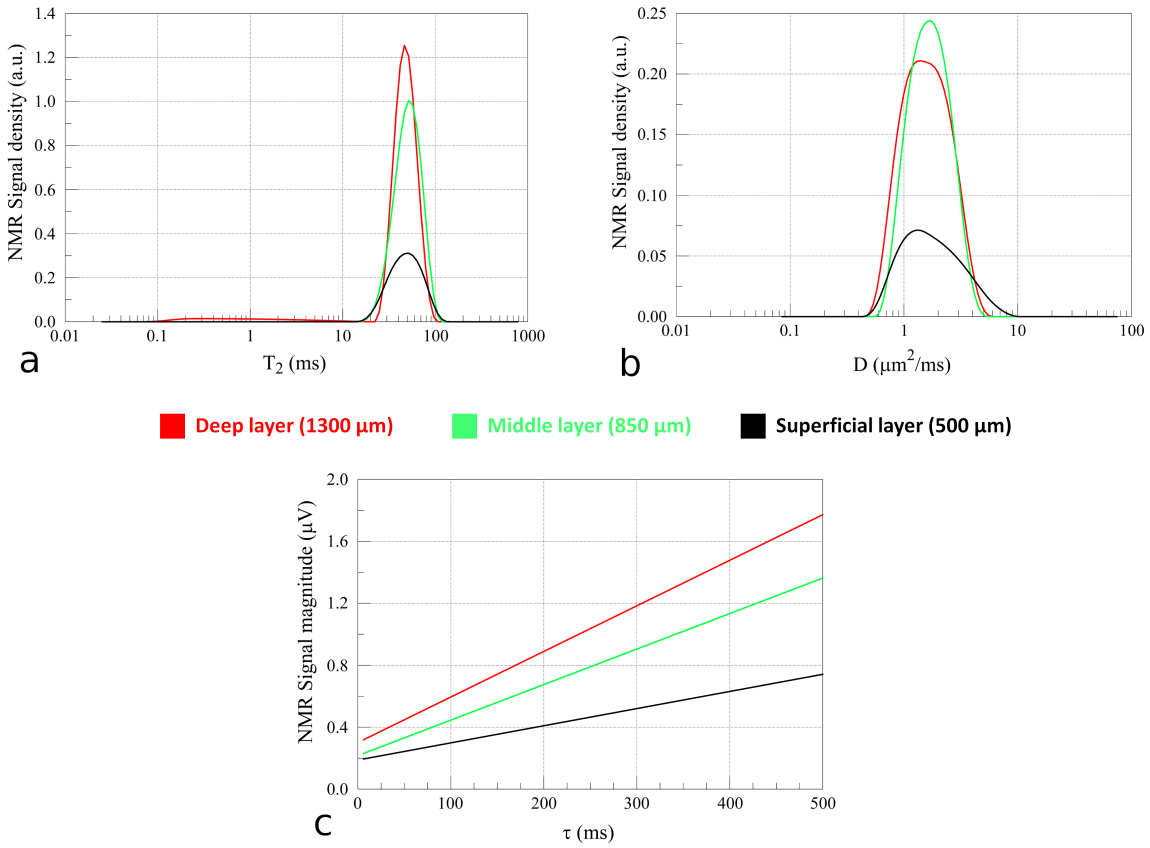

Figure A.1: *(a) T_2, (b) D, (c) T_1 distributions computed with CPMG, SSE and SR signals inversion made by the UPEN algorithm for the three cartilage layers of the B3FA sample. (d) DQ sequence linear data fit for each cartilage layer. Results were obtained with the automatized three-layer analysis on B1FA sample using* 500, 850 *and* 1300 μm *as centers of the sensitive volumes for superficial, middle and deep layers, respectively.*

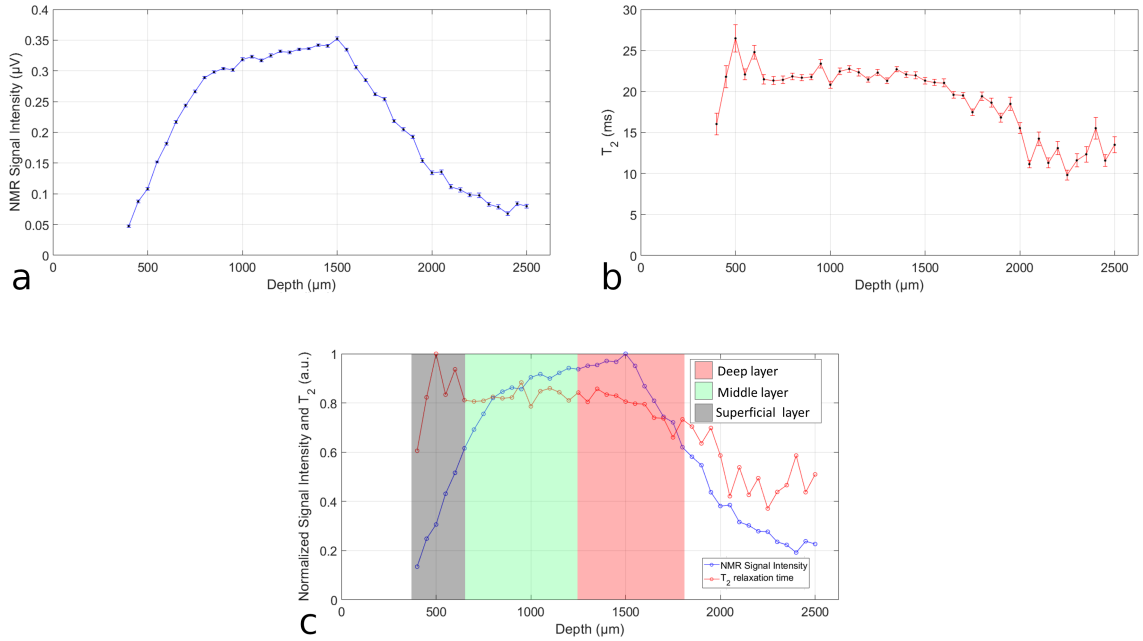

Figure A.2: *CPMG profile sequence results on B1FA sample. (a) The Nuclear Magnetization amplitude and (b) the transverse relaxation time trends as a function of the sample depth. Values and error bars were computed by the MATLAB exponential data fit. (c) Overlap of the two trends obtained by a normalization of the previous profiles by their maximum value. Superficial (black), middle (green) and deep (red) cartilage layers are assumed to be distributed as the colors indicate.* 500, 850 *and* 1300 μm *were chosen as centers of the sensitive volumes for the three layers.*

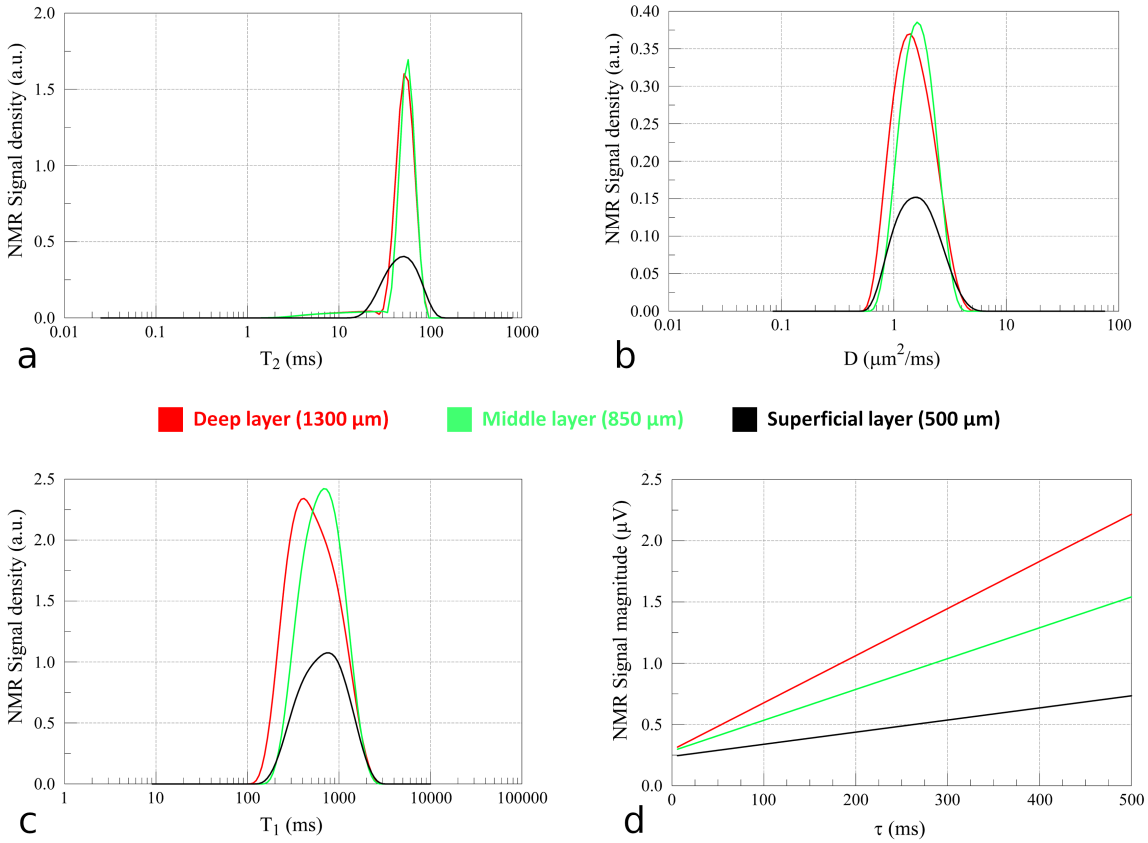

Figure A.3: *(a) T_2, (b) D, (c) T_1 distributions computed with CPMG, SSE and SR signals inversion made by the UPEN algorithm for the three cartilage layers of the B3FA sample. (d) DQ sequence linear data fit for each cartilage layer. Results were obtained with the automatized three-layer analysis on B2FA sample using* 500, 850 *and* 1300 μm *as centers of the sensitive volumes for superficial, middle and deep layers, respectively.*

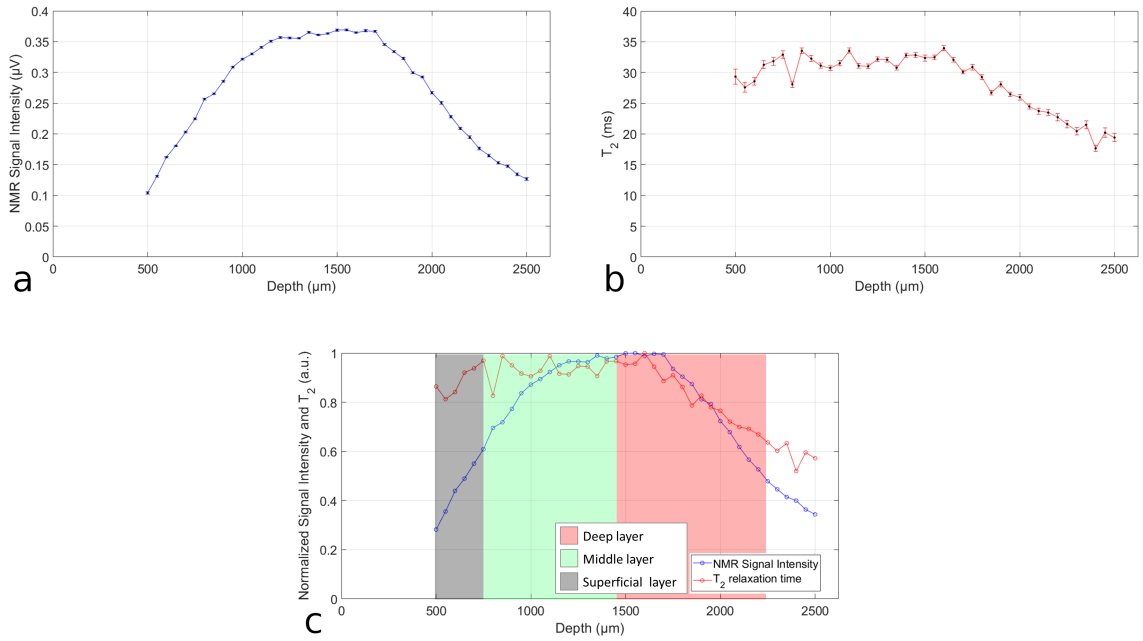

Figure A.4: *CPMG profile sequence results on B2FA sample. (a) The Nuclear Magnetization amplitude and (b) the transverse relaxation time trends as a function of the sample depth. Values and error bars were computed by the MATLAB exponential data fit. (c) Overlap of the two trends obtained by a normalization of the previous profiles by their maximum value. Superficial (black), middle (green) and deep (red) cartilage layers are assumed to be distributed as the colors indicate.* 500, 850 *and* 1300 μm *were chosen as centers of the sensitive volumes for the three layers.*

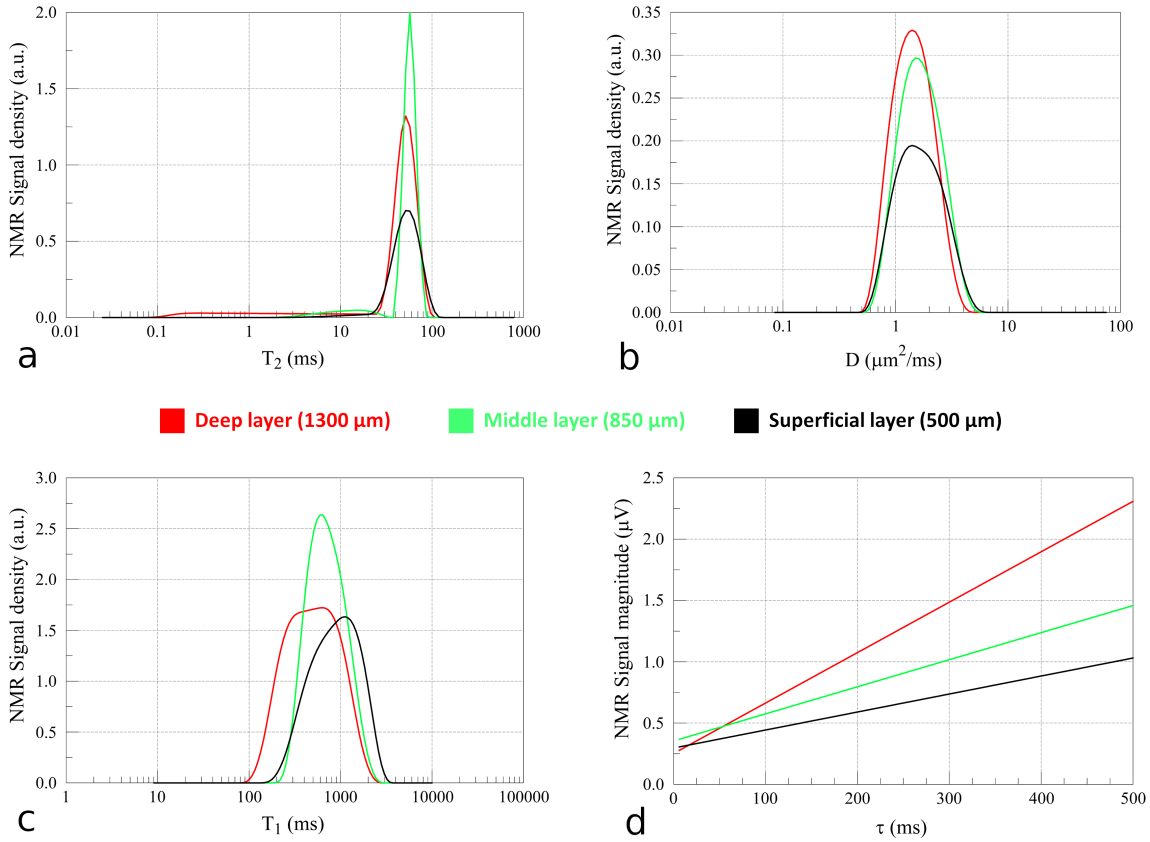

Figure A.5: *(a) T_2, (b) D, (c) T_1 distributions computed with CPMG, SSE and SR signals inversion made by the UPEN algorithm for the three cartilage layers of the B3FA sample. (d) DQ sequence linear data fit for each cartilage layer. Results were obtained with the automatized three-layer analysis on B12TB sample using* 850, 1100 *and* 1600 μm *as centers of the sensitive volumes for superficial, middle and deep layers, respectively.*

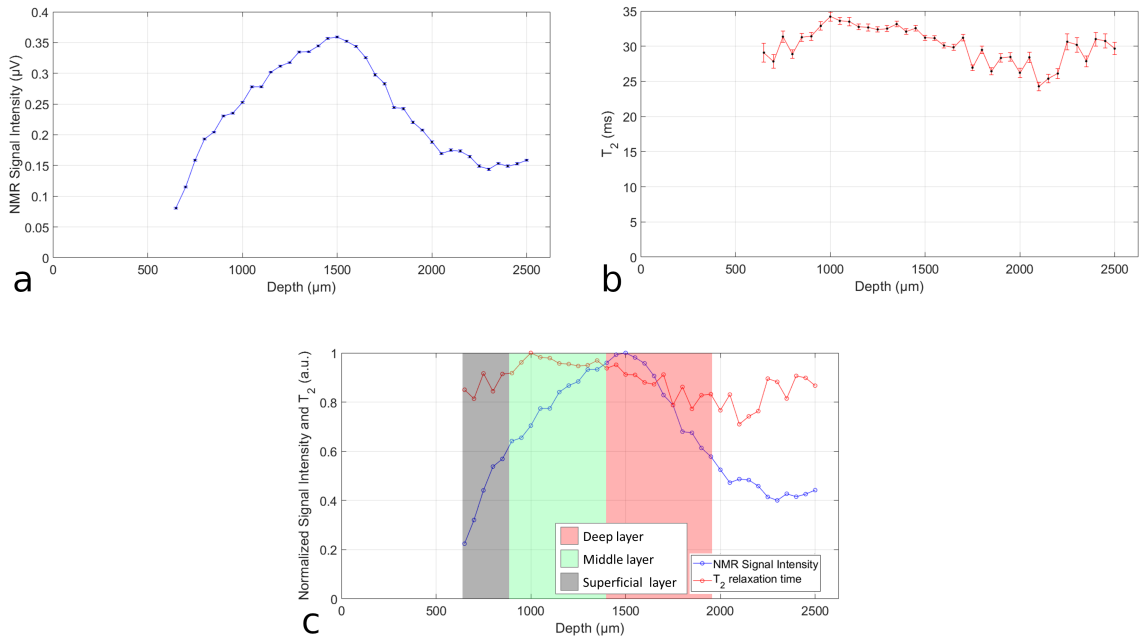

Figure A.6: *CPMG profile sequence results on B12TB sample. (a) The Nuclear Magnetization amplitude and (b) the transverse relaxation time trends as a function of the sample depth. Values and error bars were computed by the MATLAB exponential data fit. (c) Overlap of the two trends obtained by a normalization of the previous profiles by their maximum value. Superficial (black), middle (green) and deep (red) cartilage layers are assumed to be distributed as the colors indicate.* 850, 1100 *and* 1600 μm *were chosen as centers of the sensitive volumes for the three layers.*

Appendix B

Procedure results

Here the results of D, T_1 and Slp trend among cartilage layers for the four knee zones of the twenty bovine samples under study are reported. T_2 results are shown in Chapter 7.

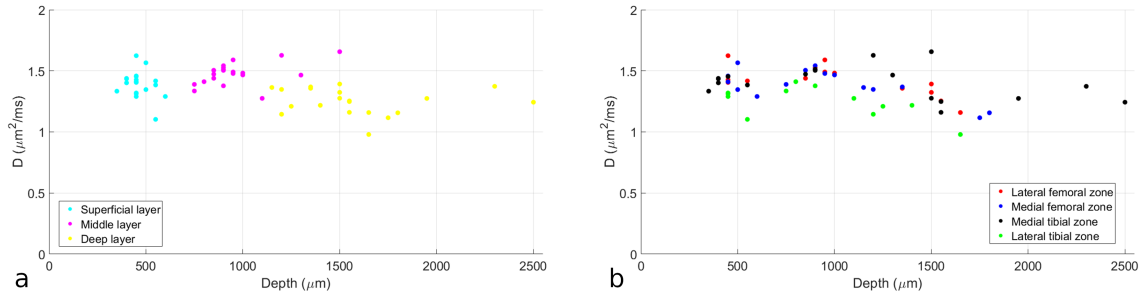

Figure B.1: *D values as a function of the sample's depths. The same plot has been colored considering two different samples information: (a) the three cartilage layers and (b) the four knee zones. Each sample is represented by three points in each of the two plots, i.e. one for each cartilage layer. The D uncertainties computed by the MATLAB data fits have not been represented because almost all the bars have a length similar to the circles' diameter.*

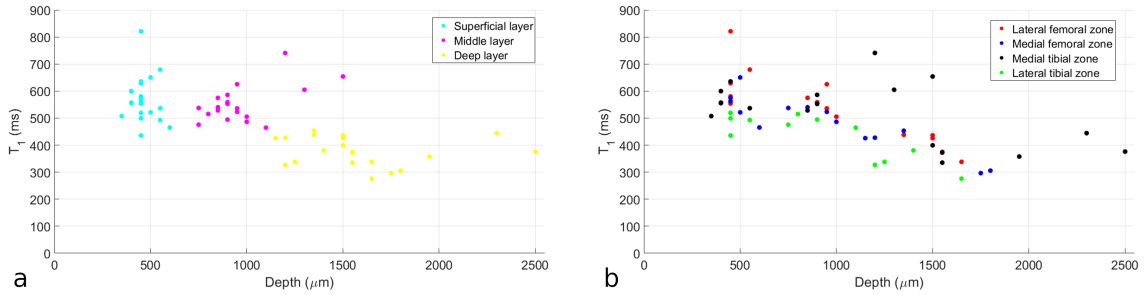

Figure B.2: *T_1 values as function of the samples depths. The same plot has been colored considering two different samples information: (a) the three cartilage layers and (b) the four knee zones. Each sample is represented by three points in each of the two plots, i.e. one for each cartilage layer. The T_1 uncertainties computed by the MATLAB data fits have not been represented because almost all the bars have a length similar to the circles' diameter.*

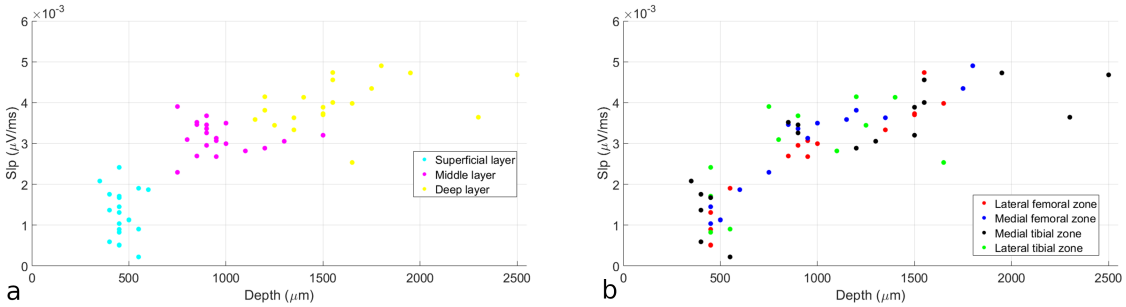

Figure B.3: *Slp values as function of the samples depths. The same plot has been colored considering two different samples information: (a) the three cartilage layers and (b) the four knee zones. Each sample is represented by three points in each of the two plots, i.e. one for each cartilage layer. The Slp uncertainties computed by the MATLAB data fits have not been represented because almost all the bars have a length similar to the circles' diameter.*

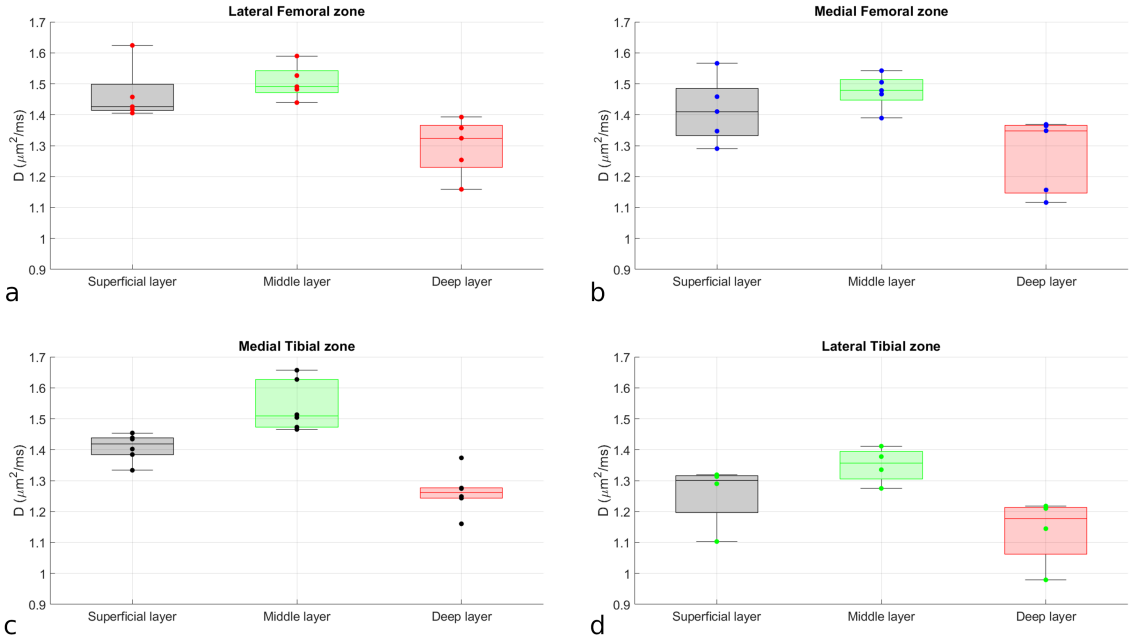

Figure B.4: *D trend among cartilage layers for the four knee zones: (a) Lateral femoral zone, (b) Medial femoral zone, (c) Medial tibial zone and (d) Lateral tibial zone. A box plot (by boxchart MATLAB function) representation is shown for each layer. The parameters uncertainties computed by the MATLAB data fits have not been represented because almost all the bars have a length similar to the circles diameter.*

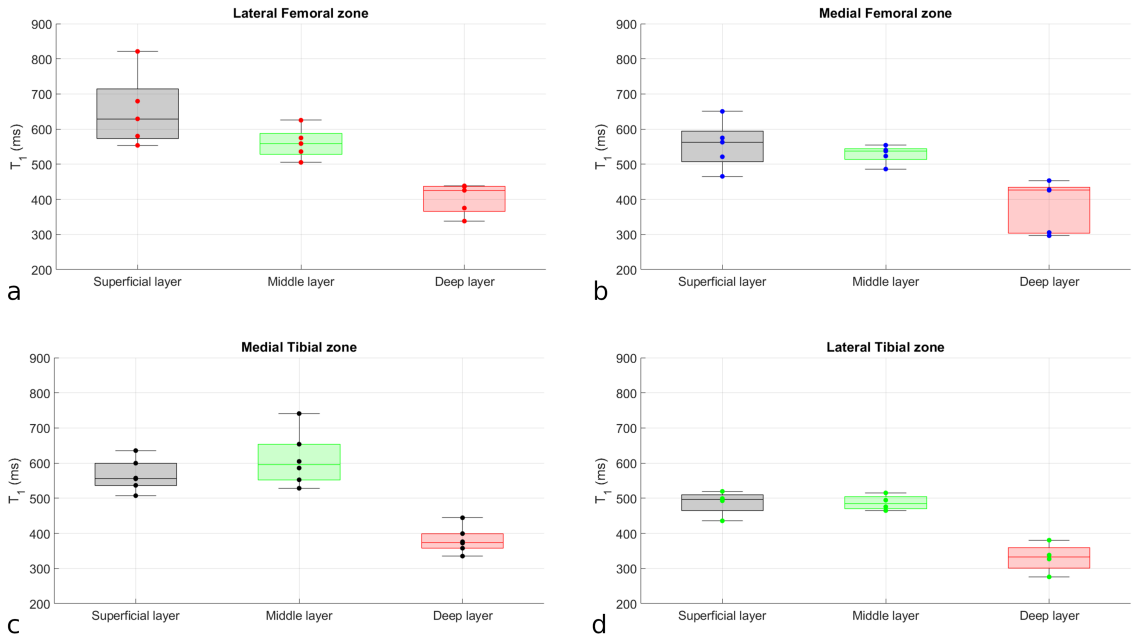

Figure B.5: *T_1 trend among cartilage layers for the four knee zones: (a) Lateral femoral zone, (b) Medial femoral zone, (c) Medial tibial zone and (d) Lateral tibial zone. A box plot (by boxchart MATLAB function) representation is shown for each layer. The parameters uncertainties computed by the MATLAB data fits have not been represented because almost all the bars have a length similar to the circles' diameter.*

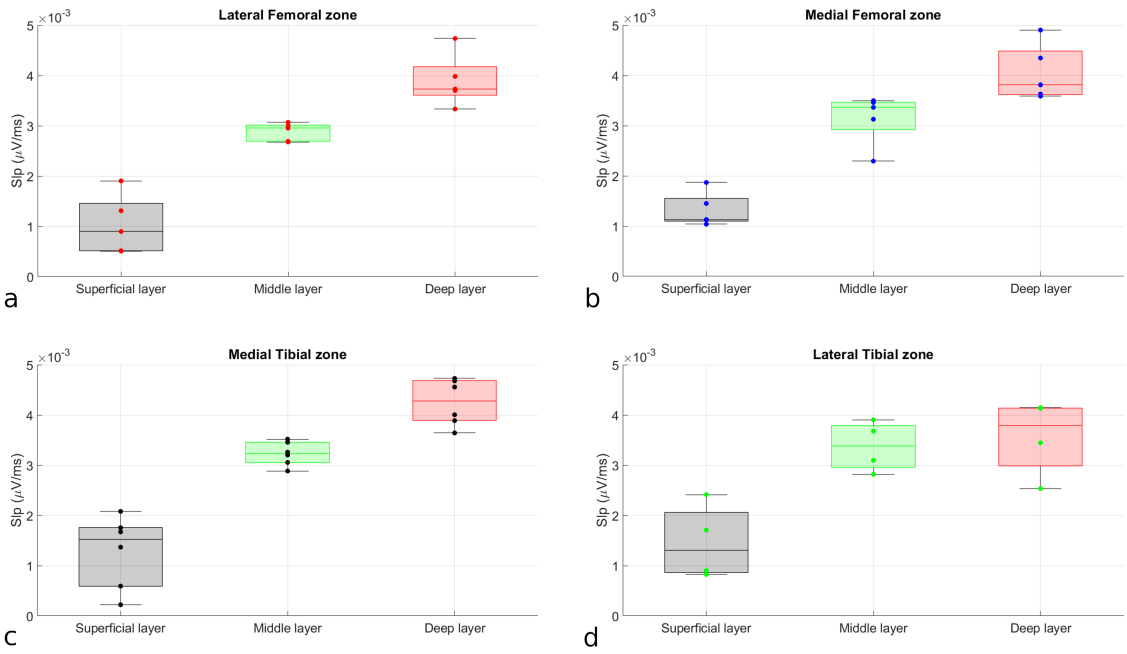

Figure B.6: *Slp trend among cartilage layers for the four knee zones: (a) Lateral femoral zone, (b) Medial femoral zone, (c) Medial tibial zone and (d) Lateral tibial zone. A box plot (by boxchart MATLAB function) representation is shown for each layer. The parameters uncertainties computed by the MATLAB data fits have not been represented because almost all the bars have a length similar to the circles' diameter.*

Bibliography

[1] Muratovic D. Findlay D.M. Cicuttini F.M. Wluka A.E. Lee Y.R. Edwards S. and Kuliwaba J.S. "Bone marrow lesions in knee osteoarthritis: regional differences in tibial subchondral bone microstructure and their association with cartilage degeneration." In: *Osteoarthritis and Cartilage* 27 (2019), pp. 1653–1662. DOI: https://doi.org/10.1016/j.joca.2019.07.004.

[2] Murray C.J.L. et al. "Disability-adjusted life years (DALYs) for 291 diseases and injuries in 21 regions, 1990–2010: a systematic analysis for the Global Burden of Disease Study 2010." In: *The Lancet* 380 (2012), pp. 2197–223.

[3] Rossler E. Mattea C. Stapf S. "Feasibility of high-resolution one-dimensional relaxation imaging at low magnetic field using a single-sided NMR scanner applied to articular cartilage." In: *Journal of Magnetic Resonance* 251 (2015), pp. 43–51. DOI: http://dx.doi.org/10.1016/j.jmr.2014.10.014.

[4] Sophia Fox A.J. Bedi A. Scott A. "The Basic Science of Articular Cartilage: Structure, Composition, and Function." In: *Orthopaedics* 1.6 (2009), pp. 461–468. DOI: 10.1177/1941738109350438.

[5] Fantazzini P. Galassi F. Bortolotti V. Brown R.J.S. Vittur F. "The search for negative amplitude components in quasi-continuous distributions of relaxation times: the example of ^1H magnetization exchange in articular cartilage and hydrated collagen." In: *New Journal of Physics* 13 (2011), pp. 1–15. DOI: 10.1088/1367-2630/13/6/065007.

[6] Kester B.S. Carpenter P.M. Yu H.J. Nozaki T. Kaneko Y. Yoshioka H. Schwarzkopf R. "$T_{1\rho}/T_2$ mapping and histopathology of degenerative cartilage in advanced knee osteoarthritis." In: *World Journal of Orthopedics* 8.4 (2017), pp. 350–356. DOI: 10.5312/wjo.v8.i4.350.

[7] Link T.M. Neumann J. Li X. "Prestructural Cartilage Assessment Using MRI." In: *Journal of Magnetic Resonance Imaging* (2016), pp. 1–17. DOI: 10.1002/jmri.25554.

[8] Guermazi A. Alizai H. Crema M.D. Trattnig S. Regatte R.R. Roemer F.W. "Compositional MRI techniques for evaluation of cartilage degeneration in osteoarthritis." In: *Osteoarthritis and Cartilage* 23 (2015), pp. 1639–1653. DOI: http://dx.doi.org/10.1016/j.joca.2015.05.026.

[9] Rossler E. Mattea C. Stapf S. "NMR Dispersion Investigations of Enzymatically Degraded Bovine Articular Cartilage." In: *Magnetic Resonance in Medicine* 73 (2015), pp. 2005–2014. DOI: 10.1002/mrm.25292.

[10] Rossler E. Mattea C. Saarakkala S. Lehenkari P. Finnila M. Rieppo L. Karhula S. Nieminen M.T. Stapf S. "Correlations of low-field NMR and variable-field NMR parameters with osteoarthritis in human articular cartilage under load." In: *NMR in Biomedicine* 30 (2017), pp. 1–14. DOI: 10.1002/nbm.3738.

[11] Barbieri M. Fantazzini P. Bortolotti V. Baruffaldi F. Festa A. Manners D.N. Testa C. Brizi L. "Single-sided NMR to estimate morphological parameters of the trabecular bone structure." In: *Magnetic Resonance in Medicine* 85 (2021), pp. 3353–3369. DOI: 10.1002/mrm.28648.

[12] Casanova F. Perlo J. Blumich B. *Single-Sided NMR*. Springer, 2011. ISBN: 978-3-642-16306-7.

[13] Eidmann G. Savelsberg R. Blumler P. Blumich B. "The NMR MOUSE, a Mobile Universal Surface Explorer." In: *Journal of Magnetic Resonance* 122 (1996), pp. 104–109.

[14] Rossler E. Mattea C. Mollova A. Stapf S. "Low-field one-dimensional and direction-dependent relaxation imaging of bovine articular cartilage." In: *Journal of Magnetic Resonance* 213 (2011), pp. 112–118. DOI: 10.1016/j.jmr.2011.09.014.

[15] Rossler E. Mattea C. Stapf S. Karhula S. Saarakkala S. Nieminen M.T. "Load-dependent NMR low-field profiling and relaxation dispersion study of osteoarthritic articular cartilage." In: *Microporous and Mesoporous Materials* 269 (2018), pp. 160–165. DOI: http://dx.doi.org/10.1016/j.micromeso.2017.02.069.

[16] Cretu A. Mattea C. Stapf S. "Low-field and variable-field NMR relaxation studies of H_2O and D_2O molecular dynamics in articular cartilage." In: *PLOS ONE* 16.8 (2021), pp. 1–34.

[17] Kuettner K.E. "Biochemistry of Articular Cartilage in Health and Disease." In: *Clinical Biochemistry* 25 (1992), pp. 155–163.

[18] Pearle A.D. Warren R.F. Rodeo S.A. "Basic Science of Articular Cartilage and Osteoarthritis." In: *Clinics in Sports Medicine* 24 (2005), pp. 1–12. DOI: 10.1016/j.csm.2004.08.007.

[19] Riesle J. Hollander A.P. Langer R. Freed L.E. Vunjak-Novakovic G. "Collagen in Tissue-Engineered Cartilage: Types, Structure, and Crosslinks." In: *Journal of Cellular Biochemistry* 71 (1998), pp. 313–327.

[20] Snedeker J.G. and Gautieri A. "The role of collagen crosslinks in ageing and diabetes - the good, the bad, and the ugly." In: *Muscles, Ligaments and Tendons Journal* 4.3 (2014), pp. 303–308.

[21] Buckwalter J.A. Mankin H.J. "Articular Cartilage." In: *The Journal of Bone and Joint Surgery* 79.4 (1997), pp. 600–611.

[22] Moore A.C. and Burris D.L. "Tribological and material properties for cartilage of and throughout the bovine stifle: support for the altered joint kinematics hypothesis of osteoarthritis." In: *Osteoarthritis and Cartilage* 23 (2015), pp. 161–169. DOI: http://dx.doi.org/10.1016/j.joca.2014.09.021.

[23] Budras K.D. Habel R.E. Wunsche A. Buda S. *Bovine Anatomy*. Environment and Agriculture. Schluetersche, 2011. ISBN: 9780429068522.

[24] Paul T. Callaghan. *Principles of Nuclear Magnetic Resonance Microscopy*. Oxford Science Publications. Clarendon Press Oxford, 1993. ISBN: 0-19-853997-5.

[25] Joseph P. Hornak. *The Basics of NMR*. 1997. URL: https://www.cis.rit.edu/htbooks/nmr/inside.htm.

[26] Price William S. "Pulsed-Field Gradient Nuclear Magnetic Resonance as a Tool for Studying Translational Diffusion: Part 1. Basic Theory." In: *Concepts in Magnetic Resonance* 9 (1997), pp. 299–336. DOI: https://doi.org/10.1002/(SICI)1099-0534(1997)9:5<299::AID-CMR2>3.0.CO;2-U.

[27] Blumich B. Haber-Pohlmeier S. Zia W. *COMPACT NMR*. De Gruyter, 2014. ISBN: 978-3110266283.

[28] Blumich B. Perlo J. Casanova F. "Mobile single-sided NMR." In: *Progress in Nuclear Magnetic Resonance Spectroscopy* 52 (2008), pp. 197–269. DOI: 10.1016/j.pnmrs.2007.10.002.

[29] Voda M.A. Demco D.E. Perlo J. Orza R.A. Blumich B. "Multispin moments edited by multiple-quantum NMR: application to elastomers." In: *Journal of Magnetic Resonance* 172 (2005), pp. 98–109. DOI: 10.1016/j.jmr.2004.10.001.

[30] Wiesmath A. Filip C. Demco D.E. Blumich B. "Double-Quantum-Filtered NMR Signals in Inhomogeneous Magnetic Fields." In: *Journal of Magnetic Resonance* 149 (2001), pp. 258–263. DOI: 10.1006/jmre.2001.2299.

[31] Schneider M. Gasper L. Demco D.E. Blumich B. "Residual dipolar couplings by ^1H dipolar-encoded longitudinal magnetization, double- and triple-quantum nuclear magnetic resonance in cross-linked elastomers." In: *JOURNAL OF CHEMICAL PHYSICS* 111.1 (1999), pp. 402–415. DOI: https://doi.org/10.1063/1.479291.

[32] *Profile NMR-MOUSE probe with the Kea2 spectrometer*. URL: https://magritek.com/products/nmr-mouse.

[33] McDonald P.J. Gajewicz A.M. Morrell R. *The Characterisation of Cement Based Materials Using T_2 ^1H Nuclear Magnetic Resonance Relaxation Analysis*. Good Practice Guide No. 144 - Version 1.0. National Physical Laboratory - University of Surrey, 2016.

[34] Wiesmath A. Filip C. Demco D.E. Blumich B. "NMR of Multipolar Spin States Excited in Strongly Inhomogeneous Magnetic Fields." In: *Journal of Magnetic Resonance* 154 (2002), pp. 60–72. DOI: 10.1006/jmre.2001.2458.

[35] Bortolotti V. Brown R.J.S. Fantazzini P. *UpenWin: a software for inversion of multiexponential decay data for Windows system. Alma Mater Studiorum - Università di Bologna*. 2012. URL: http://software.dicam.unibo.it/upenwin.

[36] Borgia G. C. Brown R.J.S. and Fantazzini P. "Uniform-Penalty Inversion of Multiexponential Decay Data." In: *Journal of Magnetic Resonance* 132 (1998), pp. 65–77.

[37] Ostertagova E. Ostertag O. Kovac J. "Methodology and Application of the Kruskal-Wallis Test." In: *Applied Mechanics and Materials* 611 (1952), pp. 115–120. DOI: 10.4028/www.scientific.net/AMM.611.115.

[38] Kruskal W.H. and Wallis W.A. "Use of Ranks in One-Criterion Variance Analysis." In: *Journal of the American Statistical Association* 47.260 (1952), pp. 583–621. DOI: https://www.jstor.org/stable/2280779.

[39] Bewick V. Cheek L. Ball J. "Statistics review 10: Further nonparametric methods." In: *Critical Care* 8.3 (2004), pp. 196–199. DOI: 10.1186/cc2857.

[40] Chen S. Feng Z. Yi X. "A general introduction to adjustment for multiple comparisons." In: *Journal of Thoracic Disease* 9.6 (2017), pp. 1725–1729. DOI: 10.21037/jtd.2017.05.34.

[41] Abdi H. and Williams L.J. "Principal component analysis." In: *WIREs Computational Statistics* 2 (2010), pp. 433–459. DOI: 10.1002/wics.101.

[42] Wold S. Esbensen K. Geladi P. "Principal Component Analysis." In: *Chemometrics and Intelligent Laboratory Systems* 2 (1987), pp. 37–52.

[43] Omran M.G.H. Engelbrecht A.P. Salman A. "An overview of clustering methods." In: *Intelligent Data Analysis* 11 (2007), pp. 583–605.

[44] Pei J. Tseng V.S. Cao L. Motoda H. Xu G. *Advances in Knowledge Discovery and Data Mining*. Density-Based Clustering Based on Hierarchical Density Estimates. Springer, 2013. ISBN: 978-3-642-37455-5.

[45] McInnes L. Healy J. Astels S. (GitHub). *How HDBSCAN Works*. 2016. URL: https://hdbscan.readthedocs.io/en/latest/how_hdbscan_works.html#how-hdbscan-works.

[46] Rieppo J. Hyttinen M. Lappalainen R. Jurvelin J.S. Helminen H.J. "Spatial determination of water, collagen and proteoglycan contents by fourier transform infrared imaging and digital densitometry." In: *50th Annual Meeting of the Orthopaedic Research Society* 1021 (2004).

Acknowledgements

Vorrei anzitutto ringraziare Leonardo e Claudia per avermi offerto la possibilità di lavorare a un progetto così interessante e ambizioso. Grazie davvero per la vostra disponibilità, pazienza, competenza e per la profonda umanità che mi avete regalato.

Ringrazio anche Massimiliano, Matteo, Roberta e tutti i ragazzi che ho incontrato nel Laboratorio di Tecnologia Medica del Rizzoli per avermi fatto sentire a casa fin dall'inizio accogliendomi in un ambiente meraviglioso. Sarò ripetitivo, ma anche con voi ho sperimentato una grande umanità.

Grazie babbo e mamma per la vostra costante e preziosissima presenza.

E grazie Sofi per esserci stata ed esserci sempre di più.

Grazie brothers (i.e. Ire e Matto) e grazie Zanna, Anna, Mati e Robin Hood :) per il dialogo, l'ascolto e la vostra potente testimonianza.

Grazie nonni per la vostra semplicità e profonda saggezza: Ezio, Emma, Pina, Domenico, Rina, Antonietta e Gino.

Grazie a tutti gli amici, cugini e zii che in un modo o nell'altro mi vogliono bene, così come sono.

Grazie di cuore fra Tommy, Marco e Franca.

E in ultimo grazie Bellaria perchè in ben due occasioni della vita mi hai dato la possibilità di innamorarmi della Risonanza Magnetica e di una fisica a servizio della salute e della medicina.
Non c'è niente di più bello che dare speranza a chi è in difficoltà.